A NOVEL ELECTRIC POWER QUALITY MONITORING SYSTEM FOR TRANSIENT ANALYSIS

A thesis submitted to

CITY UNIVERSITY LONDON

for the Degree of

DOCTOR OF PHILOSOPHY

By

CHAN YAU CHUNG, JOHN

School of Engineering and Mathematical Sciences

City University London
Northampton Square
London EC1V 0HB
United Kingdom

October 2014

Abstract

Electricity is vital for our daily life in modern cites. In order to ensure its reliability and supply, an electric power monitoring system is indispensable in an electric power system. Currently, most electric power monitoring systems are designed for steady-state monitoring only. They may not be able to monitor instantaneous power disturbances, such as voltage surge, happened in electric power systems. In fact, instantaneous power disturbances are frequently found in electric power systems, which result in equipment failures and cause financial losses.

Therefore, a novel electric power monitoring system is proposed in this thesis. Besides traditional functions, the proposed system is capable of monitoring and analyzing instantaneous power disturbances in electric power systems. Novelties of the proposed monitoring system are in the following three major aspects.

Firstly, the proposed system is capable of monitoring instantaneous power disturbances. Unlike traditional monitoring systems, the proposed system captures not only statistical power quantities (e.g. kW, kWh), but also voltage and current waveforms. Since a considerable communication network bandwidth is required to transmit electric waveforms in a remote monitoring system, a novel waveform compression algorithm is proposed to realize real-time electric power waveform monitoring on low-speed communication networks (e.g. Zigbee).

Secondly, the proposed system is capable of identifying various kinds of power disturbances automatically. It relieves electrical engineers from manned disturbance identification on preserved waveforms. Unlike traditional disturbance identification algorithms, the proposed system can identify not only voltage disturbances, but also

current disturbances. Hence, it can provide a better chance in identifying more problems and disturbances in electric power systems.

Thirdly, a novel time-frequency analysis method is proposed to analyze preserved waveforms. The proposed method is an improvement to the well-known Discrete Wavelet Packet Transform (DWPT). DWPT has been used by researchers and engineers to analyze disturbances and harmonics in electric power systems. However, DWPT is subjected to a non-uniform leakage problem, which has been discussed intensively in many studies. In order to tackle this issue, a frequency shifting scheme is introduced in the proposed method.

A prototype has been implemented to demonstrate the feasibility of the proposed electric power monitoring system. There are two major components – a prototype meter and a central monitoring system. The performance of the prototype has been evaluated by conducting experiments and field tests. The capability of the proposed system for real-time remote monitoring has been verified on Zigbee network, which is a low-power, low speed wireless communication network.

Summary of Original Contributions

The following summarizes the original contributions made in my research studies.

[1] A hybrid sinusoidal and lifting wavelet compression algorithm for real-time electric power quality monitoring (Chapter 3).

[2] An electric power disturbances identification algorithm extended from the waveform compression algorithm in [1] above (Chapter 3).

[3] A novel power quality analysis method utilizing wavelet and Hilbert transform (Chapter 3).

[4] A prototype power quality meter and its application software (Chapter 4).

[5] A novel automatic calibration system for current measurement by coreless sensor and its prototype (Appendix I).

Acknowledgments

I would like to express my sincere gratitude to my PhD supervisor Professor Lai Loi Lei and my local PhD supervisor Dr. Tse Chung Fai, Norman, who have had the faith in me and have provided me the opportunity to carry out the research study. Under the guidance from Professor Lai and Dr. Tse, my entire research study has been a very exciting and interesting journey. Their experienced insights have pointed me to my research topic on electric power monitoring system. Their valuable advices have guided my way out from challenges and difficulties for many times. They have always provided me the best possible resource to complete my study. This research study is definitely a wonderful experience in my life. I am grateful for their guidance and supports in these years. I would like to thank Professor Lai and his family for their warm reception in London, when I first left my hometown to start my amazing research journey.

I would like to express my sincere gratitude to Dr. Lau Wing Hong, Ricky, who has been my teacher and supervisor since the first day in my undergraduate study. He is always willing to help and give his best suggestions for my study and career. I am grateful for his deepest trust in my ability by introduced me to his colleagues Dr. Tse to begin my fantastic journey.

I would like to thank Professor Chung Shu Hung, Henry and his research team, in particular Dr. Li Tin Ho, River, for allowing me to access their well-equipped laboratory and giving me their helpful supports. I would like to thank Mr. Leung Ming Chiu for his valuable data and supports on electric power quality measurement in buildings.

Finally, I would like to thank my parents and my sister. It would have been impossible for me to complete the research study if they are not always supporting me and encouraging me with their best wishes. They have tolerated me to willfully extend my

wonderful journey in exploring and developing more new ideas. To them, I am eternally grateful.

Copyright Declaration

I, “Chan Yau Chung”, of Hong Kong, “the Depositor”, would like to deposit “A Novel Power Quality Monitoring and Analysis System – Waveform Capturing, Identifying and Analyzing”, hereafter referred to as the “Work”, in the City University Institutional Repository and agree to the following:

NON-EXCLUSIVE RIGHTS

Rights granted to the City University Institutional Repository through this agreement are entirely non-exclusive and royalty free. I am free to publish the Work in its present version or future versions elsewhere. I agree that the City University Institutional Repository administrators or any third party with whom the City University Institutional Repository has an agreement to do so may, without changing content, translate the Work to any medium or format for the purpose of future preservation and accessibility.

DEPOSIT IN THE CITY UNIVERSITY INSTITUTIONAL REPOSITORY

I understand that work deposited in the City University Institutional Repository will be accessible to a wide variety of people and institutions - including automated agents - via the World Wide Web. I also agree to an electronic copy of my thesis being included in the British Library Electronic Theses On-line System (EThOS).

I understand that once the Work is deposited, a citation to the Work will always remain visible. Removal of the Work can be made after discussion with the City University Institutional Repository, who shall make best efforts to ensure removal of the Work from any third party with whom the City University Institutional Repository has an agreement.

I AGREE AS FOLLOWS:

- That I am the author or co-author of the work and have the authority on behalf of the author or authors to make this agreement and to hereby give the City University Institutional Repository administrators the right to make available the Work in the way described above.

- That I have exercised reasonable care to ensure that the Work is original, and does not to the best of my knowledge break any UK law or infringe any third party's copyright or other Intellectual Property Right. Where I have included third party copyright material, I have fully acknowledged its source.

- The administrators of the City University Institutional Repository do not hold any obligation to take legal action on behalf of the Depositor, or other rights holders, in the event of breach of intellectual property rights, or any other right, in the material deposited.

Chan Yau Chung

October 2014

Table of Contents

Glossary

Abbreviation

AC	Alternating Current
ADC	Analog-to-Digital Converter
AFE	Analog Front-End
AMR	Automatic Meter Reading
ANN	Artificial Neural Network
CR	Compression Ratio
DC	Direct Current
DFT	Discrete Fourier Transform
DMA	Direct memory access
DSP	Digital Signal Processor
DVR	Dynamic Voltage Restorer
DWPT	Discrete Wavelet Packet Transform
DWT	Discrete Wavelet Transform
FFT	Fast Fourier Transform
FIR	Finite Impulse Response
FT	Fourier Transform
HT	Hilbert Transform
IDWT	Inverse Discrete Wavelet Transform
IEC	International Electrotechnical Commission
IEEE	Institute of Electrical and Electronics Engineers
ILWT	Lifting Wavelet Transform with Integer to Integer Mapping
LWT	Lifting Wavelet Transform
p.f.	Power Factor
PQ	Power Quality
RMS	Root Mean Square

RTOS	Real-Time Operation System
SNR	Signal-to-Noise Ratio
SPI	Serial Peripheral Interface
THD	Total Harmonic Distortion
UPS	Uninterruptible Power Supply
WPT	Wavelet Packet Transform
WT	Wavelet Transform

Mathematical Notations

$x[\ ]$	Finite sequence of sampled data
$X[\ ]$	Finite sequence of complex sinusoids
θ	Initial phase angle of sinusoid component
$\theta(\ )$	Instantaneous phase angle of sinusoid component
ω	Frequency of sinusoid component
$\omega(\ )$	Instantaneous frequency of sinusoid component
a	Amplitude of sinusoid component
$a(\ )$	Instantaneous amplitude of sinusoid component
$\delta[\ ]$	Dirac delta function (or Impulse function)
$H[\ ]$	Hilbert transform
$F[\ ]$	Fourier transform
$y(\ )$	Hilbert transform of $x[\ ]$
$z(\ )$	Analytic signal
$g[\ ]$	Wavelet filter of Discrete Wavelet Transform
$h[\ ]$	Scaling filter of Discrete Wavelet Transform
$\downarrow 2$	Downsampling coefficients by 2 in Discrete Wavelet Transform
d_j	Wavelet coefficients of Discrete Wavelet Transform
a_j	Approximation coefficients of Discrete Wavelet Transform
w_j	Wavelet coefficients of Discrete Wavelet Packet Transform
$s[\ ]$	Stationary component of $x[\ ]$
$\varphi[\ ]$	Non-stationary component of $x[\ ]$
$m[\ ]$	Modified wavelet coefficient for Otsu's Method

Definition of Common Terms

Harmonics of a signal are the frequency components of the signal.

Sub-harmonics of a signal are frequency components of the signal with frequencies below the fundamental frequency.

Inter-harmonics of a signal are frequency components of the signal with frequencies not integer multiples of the fundamental frequency.

Integer harmonics of a signal are frequency components of the signal with frequencies equal to integer multiples of the fundamental frequency

Stationary signal is a signal for which the signal properties such as amplitude and frequency do not vary with time.

Non-stationary signal is a signal for which the signal properties such as amplitude and frequency vary with time.

List of Figures and Tables

List of Figures

List of Tables

Chapter 1

Introduction

1.1 Motivation of the Research

Nowadays electricity is a basic necessity in modern cities. Our daily activities are now sustained by various kinds of electric appliances such as electric lights and electrified transports. A reliable electric power supply is essential to maintain our normal activities. Any interruption of electricity supply is very likely to cause huge damages and inconveniences to our societies.

As global electricity demand is increasing, it poses many challenges to the reliability of the electric power systems. Firstly, electricity shortage has become a serious problem. In many developing counties, intended electricity cutoffs have been very common to prevent overloading of the electric power systems. While more electric power stations are to be built to cater for the increasing demand of electricity, energy efficiencies are also becoming more and more important for maximizing capacities of electric power systems

Secondly, electric power systems are getting more complicated than in the past. Electricity generation is no longer centralized. Many renewable energy collectors are now penetrating into various levels of electric power systems. They can be found in remote areas, where suitable weathers warrant a stable supply, or simply on top of our building roof. The power flow of the electric power system is no longer unidirectional and therefor is more difficult to manage. Moreover, most renewable energy sources (e.g. solar, wind) are weather-dependent. Their reliabilities are lower than traditional energy sources (e.g. coal-fire, nuclear). As a result, they would cause many power quality problems (e.g. harmonics) to the electric power systems.

Thirdly, the varieties of electric-driven devices are increasing. More and more devices with different electric characteristics are connected to electric power systems. The status of the electric power systems are more and more difficult to predict. In the past, electric devices are mostly passive in nature, i.e. they contain passive components only (e.g. resistor, capacitor and inductor). However, many modern electric devices contain active components (e.g. transistor, diode) nowadays. Their electric characteristics are controlled by their own internal mechanisms. Unlike passive electric devices (e.g. incandescent light bulb), their voltage and current relationship are not necessarily linear and repetitive. Hence, many of these devices have posed various reliability problems (e.g. overheat, tripping of circuit breaker) to the electric power systems.

Besides the problems mentioned above, new technologies, such as electric vehicle charging, smart home, and demand response management, will also integrate into the electric power systems. While the electric power systems are getting more complicated, the reliability of existing electric power systems is unavoidably being influenced. Hence, maintaining the reliability of the power systems has become the number one challenge to many electrical engineers.

1.2 Power Quality Problems

A reliable electric power supply is vital for any electric equipment to function properly. In an ideal scenario, the voltage supply to electric equipment is presumed to remain constant and purely sinusoidal under all circumstances. However, practical power systems are far from ideal. Their voltage supplies are varying time to time and even occasionally interrupted.

In general, electricity suppliers are responsible to provide a reliable electricity source for end-users. Their voltage qualities have to comply with electricity regulations and stay within specifications (e.g. magnitude and frequency). However, electric power systems in these days are enormous. Electricity is usually transmitted from a long distance to end-users. Their service area usually covers multiple cities and even countries. An electric power system may have millions of consumers at the same time. Hence, electric power systems are liable to many unpredictable events (e.g. parts failure, tree collapse). Although modern electric power systems are far more reliable than in the past, occasional

power interruptions are still unavoidable. For example it is reported that in 2012 alone, the number of electricity interruption experienced per customer in UK is around 0.7 [5].

Beside interruption, other power quality problems such as low power factor, harmonics, and disturbances are also found in electric power systems. These problems raise a huge concern in both reliability and efficiency of electric power systems.

1.2.1 Low Power Factor

Power factor (p.f.) is a ratio of active power and apparent power (1.1). It is widely used to indicate the efficiency of electric power delivery. Normally, power factors of electric equipment are preferred to be 1, where the active power is equal to the apparent power. Equipment with low power factor often spoils the efficiency of the electric power system, as they demand unnecessary current flowing through distribution networks which result in extra conduction loss. The cost of the unnecessary current is enormous. A rough estimate of the energy loss in conduction is exponentially proportional to the current ($P = I^2R$). Moreover, the unnecessary current also undermines maximum throughputs of electric power systems by occupying their distribution networks. Thus in addition to energy consumption (kWh), industrial and commercial customers are also required to pay for the apparent power.

$$Power\ factor\ (p.f.) = \frac{Active\ Power\ (P)}{Apparent\ Power\ (S)} \tag{1.1}$$

Instead of (1.1), power factor can also be calculated by the phase difference between voltage and current for linear (or passive) load (e.g. heater, motor), where the current is either lagging or leading the voltage.

1.2.2 Harmonics

Electric power systems have become more and more complicated, when non-linear loads (e.g. Switch Mode Power Supply, Adjustable Speed Device and Electronic Ballast) are used extensively nowadays. Different from passive loads, the impedance of the non-linear loads is voltage-dependent. The current drawn by the non-linear loads is non-sinusoidal and non-linear to the voltage supply. As a result, harmonic currents are introduced in the electric power systems by the non-linear loads.

Theoretically, harmonic currents (e.g. 3rd – 150/180 Hz) cause only conduction loss in electric power systems. They cannot generate any useful energy for electric appliances. For example, taking integral on products of a sinusoidal supply voltage (e.g. 50/60 Hz) and a harmonic current (e.g. 150/180 Hz), its net energy is always zero. Therefore, the presence of harmonic currents would degrade the power system efficiency. Nevertheless, non-linear loads (e.g. electronic products) have been becoming very popular in these days. Billions of electronic products (e.g. computer, electronic ballast) are installed in the electric power systems. The growing amount of harmonic current has become a serious problem to electrical engineers.

In addition to lowering the efficiency of the electric power systems, harmonic currents also threaten the reliability of the electric power systems. In distribution networks, excessive harmonic currents often lead to voltage distortion (e.g. flat-top). In three phase circuits, neutral conductors have to be oversized for handling triplen harmonics (e.g. 3rd, and 9th). In transformers, k-rated transformers are to be specified to avoid overheating. Moreover, many electric meters in the past are only sensitive to 50/60 Hz current; hence, replacements are needed to prevent false reading.

1.2.3 Voltage Disturbance

Generally, voltage supplies in electric power systems are fairly stable in these days. Their voltage derivations are usually insignificant and even unperceivable. The voltage supplies are hardly affected by individual demands (or loads), as their demands are relatively negligible to the enormous power supply systems. Nevertheless, undesired voltage disturbances are occasionally found in the electric power systems. They are usually classified into 7 categories with different characteristics (e.g. spectral content, duration, magnitude) as shown in Table 1.1 [3]. These disturbances are usually caused by various predictable or accidental events. Details of their typical causes can be found in IEEE standard 1159-2009 [3].

Table 1.1
Categories and typical characteristics of power system electromagnetic phenomena [3]

Categories	Typical spectral content	Typical duration	Typical voltage magnitude
1.0 Transient			
1.1 Impulsive	-	-	-
1.2 Oscillatory	< 5MHz	5 μs – 50 ms	0 – 8 pu
2.0 Short-duration variations			
2.1 Interruption	-	10 ms – 1 min	< 0.1 pu
2.2 Sag	-	10 ms – 1 min	0.1 – 0.9 pu
2.3 Swell	-	10 ms – 1 min	1.1 – 1.8 pu
3.0 Long-duration variations			
3.1 Interruption	-	> 1 min	0.0 pu
3.2 Undervoltage	-	> 1 min	0.8 – 0.9 pu
3.3 Overvoltage	-	> 1 min	1.1 – 1.2 pu
4.0 Imbalance			
4.1 Voltage	-	steady state	0.5 – 2%
4.2 Current	-	steady state	1.0 – 30%
5.0 Waveform distortion			
3.1 DC offset	-	steady state	0 – 0.1%
3.2 Harmonics	0 – 9 kHz	steady state	0 – 20%
3.3 Interharmonics	0 – 9 kHz	steady state	0 – 2%
3.2 Notching	-	steady state	-
3.3 Noise	broadband	steady state	0 – 1%
6.0 Voltage fluctuation	< 25 Hz	intermittent	0.1 – 7% 0.2 – 2 P_{st}
7.0 Power frequency variations	-	< 10 s	± 0.10 Hz

1.3 The Cost of Poor Power Quality

As more and more fossil fuel power generating plants are built all over the world to cater for the increasing electricity demand, the already alarming pollution problem is even worsened. For instance, in 2009, fossil fuel (e.g. Coal, Oil and Gas) power plants accounted for 65% of global electricity generation [6]. They are identified as a major source of air pollution in many cities. Poor air quality has led to various respiratory diseases, which incurs huge medical expenses and financial burdens to many countries. The trend of global electricity demand has suggested that the global electricity demand is unlikely to cut back in the coming years; hence, maximizing energy efficiencies of

electric power systems are definitely essential to mitigate the worsening living environment of our society.

Compared to efficiency, the reliability of an electric power system is usually more concerned by end-users, as their consequences are much more visible and direct. Even though electric power interruptions are costly for the society, it is rarely happened (e.g. perhaps once a year) especially in developed countries.

In contrast to electric power interruption, many surveys have already found that even a small voltage disturbance lasting less than a second (e.g. voltage sag) can be very costly. Despite the voltage supply is recovered rapidly, these undesired disturbances can lead to unpredictable behavior of electric equipment (e.g. motor stall, computer restart). These unpredictable behaviors can cascade to entire production systems, where downtime and material loss can be very costly. Table 1.2 shows a survey which is done by the European Copper Institute in 2001 [7], estimating typical financial loss due to power quality incident.

Table 1.2
Typical financial loss due to power quality incident (2001) [7]

Industry	Typical financial loss per event (euro)
Semiconductor production	€3,800,000
Financial trading	€6,000,000 per hour
Computer centre	€750,000
Telecommunications	€30,000 per minute
Steel works	€350,000
Glass industry	€250,000

Moreover, studies have found that poor power quality can lead to various unexpected expenses. Besides damaging equipment directly, harmonics can raise equipment operational temperature and eventually shorten their life expectancy. Furthermore, the poor power quality may lead to unexpected installation cost, such as oversized cables, dynamic voltage restorer (DVR) and even uninterruptible power supply (UPS), for reliability reinforcement.

1.4 Power Quality Monitoring and Analysis

Traditionally electricity meters were mainly used to record energy consumption (e.g. kWh). The meters are usually electromechanical meters (or so called watt-hour meters), which can record only total energy consumed. Remote communication is rarely available in these meters; hence, electric power companies have to read their meters manually for billings. Nevertheless, they are still the most common electricity meters found in residential buildings these days.

With the advance in reliability and capability of solid-state devices, solid-state electricity meters are becoming more and more popular. Currently, they are mostly utilized in crucial locations for monitoring and diagnosing. Besides total energy consumption, they are able to measure and record other electric power quantities, such as reactive power, harmonics distortion and power factor, in complying with various electric power quality measurement standards like IEC 61000-4-7 [1], IEC 61000-4-30 [2] and IEEE 1159 [3]. Moreover, many of these meters (e.g. smart meters) are now integrated with communication (e.g. Zigbee) and storage functions to realize remote data access (e.g. Automatic Meter Reading (AMR)).

1.4.1 Power Quality Measurement and Waveform Capturing

The electric power quantities measured by electricity meters are usually represented in numerical-based parameters, which are either accumulated or averaged value. Kilo-Watt hour (kWh) is a typical example of accumulated measurement representing total energy consumption. On the other hand, active power (kW), power factor (p.f.) and total harmonic distortion (THD) are usually averaged and recorded in a fixed interval (e.g. 15 minutes). These kinds of parameters are very useful in steady state analysis. However, neither of these parameters is suitable for identifying and analyzing disturbances (e.g. transients) in electric power systems, as their time information is diminished (e.g. averaged).

Identifying and analyzing non-steady state events in electric power systems often require raw samples on voltage and current waveforms as mentioned in IEC 61000-4-30 [2]. Nevertheless, raw sampling equipment for long term (e.g. hours) monitoring are usually very expensive, as they require massive computer memory to preserve samples, and also

huge networking bandwidth for remote monitoring. Hence, they are usually installed for temporary (e.g. hours) and local diagnosis only.

1.4.2 Electric Power Disturbance Identification and Classification

Identifying disturbances in an electric power system are useful for diagnostics and power quality improvements. Through visual inspection on a captured waveform, electrical engineers can identify and classify disturbances easily. Nevertheless, manual inspection on captured waveforms is an enormous task. It is inefficient and almost impossible as data are sampling from the electric power systems continuously.

So far researchers have developed various methods to automate disturbance identification and classification. Many methods are based on various time-frequency analysis (e.g. Wavelet, S- Transform) and artificial intelligences (e.g. neural network) to extract features and classify disturbances in voltage waveforms. On the other hand, as current is time-varying and load-dependent; hence, identifying disturbances in current are more challenging and less obvious. Nevertheless, it is useful for locating the problems and identifying small disturbances in the electric power system.

1.4.3 Harmonics and Disturbance Analysis

Traditionally, Discrete Fourier Transform (DFT) has been employed for harmonics analysis in electric power systems. It is well-known that DFT is only suitable for steady state analysis and would produce significant errors in the presence of non-integer harmonics, sub-harmonics and time-variant harmonics. Studies have already confirmed that Discrete Wavelet Packet Transform (DWPT) can outperform DFT for time-varying harmonics analysis in electric power systems. With time information is preserved, it is more suitable for disturbance analysis (e.g. transient) comparing to DFT. Nevertheless, some research results also illustrated that DWPT suffers a non-uniform leakage problem [4] which causes errors in some orders of harmonics.

1.5 Objectives of the Study

This research study is aimed at investigating into a novel electric power monitoring system that is capable of monitoring and analyzing transients in electric power systems. Three main objectives are included.

Raw sample capturing is a key to analyze transients or non-steady state events in electric power systems as mentioned in IEC 61000-4-30 [2]. Yet, traditional equipment is either unsuitable for long-term monitoring (e.g. oscilloscope) or in needs of massive memory storage. Therefore, the first objective of this study is to develop a novel power quality meter with an electric waveform compression algorithm. The meter is aimed at reducing storage requirement for continuous waveform capturing and realizing real-time electric waveform monitoring on low-speed communication networks (e.g. Zigbee).

The second objective of the research study is to investigate into a disturbance identification algorithm to relieve electrical engineers from manual inspections. In order to maximize computational efficiency, the disturbance identification algorithm is to be integrated with the proposed compression algorithm mentioned above. Data and processes are aimed to be shared and reused by both algorithms.

Once disturbances are identified, further analysis should be carried out. Hence, the third objective of the research study is to enhance the existing method for time-varying harmonics and disturbance analysis. It is targeted to overcome a non-uniform leakage problem in DWPT for harmonics analysis. Furthermore, it is aimed to provide a more detailed analysis for various kinds of electric power disturbances (e.g. voltage flickering, frequency variation and transient).

1.6 Organization of the Thesis

Findings of the research study are summarized in this thesis, which consists of six chapters.

Chapter 2 briefly reviews existing technologies related to this thesis. Firstly, three important mathematical tools are reviewed. They are Fourier transform, Hilbert transform, and Wavelet transform. Thereafter, existing methods for electric power monitoring and analysis are discussed.

Chapter 3 presents three novel methods – the waveform compression algorithm, the disturbances identification algorithm and the analysis method, which are proposed for addressing the three objectives of this thesis respectively.

Chapter 4 illustrates a prototype electric power monitoring system integrated with the three proposed methods of Chapter 3. The prototype meter and the central monitoring system of the prototype electric power monitoring system are introduced.

Chapter 5 evaluates feasibilities and performances of the three proposed methods. Using the prototype monitoring system in Chapter 4, different tests are designed and performed for the proposed methods.

Finally, Chapter 6 summarizes work done in the research study.

Chapter 2

Review of Existing Technologies

2.1 Introduction

As Fourier transform, Hilbert transform and Wavelet transform are to be involved in many parts of this thesis, this review chapter begins with a short review of these transforms for completeness of the thesis. Thereafter, existing monitoring and analyzing methods of electric power quality related to the thesis are reviewed in the later sections of this chapter.

2.2 Review of Fourier Transform, Hilbert Transform and Wavelet Transform

In analyses of electric power quality, mathematical tools related to frequency transformation have been widely used in these days. They are useful in transforming a time domain signal (e.g. raw sample of voltage) into frequency components or bands for distortion analysis of voltages and currents in electric power system. These transforms have different characteristics with respective advantages and limitations. For example, it is well-known that Fourier Transform is more useful in steady-state analysis than transient analysis. On the other hand, Wavelet Transform is useful in analyzing time-frequency characteristics of disturbed voltages and currents.

2.2.1 Fourier Transform

Fourier transform has been the most popular analytical tool for frequency analysis in many areas, especially in physics and engineering [8 - 9]. It decomposes and represents a signal in a summation of sine and cosine functions. Fourier transform has four family members – (Continuous) Fourier transform, Fourier series, Discrete-time Fourier transform and Discrete Fourier transform. They are derived from Fourier transform to handle either a continuous or discrete signal, and also it can be either periodic or aperiodic. Discrete Fourier transform (DFT) is the most important one for practical

applications. It is widely used for harmonic analysis in electric power systems. Thus, only the Discrete Fourier Transform is discussed here.

2.2.1.1 Discrete Fourier Transform

DFT is defined as:

$$X[k] = \sum_{n=0}^{N-1} x[n] \cdot e^{-\frac{2 \cdot \pi \cdot i}{N} \cdot k \cdot n}, k = 0, 1, 2, \dots, N-1 \quad (2.1)$$

where *N* is length of the signal *x*.

In the family of Fourier Transform, DFT is derived to handle discrete and periodic signal. It transforms a finite sequence of sampled data (*x[n]*), either complex number or real number, into a finite sequence of complex sinusoids (*X[k]*) ordered by their frequencies.

In an electric power system, DFT is often utilized to transform the sampled voltage and current waveform into frequency domain for harmonic analysis. The obtained complex sinusoids are then utilized to compute the amplitude and phase of individual frequency by equations (2.2) and (2.3) respectively. Once the amplitudes and phases are obtained, they are employed to calculate various parameters such as Total Harmonic Distortion (THD).

$$|X[k]| = \sqrt{Re(X[k])^2 + Im(X[k])^2} \quad (2.2)$$

$$\theta(X[k]) = tan^{-1} \frac{Im(X[k])}{Re(X[k])} \quad (2.3)$$

Furthermore, fast Fourier Transform (FFT) is extensively used to compute DFT. FFT is a unified name referring to various fast numerical algorithms (e.g. Cooley-Tukey algorithm) for DFT. Instead of computing (2.1) iteratively, these algorithms reduce DFT's complexity from $\mathrm{O}(\mathrm{N}^2)$ to $\mathrm{O}(\mathrm{N} \log_2 \mathrm{N})$ with the same outcomes, making it easier to implement in many application systems.

2.2.1.2 Examples

Two distinctive examples of DFT are shown in (2.4) and (2.5). Theoretically, when a supply voltage is perfectly sinusoidal, only two symmetric impulses will appear in frequency domain as in (2.4). On the other hand, impulse (e.g. transient) in time domain spreads to a constant in frequency domain as in (2.5).

DFT of cosine function:

$$\mathrm{DFT}\left\{\cos\left(2\pi \times \mathrm{M} \times \frac{\mathrm{n}}{\mathrm{N}}\right)\right\} = \frac{\mathrm{N}}{2}\left[\delta[\mathrm{k}-\mathrm{M}] + \delta[\mathrm{k}+\mathrm{M}]\right] \tag{2.4}$$

DFT of impulse function $\delta[n]$:

$$\mathrm{DFT}\{\delta[\mathrm{n}]\} = 1, \quad \delta[\mathrm{n}] = \begin{cases} 0, & \mathrm{n} \neq 0 \\ 1, & \mathrm{n} = 1 \end{cases} \tag{2.5}$$

2.2.2 Hilbert Transform

Hilbert transform (HT) [9 - 10] is a time-invariant and linear transform, defined as

$$\mathrm{y}(\mathrm{t}) = \mathrm{H}[\mathrm{x}(\mathrm{t})] = \frac{1}{\pi}\,\mathrm{p.v.}\int_{-\infty}^{\infty}\frac{\mathrm{x}(\tau)}{\mathrm{t}-\tau}\mathrm{d}\tau\,, \tag{2.6}$$

where p.v. represents the Cauchy principal value.

It convolutes a signal $\mathrm{x}(\mathrm{t})$ with $1/\pi\mathrm{t}$, and shifts each frequency component of $\mathrm{x}(\mathrm{t})$ by 90^{o}. HT is related to Fourier Transform as shown in (2.7), and can be computed by DFT.

$$\mathrm{Y}(\omega) = \mathcal{F}\left[\mathrm{H}[\mathrm{x}(\mathrm{t})]\right] = -\mathrm{j}\cdot\mathrm{sgn}(\omega)\cdot\mathrm{X}(\omega)\,. \tag{2.7}$$

2.2.2.1 Analytic Signal

HT can convent a signal $\mathrm{x}(\mathrm{t})$ into an analytic signal $\mathrm{z}(\mathrm{t})$, which is useful to obtain instantaneous amplitudes, phases and frequencies for monotone $\mathrm{x}(\mathrm{t})$ signal [10]. The

analytic signal $z(t)$ is formed by simply putting the transformed signal $y(t)$ as an imaginary part of the original signal $x(t)$,

$$z(t) = x(t) + j \cdot y(t) \tag{2.8}$$

where $y(t)$ is the transformed $x(t)$ as in (2.6).

2.2.2.2 Instantaneous Amplitude, Phase and Frequency

Through the analytic signal (2.8), the instantaneous amplitude and phase of $x(t)$ can be obtained,

$$z(t) = a(t) \cdot e^{j\theta(t)}, \tag{2.9}$$

where $a(t) = \sqrt{x(t)^2 + y(t)^2}$ and $\theta(t) = \tan^{-1}\frac{y(t)}{x(t)}$, by Euler's formula.

Furthermore, the instantaneous (angular) frequency $\omega(t)$ can also be obtained by

$$\omega(t) = \frac{d\theta(t)}{dt}. \tag{2.10}$$

Its instantaneous amplitude $a(t)$ and phase $\theta(t)$ are very useful for monotone signal analysis, yet it is not suitable for a signal with multiple frequencies. An example of monotone and multiple frequencies signal is shown below.

2.2.2.3 Example - Monotone

Let $x(t)$ be defined as

$$x(t) = \cos(\omega t + \alpha), \tag{2.11}$$

Its HT gives

$$y(t) = \cos(\omega t + \alpha + 90^{o}) = \sin(\omega t + \alpha). \tag{2.12}$$

From (3.8) and (3.9), its analytic signal is

$$z(t) = \cos(\omega t + \alpha) + j \cdot \sin(\omega t + \alpha) = e^{j(\omega t+\alpha)}, \tag{2.13}$$

where its instantaneous amplitude $a(t) = 1$ and phase $\theta(t) = \omega t + \alpha$.

2.2.2.4 Example - Multiple Frequencies

If a signal $x(t)$ contains more than one frequency components, say,

$$x(t) = \cos(\omega t) + \cos(2\omega t), \tag{2.14}$$

from (2.8) and (2.9), its instantaneous amplitude is

$$a(t) = \sqrt{(\cos(\omega t) + \cos(2\omega t))^2 + (\sin(\omega t) + \sin(2\omega t))^2} \tag{2.15}$$

The computed instantaneous amplitude $a(t)$ in (2.15) contains both frequency components. Hence, the instantaneous amplitude $a(t)$ and phase $\theta(t)$ of individual frequency component cannot be estimated.

2.2.2.5 Application - Frequency Shifting

Moreover, HT can be used for shifting frequency components in a signal, commonly known as single side-band modulation [11]. Frequency shifting is accomplished by multiplying $e^{j\omega_1 t}$ to the analytic signal, in which ω_1 is the frequency shift in the spectrum. The shifted signal is obtained readily from the real part of the signal as

. $$s_{\omega_1}(t) = \mathrm{Re}\left((x(t) + j \cdot H[x(t)]) \cdot e^{j\omega_1 t}\right). \tag{2.16}$$

As $e^{j\omega_1 t}$ shifts the whole spectrum by ω_1, including both the negative and positive frequency as in (2.17), it creates a new redundant frequency component in time domain,

$$\mathcal{F}\left[\cos(\omega_0 t) \cdot e^{j\omega_1 t}\right](\omega) = \int_{-\infty}^{\infty} \left(\frac{e^{j(\omega_0+\omega_1)t} + e^{-j(\omega_0-\omega_1)t}}{2}\right) e^{-j\omega t} dt$$

$$= \frac{1}{2}[\delta(\omega - \omega_0 - \omega_1) + \delta(\omega + \omega_0 - \omega_1)]. \tag{2.17}$$

The analytic signal helps to remove the negative frequency component and thus the redundant frequency will not be produced as in (2.18).

$$\mathcal{F}\left[(\cos(\omega_0 t) + \mathrm{j}\cdot\sin(\omega_0 t))\cdot e^{\mathrm{j}\omega_1 t}\right](\omega)$$

$$= \int_{-\infty}^{\infty} e^{\mathrm{j}(\omega_0+\omega_1)t} e^{-\mathrm{j}\omega t} dt = \delta(\omega - \omega_0 - \omega_1). \quad (2.18)$$

Hence,

$$s_{\omega_1}(t) = \mathrm{Re}[(\cos\omega_0 t + \mathrm{j}\cdot\sin\omega_0 t)\cdot e^{\mathrm{j}\omega_1 t}] = \cos\big((\omega_0+\omega_1)t\big). \quad (2.19)$$

2.2.3 Wavelet Transform

Wavelet transform (WT) is commonly regarded as a time-frequency transform. Instead of transforming signals to frequency domain entirely like the Fourier transform, the time-frequency transform, such as wavelet, take a balance between time and frequency. It retains partial time information on one hand, and supplies partial frequency information on the other hand. Similar to uncertainty principle, time and frequency information are limited by each other, both cannot be obtained precisely [12].

Despite this limitation, WT is very useful for analyzing non-stationary signals, and is widely adopted for power disturbance analysis (e.g. transient) in these days. A variety of Wavelet transforms is derived by mathematicians, and mainly classified into two categories – continuous and discrete. Since the continuous Wavelet transform will not be involved in this thesis, only Discrete Wavelet transform (DWT) is discussed below.

2.2.3.1 Discrete Wavelet Transform (DWT)

DWT is an orthonormal transform that dilates an orthogonal wavelet by a factor of 2 and translates a finite sequence into multi-resolutions from fine to coarse levels [12]. It is commonly implemented by a pair of conjugate mirror filters and the output sequence is down-sampled. Thus a sequence with N coefficients is decomposed into two sequences with N/2 coefficients in each level. This is done by down-sampling the output of the high-pass filter (wavelet filter, g[n]) and the low-pass filter (scaling filter, h[n]). Its

output coefficients are called wavelet coefficients (d_{j+1}) and approximation coefficients (a_{j+1}), defined as

$$d_{j+1}[n] = \sum_{m=-\infty}^{+\infty} a_j[n]g[2n - m], \tag{2.20}$$

$$a_{j+1}[n] = \sum_{m=-\infty}^{+\infty} a_j[n]h[2n - m]. \tag{2.21}$$

The approximation coefficients at a given level can be further decomposed in the next level to form a hierarchical structure. Thus, a sampled signal x[n] can be decomposed into several frequency bands, as in Fig. 2.1.

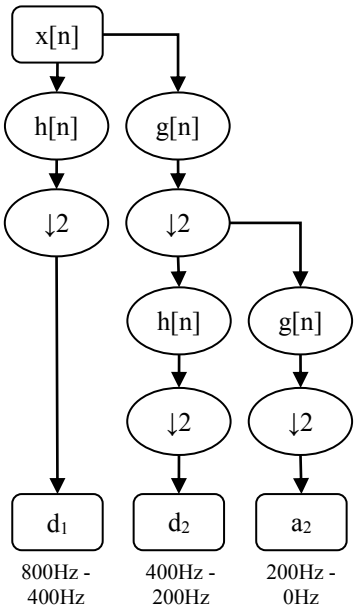

Fig. 2.1 Flowchart of Discrete Wavelet Transform

2.2.3.2 Integer-to-integer mapping via Lifting Scheme

Practically, the DWT filters (g[n] and h[n]) are usually implemented in sequences of floating-point numbers, which is the same as the Finite Impulse Response (FIR) filter. Hence, their outputs (e.g. d_1, d_2, a_2) are also bounded to be floating-point numbers. For data compression, floating-point numbers are not always desirable, as their data sizes are usually bigger compared to integers. Moreover, their computational time are longer, and

they are more likely to introduce rounding-off error during calculation. It spoils both compression ratio (CR) and signal-to-noise ratio (SNR).

Integer-to integer mapping is a desired property for data compression, especially when the raw data is in integer. For instance, the data retrieved from an analog-to-digital converter is always integers. Hence, the Lifting Wavelet Transform (LWT) derived from DWT is introduced [13]. LWT factorizes the DWT filters (g[n] and h[n]) into a sequence of steps[14]. Those factorized steps form a ladder structure similar to Fig. 2.2.

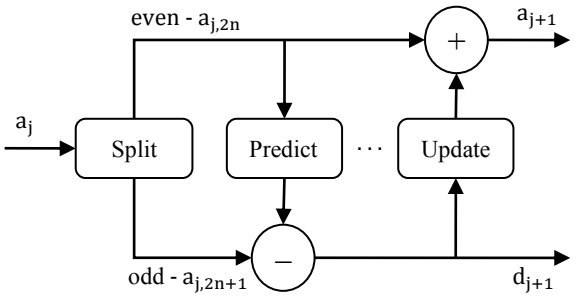

Fig. 2.2 A ladder structure of the Lifting Discrete Wavelet Transform

The coefficients (a_j) representing sampled signal are first split into two parts – even samples and odd samples. They are then fed into a series of filtering steps, so called 'Prediction' and 'Update', to produce the wavelet coefficient (d_{j+1}) and the approximate coefficient (a_{j+1}), as in (2.20) and (2.21). Moreover, these filtering steps reduce the computation complexity of the transform by a factor of two asymptotically, making it very suitable for implementation on small-scale embedded system.

According to [13], a Lifting Scheme based on the Daubechies-4 wavelet is formulated as in (2.22) - (2.24), where (2.22) and (2.24) are prediction steps, (2.23) is an update step.

$$d_{j+1,n}^{(1)} = a_{j,2n+1} - \sqrt{3}a_{j,2n} \tag{2.22}$$

$$a_{j+1,n} = a_{j,2n} + \frac{\sqrt{3}}{4}d_{j+1,n}^{(1)} + \frac{\sqrt{3}-2}{4}d_{j+1,n+1}^{(1)} \tag{2.23}$$

$$d_{j+1,n} = d_{j+1,n}^{(1)} - a_{j+1,n+1} \tag{2.24}$$

Once the finite filter is factorized into lifting steps, the wavelet can be customized by modifying the steps in the algorithm. A LWT that maps an integer input to an integer wavelet coefficient output can be implemented by rounding off the result in each steps of the ladder, as stated in [15]. An example for Daubechies-4 wavelet is formulated in (2.25) to (2.27). In these steps, the real numbers (or terms) are rounding off into integers, such as $\lfloor \sqrt{3} a_{j,2n} + 1/2 \rfloor$ in (2.25). The transform can be fully reversible by simply reversing all steps.

$$d^{(1)}_{j+1,n} = a_{j,2n+1} - \left\lfloor \sqrt{3} a_{j,2n} + \frac{1}{2} \right\rfloor \tag{2.25}$$

$$a_{j+1,n} = a_{j,2n} + \left\lfloor \frac{\sqrt{3}}{4} a^{(1)}_{j+1,n} + \frac{\sqrt{3}-2}{4} a^{(1)}_{j+1,n+1} + \frac{1}{2} \right\rfloor \tag{2.26}$$

$$d_{j+1,n} = d^{(1)}_{j+1,n} - a_{j+1,n+1} \tag{2.27}$$

2.3 Review of Electric Power Quality Monitoring and Analysis Methods

There are numerous methods for electric power quality monitoring and analysis. This section will only review existing methods related to the three objectives of this thesis. In order to focus on each objective, this section is divided into three parts respectively. Firstly, it will discuss limitations of existing measurement methods of electric power quality. Secondly, it will briefly review existing identification methods for electric power disturbances. Thirdly, it will review some common time-frequency methods for electric power quality analysis and will discuss the non-uniform leakage problem of DWPT.

2.3.1 Measurement of Electric Power Quality

Electricity meters are widely used in measuring electric power quantities on electric power systems. In the past, electricity meters were mostly electromechanical. They are embedded with a rotating disk, which is driven by magnetic forces generated from currents flowing through. They record only total energy consumption via counting disk revolution mechanically.

Solid-state electricity meters are very popular nowadays. They are commonly used in accessing electric power quality in crucial locations of electric power systems. Besides

total energy consumption, they are capable of measuring and recoding voltage, current, active power, reactive power, power factor and even harmonic distortion [1-3].

In general, the measurement results and records of these electric power quantities are represented in numerical-based parameters, which are either accumulated or averaged. For instance, the total energy consumption is often accumulated in a single parameter (e.g. kilo-Watt hour), while the others are usually averaged and recorded in a periodic interval (e.g. 15 minutes per record) [2].

Using these measurement records, electrical engineers are able to identify the status of electric power systems in different periods of time (e.g. summer, weekdays, afternoon), which is very useful for efficiency and reliability improvement. For example, it is beneficial to schedule generators for various demand patterns and also identify poor power quality source in distribution networks.

2.3.1.1 Problems of Existing Measurement Methods

The measurement results of existing electricity meters are indeed useful in steady-state power quality analysis; however, these measurement results are not able to identify and analyze non-steady state events (e.g. transient) in electric power systems. The non-steady state events are usually short in duration comparing with the measurement periods of the electricity meters. Hence, these events cannot be represented by the averaged measurement results of electricity meters. An example is shown in Fig 2.3. The voltage transient in Fig. 2.3(b) at 0.1 second makes this waveform different from the waveform in Fig 2.3(a). Except at 0.1 second, their voltages are same. For electricity meters, the measured results are 220.00 Vrms and 220.08 Vrms respectively. Their difference is only 0.08 V. Both voltages are within the limit of the voltage regulation (e.g. ±5% of nominal voltage); hence, the transient voltage in Fig. 2.3(b) is not observable from the measurement of the electricity meters.

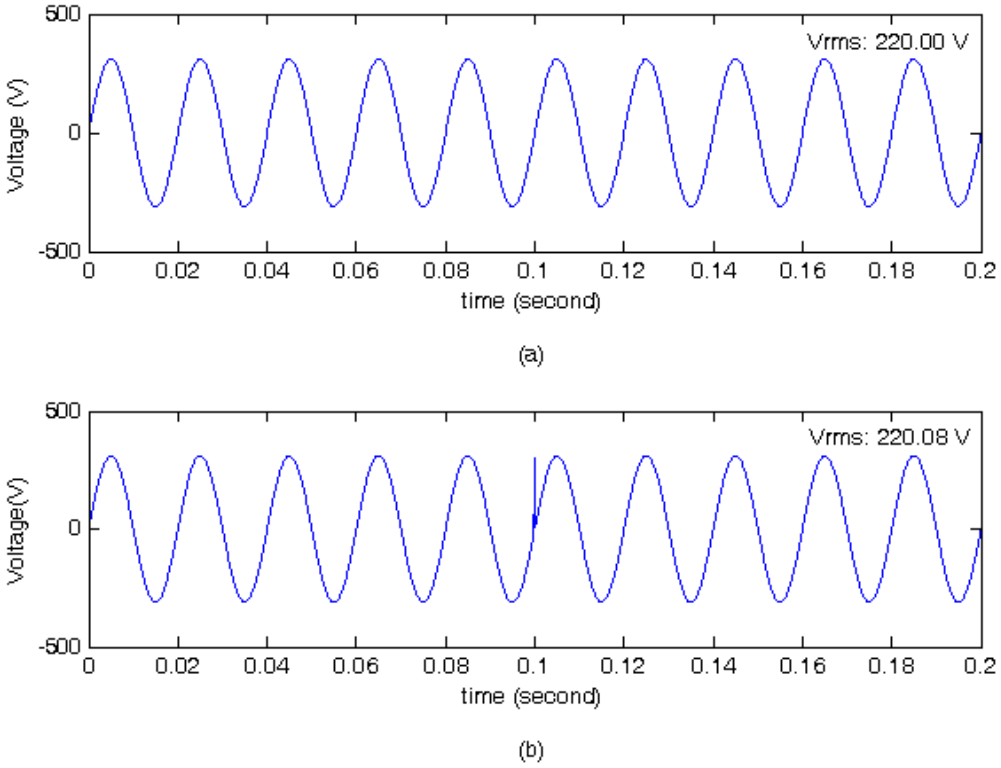

Fig. 2.3 (a) A normal voltage waveform, (b) A transient voltage waveform

Non-steady events, such as the transient in Fig. 2.3(b), are known as disturbances of electric power systems. Even though they only occur occasionally and are short in duration (e.g. 0.01 second), these disturbances may lead to device damage and malfunction, which can be catastrophic (e.g. fire). They are always serious threats to reliability of electric power systems.

In order to evaluate electric power qualities of non-steady state events, waveforms of voltage and current are always preferred as suggested in IEC 61000-4-30 [2]. The waveforms are able to retain the most fundamental information, especially time information, for non-steady state events. Preserving the waveforms allow non-steady state events to be further analyzed using various methods (e.g. Wavelet transform). They are more flexible for post-processing comparing to averaged measurement results of electricity meters.

On the other hand, recording waveforms require a huge amount of storage for data preservation and huge networking bandwidth for remote monitoring. Hence, the

equipment (e.g. oscilloscope) is usually expensive and inconvenient for remote monitoring. They are usually used for temporary local diagnosis in trouble-shooting. In many cases, they are deployed only after a disturbing problem has happened repeatedly for a long period of time.

2.3.2 Identification of Electric Power Disturbances

Electric power disturbances (e.g. transient) are undesirable events in electric power systems. They threaten not only systems' reliability, but also equipment in electric power systems. A considerable number of equipment are damaged and malfunctioned every year due to electric power disturbances [7, 25 - 27].

In many scenarios, disturbances in electric power systems can be avoided, or their resultant damages can be limited by doing some modifications or enhancements to the electric circuits (e.g. changing cable size, parts replacement, and surge protection). Nevertheless, an electric power system consists of two parties – demand and supply. While the demand is dependent upon end-users, the supply is dependent upon electricity companies. In general, the electric circuits are maintained and operated by the electricity companies. On the other hand, demands of end-users are changing over time. Existing electric circuits may become inadequate, once more electric loads are installed or replaced by the end-users. Hence, electric circuits require inspections, maintenance and renovation from time to time.

Before modifications or enhancements are made in electric circuits, problems of the electric circuits must be identified and located in the first place. Thus, identifying disturbances in electric circuits are essentially the first step for improvements of electric power systems.

In recent years, renewable energy sources are plugged into the electric power system intensively. Their utilizations have made disturbance identification in electric power system even more important than before. Renewable energy resources have been penetrating into various levels of electric power distribution system. Depending on scale, their energy collectors (e.g. solar panel, wind turbine) can be found in many places, such as power stations or even on our building roof-tops. While their utilizations are increasing exponentially, they have led many unexpected disturbances in electric power systems as

well [16, 17]. These unexpected disturbances are usually related to instabilities of renewable energy sources (e.g. wind speed, sun radiation) [28]. As a result, disturbance identification has becoming more important, and it is the very tasks of electrical engineers and researchers to improve the reliability of electric power systems.

2.3.2.1 Existing Disturbance Identification Methods

Disturbances in electric power systems are usually classified into a few common categories (e.g. sag, swell, transient) with different features in terms of magnitude, duration and spectral contents as shown in Table 1.1. Through inspecting voltage and current waveforms, their distinctive features can be easily identified by electrical engineers. However, manually identifying disturbances is an inefficient task. It is impossible for real-time monitoring too. Fifty (or sixty) cycles of voltage and current waveforms are captured in a second. It is difficult for engineers to process the waveforms in this speed by visual inspection.

Hence, various methods are proposed by researchers to identify disturbance automatically. Time-frequency transforms, such as Wavelet transform [11] and S-transform [29], have been widely adopted to be part of the disturbance identification process [30]-[36]. Compared to Fourier transform, these transforms take balance between time and frequency information, which is more effective for analyzing and locating the non-stationary components (e.g. transient) in the waveforms.

Since time-frequency transform itself does not provide identification results, additional algorithms are required to interpret the result. Artificial Neural Network (ANN) [37] is by far the most popular one. Results of the time-frequency transform are usually concise into a set of parameters via statistical means (e.g. standard derivation, mean value), and then passed to ANN for disturbance classification [31]-[36]. Accuracy of these methods is reported to be fairly good. Some methods can achieve a classification accuracy of 90% or more in simulation. Fig 2.4 shows a common workflow of a disturbance identification algorithm

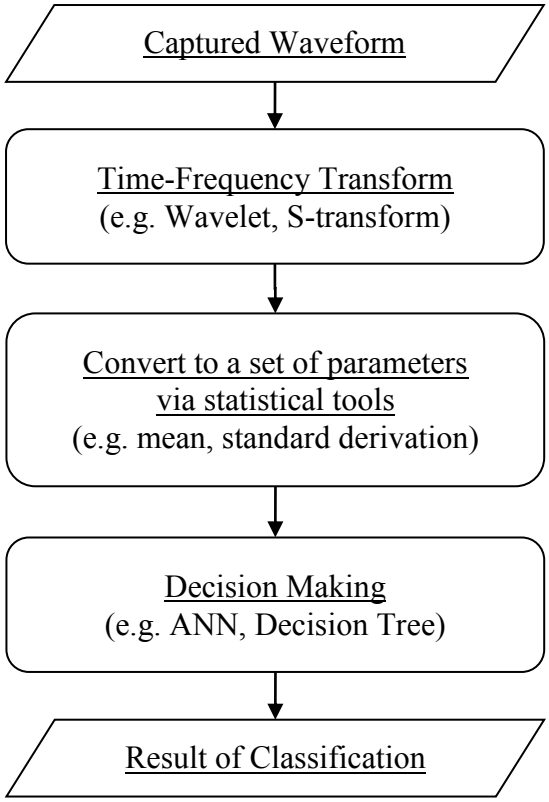

Fig. 2.4 Flowchart of a typical disturbance identification algorithm

So far existing methods are mainly focused on voltage disturbances identification. They are not suitable to identify current disturbances. In contrast to voltage disturbances, current disturbances are more difficult to be identified. Normally, voltages of electric power systems are sinusoidal and set at a standard amplitude (e.g. 220 / 110 V) and frequency (e.g. 50 / 60 Hz). The variation of the supplied voltage is usually less than 10%. On the other hand, currents of electric power systems are completely determined by users' apparatus. The currents are varying arbitrarily from time to time dependent on operation the status of the apparatus. Without a standard pattern for comparison, current disturbances are more challenging to be identified automatically than voltage disturbances. Decisions are more difficult to be made by ANNs or other decision making methods.

Nevertheless, it is known that problems of electric power systems can be arisen from current disturbances. Causes of the current disturbances are usually related to operation changes of electric equipment (e.g. inrush current of electric apparatus, impulse current of thyristor devices and harmonic current of electronic devices). The current disturbances

can overload or even destabilize (e.g. oscillation) the electric power systems. Eventually, electricity supplies are interrupted unexpectedly (e.g. tripping of circuit breaker). In many situation, these unexpected interruptions of electricity supplies do not happen frequently; thus, the current disturbances are usually overlooked and regarded as unknown behaviors or events of the electric power systems. As a result, the reliability of the electric power systems are lowered. If current disturbances can be identified automatically, it will definitely help to identify and solve the problems of electric power system more rapidly in the future [38].

2.3.3 Analysis of Electric Power Quality

Throughout the years, various analysis techniques have been applied in dealing with power quality problems for electric power systems. Fourier transform (FT) is the most popular technique for harmonic analysis in electric power systems. FT is well suited for steady state analysis. On the other hand, time-frequency transforms are always preferred for disturbance or non-steady state analysis [12]. There are many time-frequency transforms, such as Wavelet transform [12], S-transform [39], Gabor transform [40], Wigner distribution function [41], Gabor-Wigner transform [42] and Hilbert-Huang transform [43 - 45]. Wavelet based transforms have drawn many attentions in past decades. They have been utilized to analyze electric power quality in many studies [46 - 68]. In this section, only Discrete Wavelet Packet Transform (DWPT) and the non-uniform leakage problem of DWPT, which are related to the thesis, will be discussed.

2.3.3.1 Discrete Wavelet Packet Transform (DWPT)

DWPT is an extension of the Discrete Wavelet transform (DWT). Generalizing from DWT as in Fig. 2.1, DWPT decomposes both detail coefficients and approximation coefficients in each stage as in Fig. 2.5.

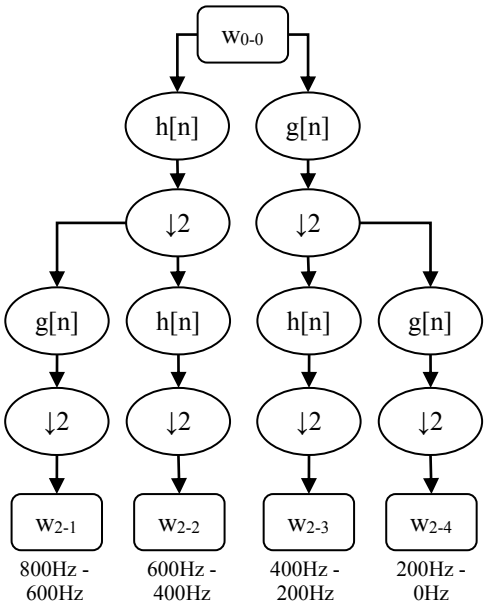

Fig. 2.5 Flowchart of Discrete Wavelet Package Transform

DWPT is a popular time-frequency transform for electric power quality analysis. It has been widely applied to decompose disturbance for ANN-based disturbance identification [31]-[36]. Moreover, some researchers also found that DWPT can outperform the FT in some particular cases. They proved that DWPT is capable of analyzing the sub-harmonics, the inter-harmonics, and also the non-steady state harmonics in electric power systems more accurately. Thus, DWPT is also used to calculate traditional power quantities such as root-mean-square (RMS) values and total harmonic distortion (THD) [4, 52 - 62].

2.3.3.2 Non-Uniform Spectra Leakage

DWPT is capable of separating a signal into multiple frequency bands evenly. For example, a signal of 800 Hz bandwidth is divided into four 200 Hz frequency bands after 2 levels of DWPT decomposition as illustrated in Fig. 2.5. In electrical engineering, DWPT is applied to waveforms of voltage and current. Those decomposed frequency bands are often utilized for harmonics and power quality analysis in an electric power system [57 - 60]. Nevertheless, researchers in [4] noted that DWPT exhibits varying spectra leakages in each frequency bands due to differences in transition length. The leakages are especially evident for the frequency bands in centre of the spectrum. Fig. 2.6 shows an example frequency spectrum decomposed by DWPT [4]. Totally, 16

frequency bands in 50 Hz bandwidth are decomposed. While the frequency bands at the two sides suffer the least, the leakage problems in the center are especially obvious.

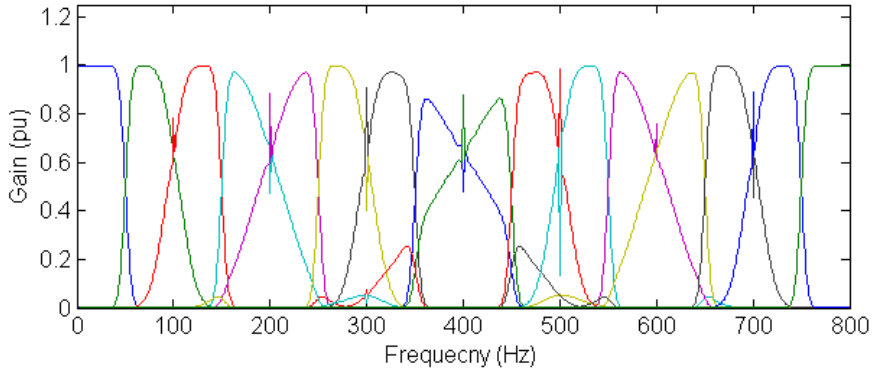

Fig. 2.6 Frequency bands of the DWPT

Their non-uniform transition lengths are caused by the hierarchy structure, the wavelet filters (g[n] and h[n]), and the down-sampling process in DWPT. As the same filters (g[n] and h[n]) are applied throughout the entire DWPT but only the frequency spectrum is halved via the down-sampling in each level, the transition length of filters (g[n] and h[n]) is halved in each level. Fig. 2.7 shows an example transition length of the 'db20' mother wavelet in the first and the second levels.

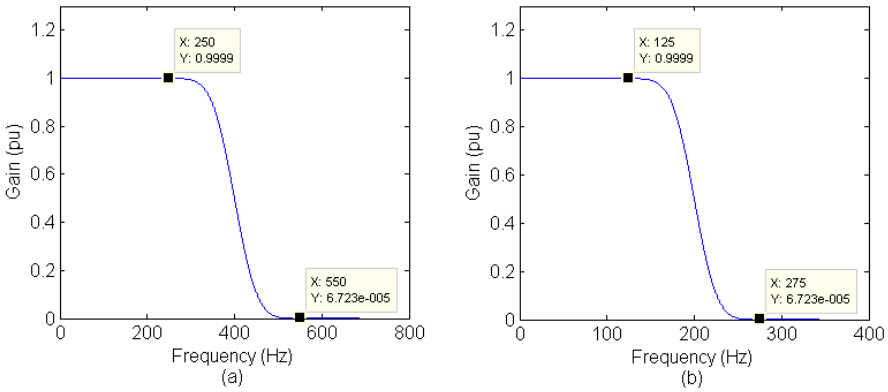

Fig. 2.7 Frequency response of the 'db20' filter h[n]: (a) Level 1; (b) Level 2

When a sampled waveform in 800 Hz bandwidth (sampling rate equal to 1600 Hz) is passed through the filter h[n] at level 1, the output contains the spectra from 0 Hz to 550 Hz (including transition length of 150 Hz). At level 2, the filters separate the signal into two bands. The first band (0 - 200 Hz) contains the spectra from 0 Hz to 275 Hz

(including a transition length of 75 Hz). The second band (200 - 400 Hz) contains the spectra from 125 Hz to 550 Hz (including a transition length of 75 Hz + 150 Hz). Thus, the non-uniform transition lengths of frequency bands are gradually formed during the filtering and the down-sampling process in each level.

As suggested in [57], this leakage problem can be minimized by merging the decomposed frequency band to make the harmonics components be located in the center of frequency band. The approach is illustrated in Fig. 2.8, in which a sampling frequency of 400 Hz must be selected to locate the 50 Hz, 100 Hz and 150 Hz component on the center of the merged frequency bands (2, 3 and 4). The approach relies on the selection of a proper sampling frequency, so that integer harmonics can be located in the center. However, it is inflexible to handle the inter-harmonics in this manner.

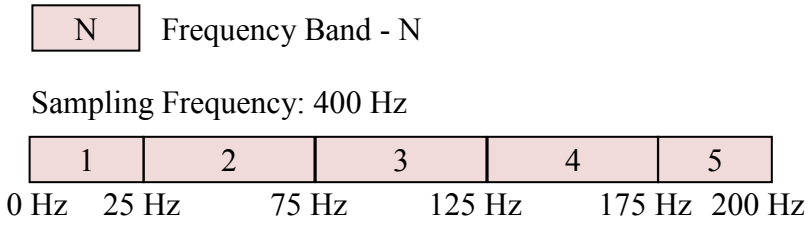

Fig. 2.8 Relationship between sampling frequency and integer harmonics [57]

Another approach suggested in [54] is to compensate the distortion caused by the filters. It can be very complicated when frequency components are already leaked to another frequency bands.

2.4 Summary

Three mathematical tools essential for the thesis are briefly reviewed in the first part of this chapter. The three mathematical tools are Fourier transform (FT), Hilbert transform (HT) and Wavelet transform (WT). Their salient properties and applications related to the thesis are discussed. FT is utilized to illustrate frequency properties of stationary and non-stationary signals. HT and its applications in analytic signal construction and frequency shifting are discussed. Discrete Wavelet transform (DWT) and Integer Lifting Wavelet transform (LWT) of WT's family are reviewed.

Furthermore, existing technologies for electric power quality monitoring and analyzing are briefly reviewed in the second part of this chapter. In respect to the three objectives of this thesis, methods and problems of existing electric power quality measurements are discussed. The importance of analyzing both voltage and current waveforms in electric power quality analysis is discussed. Secondly, existing methods for electric power disturbance identification are reviewed. Their limitations on current disturbance identification are discussed. Thirdly, Discrete Wavelet Packet transform (DWPT), a popular tool for electric power analysis, is reviewed. In the review, the non-uniform leakage problem of DWPT is discussed.

Chapter 3

Proposed Methods

3.1 Introduction

In this thesis, three methods are proposed to improve existing electric power monitoring systems. They are proposed for enhancing the capability of transient monitoring and analysis for existing electric power monitoring systems. Also, they are aimed at overcoming existing problems, which are discussed in previous chapters, and addressing the three objectives of this thesis respectively.

Firstly, a compression algorithm for voltage and current waveforms is proposed. It is specially designed to compress electric waveforms effectively. Stationary components of electric waveforms are extracted for enhancing compression ratio. It reduces memory storage requirement for continuous waveform recording. Furthermore, it is intended for applications in real-time electric power quality monitoring. It is aimed at realizing real-time electric waveform monitoring on low-speed communication networks (e.g. Zigbee).

Secondly, an identification algorithm for electric power disturbance is proposed. It identifies disturbances of electric power system from captured electric waveforms. It is capable of identifying disturbances in both voltage and current waveform. The identification algorithm is to be integrated with the compression algorithm. Their data and processes can be shared and reused to maximize computational efficiency of both algorithms.

Thirdly, an analysis method for time-varying harmonic and disturbance is proposed. It is aimed at analyzing harmonics and disturbances of electric power systems. Modified from Discrete Wavelet Packet transform (DWPT), the proposed method takes advantages of both Discrete Wavelet transform (DWT) and Hilbert transform (HT). It processes electric

waveforms in frequency shifting manner and decomposes the waveforms into multiple frequency bands for analysis. In contrast with DWPT, it suffers lesser problem of non-uniform spectra leakage, which is discussed in Section 2.3.3.2 of Chapter 2.

In this chapter, the three proposed methods – the compression algorithm (Section 3.2), the identification algorithm (Section 3.3) and the analysis method (Section 3.4) are presented in consecutive order. A prototype monitoring system is developed to evaluate feasibilities and performances of the proposed methods. Details of the prototype are presented in Chapter 4. Results of their feasibilities and performances under experiments and field tests are presented in Chapter 5.

3.2 The Proposed Waveform Compression Algorithm

The proposed compression algorithm is divided into two main stages. It presumes that electric waveforms are formed by two distinctive components – stationary and non-stationary as in (3.1). In the compression process, the two components are separated from the captured waveforms, and they are handled with different strategies.

The electric waveform is presumed as:

$$x[n] = s[n] + \varphi[n], \tag{3.1}$$

where $x[n]$ is the captured electric waveform; $s[n]$ is the stationary component; $\varphi[n]$ is the non-stationary (varying) components.

Ideally, the non-stationary component $\varphi[n]$ is preferred to be zero under normal situations, and it contains only variations (e.g. transients, pulses) caused by the electric power disturbances.

3.2.1 Modeling the stationary component

Following Fourier analysis, the proposed algorithm reduces data size by modeling the stationary component s[n] in a summation of cosine functions with various frequencies, amplitudes and phases, as

$$s[n] = \sum_m a_m \cos(2\pi n f_m + \theta_m), \quad (3.2)$$

where a_m, f_m and θ_m are frequency, amplitude and phase respectively; and m is the total number of sinusoidal components.

FFT is performed on the captured waveform to identify the parameters (a_m, f_m and θ_m). Although its frequency domain may contain both the stationary and non-stationary components, their distinctive features (discussed in Section 2.2.1.2) enable them to be clearly distinguished. Thus, while the non-stationary components spread widely in the frequency domain, only pulses in the frequency domain are recognized as the stationary components.

Once the parameters (a_m, f_m and θ_m) are identified, the stationary component f[n] are modeled and reconstructed as in (3.2). Any non-stationary component represented by φ[n] in (3.1) can be extracted readily.

3.2.2 Compressing the non-stationary component

In this stage, the stationary component is already separated from the captured waveform, and compressed into a few parameters. Lifting Discrete Wavelet Transform is then utilized to further reduce data size of the non-stationary component. Along with the integer to integer mapping (mentioned in Section 2.2.3.2), the non-stationary component is fully reversible after compression. Unlike traditional approaches, the wavelet coefficients are protected from precision loss during floating point computations.

3.2.2.1 Truncating Wavelet Coefficient by Adaptive Threshold

While lossless compression is unnecessary, or memory storage and transmission bandwidth are limited, the wavelet coefficients are truncated to further reduce data size. Yet, irreversible errors are inevitably introduced. Depending on the captured waveforms,

losses in vital features of electric power disturbance are sometimes unacceptable and should be avoided. Instead of applying constant thresholds [18 - 22], an adaptive scheme is introduced to truncate the wavelet coefficients selectively.

This adaptive scheme is derived from Otsu's method [23]. It allows vital features in electric waveforms to be located, and thus their wavelet coefficients can be chosen to be entirely preserved or truncated with smaller thresholds. Otsu's method is originally introduced for image processing. Based on pixel quantity in various intensity levels, it identifies an optimal threshold to separate an image into 'foreground' and 'background'. The optimal threshold is determined from maximum variances of foreground and background as

$$\text{optimal threshold } (k^*) = \max \{ \sigma_B^2(k) \}, \tag{3.3}$$

where $\sigma_B^2(k) = \omega_1(k)\omega_2(k)\big(\mu_1(k) - \mu_2(k)\big)^2$; k is the optimal threshold $= 1 \le k < L$; ω_n and μ_n are weights and means of foreground and background respectively; and L is the number of gray level.

In Otsu's method, it considers only the pixel intensity (amplitude) to classify a pixel into 'foreground' or 'background'. Since the amplitude change of the wavelet coefficient is also desired to be preserved in this application, the wavelet coefficients are modified to incorporate both amplitude and change (derivative), as in (3.4) for Otsu's method to classify the vital features.

The modified wavelet coefficient is given as,

$$m[n] = \sqrt{d_j[n]^2 - d_j'[n]^2}, \tag{3.4}$$

where $m[n]$ is the modified wavelet coefficients, and $d_j[n]$ and $d_j'[n]$ are the original wavelet coefficients and their first derivatives respectively.

Once Otsu's method has been used to determine the optimal threshold from the modified wavelet coefficients and to locate the vital features (foreground) in the electric waveform,

various truncation strategies can be applied to the foreground and the background. For instance, a higher threshold (th) is applied to the background to produce more zero-coefficients, and a lower threshold (or prefect reconstruction, th = 1) is applied to the foreground to preserve more significant features. A flowchart of the adaptive scheme is depicted in Fig.3.1.

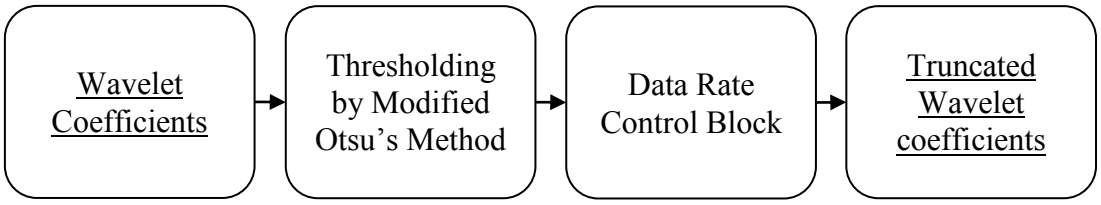

Fig. 3.1 Flowchart of the adaptive thresholding scheme

The proposed adaptive scheme also includes a data rate (or bandwidth) control block for meeting available transmission bandwidth in real time operation. The control block estimates compression ratio by estimating the number of bit required to represent non-zero wavelet coefficients. When the estimated compression ratio is not satisfactory, both the foreground and background threshold will be increased by a factor of 2. These are executed continuously until the compression ratio is satisfactory.

3.2.2.2 Compressing Wavelet Coefficient by Entropy Encoding

Huffman coding is a lossless entropy coding technique commonly used for data compression (e.g. Image: JPEG, Audio: MP3), usually implemented at the final stage of a compression algorithm. This method is useful when symbols (wavelet coefficients) are not uniformly distributed. Symbols are coded based on their occurrences in the data. For example, if a symbol appears frequently in the data, fewer binary bits are used to represent the symbol (e.g. symbol "a" = 111). More bits are used to represent symbols less frequently appeared (e.g. symbol "z" = 010101). A coding table can be generated by examining the occurrence of each symbol. Thereafter, the data (wavelet coefficient) can be translated into coded bit stream efficiently by referencing to the coding table. Table 3.1 shows an example coding table, in which the symbol '0' is assumed to appear most frequently and other symbols are more or less uniformly distributed. A coding table is updated periodically according to statistical results.

Table 3.1
Huffman Coding table

Wavelet Coefficient (Data)	Binary	Coded Symbol
0	0000	0
1	0001	10001
2	0010	10010
…	…	…
15	1111	11111

3.2.3 Flowchart of the Proposed Waveform Compression Algorithm

The overall flowchart of proposed algorithm is shown in Fig. 3.2.

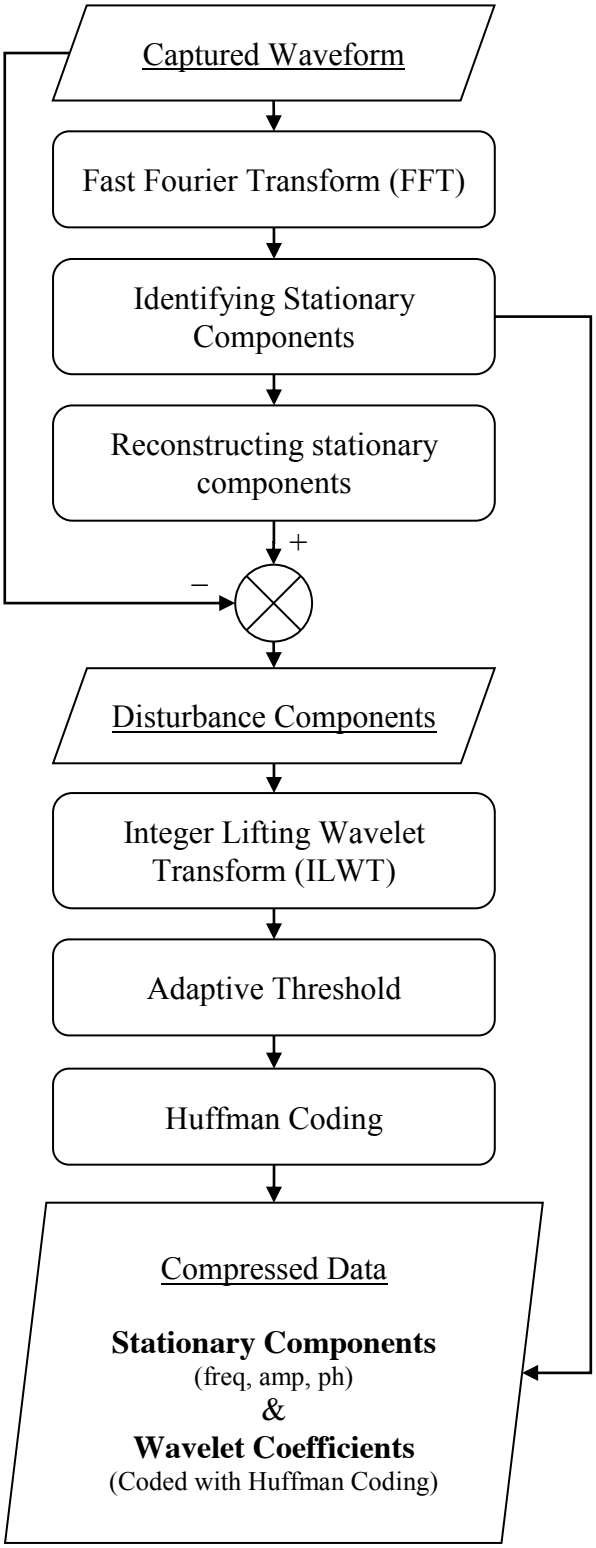

Fig. 3.2 Flowchart of the proposed waveform compression algorithm

3.3 The Proposed Disturbance Identification Algorithm

The proposed identification algorithm is capable of identifying electric power disturbances (e.g. transient) in voltage and current. It can be integrated with the proposed compression algorithm presented in previous Section 3.2. They can share data and processes to maximize computation efficiency for both algorithms. As illustrated in Fig. 3.4, the proposed algorithm is divided into three stages to identify different types of disturbance. It can be noticed that the processes in Stage 2 is almost identical to the proposed compression algorithm; hence, their processes and data can be shared during computation.

Stage 1: Identifying Fundamental Frequency Disturbances by Root-Mean-Square (RMS)

In Stage 1, RMS of the captured waveform is evaluated every half-cycle (0.01s at 50Hz). The RMS differences between adjacent half-cycles are used for classifying disturbance events – supply interruption, voltage sag & swell, and voltage fluctuation, in accordance with the requirements stipulated in IEC 61000-4-30:2008. In particular, the variation rate is calculated by using the RMS differences to identify voltage and current fluctuations.

Stage 2: Identifying Harmonics and Extracting Disturbance Components

In Stage 2, harmonics in both voltage and current are identified via FFT. Like the waveform compression algorithm (see Section 3.2.1), stationary components are identified and eliminated from the captured waveform to extract disturbance components. Fig. 3.3 shows an example of transient extraction in the current containing harmonics. The example current waveform and its frequency spectrum are shown in Fig. 3.2 (a) and (b) respectively. Once the stationary components (impulses in the frequency spectrum) are identified and reconstructed (see equation (3.2)), the disturbance components can be obtained by subtraction, as shown in Fig.3.2 (c).

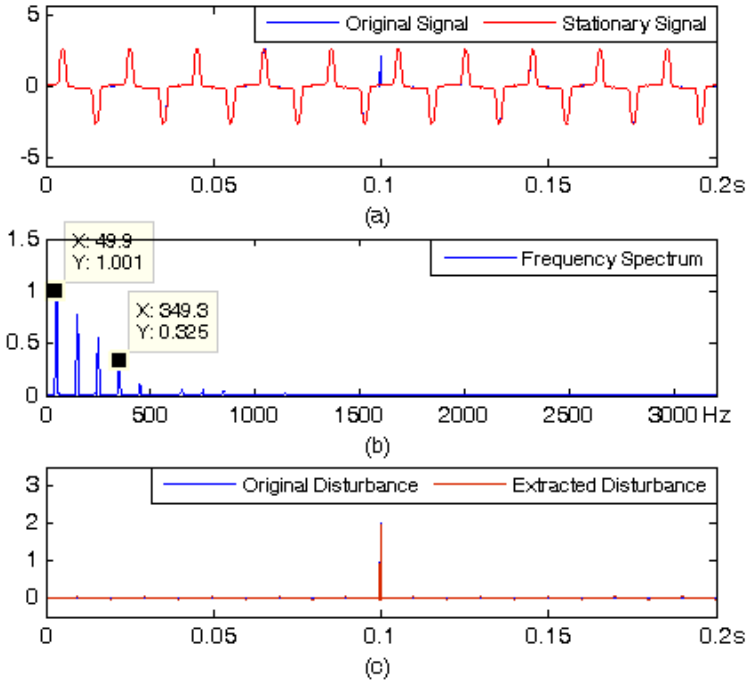

Fig. 3.3 (a) Harmonic current with an impulse transient, (b) Frequency spectrum, (c) Extracted disturbance

Stage 3: Identifying High frequency Disturbances by Crest Factor and Peak Value

Like the waveform compression algorithm, the disturbance component is further decomposed via the integer Lifting Wavelet transform (ILWT) in Stage 3 to separate high and low frequency disturbances. It is known that transients (e.g. impulse) are high in power and low in energy. Thus, the existence of transient is then determined by the crest factor and peak value of each cycle (at 50/60Hz) of the high frequency disturbance as in (3.5)-(3.6). The peak value (3.6) ensures a minimum threshold of transient to prevent false detections generated by noise. Moreover, if transient is identified in more than one cycle on the waveform, this disturbance is determined as notches.

$$\text{Crest Factor} = \frac{|d_1|_{\text{peak}}}{d_{1_{\text{rms}}}} > t_1 \tag{3.5}$$

$$\text{Peak Value} = |d_1|_{\text{peak}} > t_2 \tag{3.6}$$

where t_1 and t_2 represent the threshold settings of the crest factor and the peak value respectively.

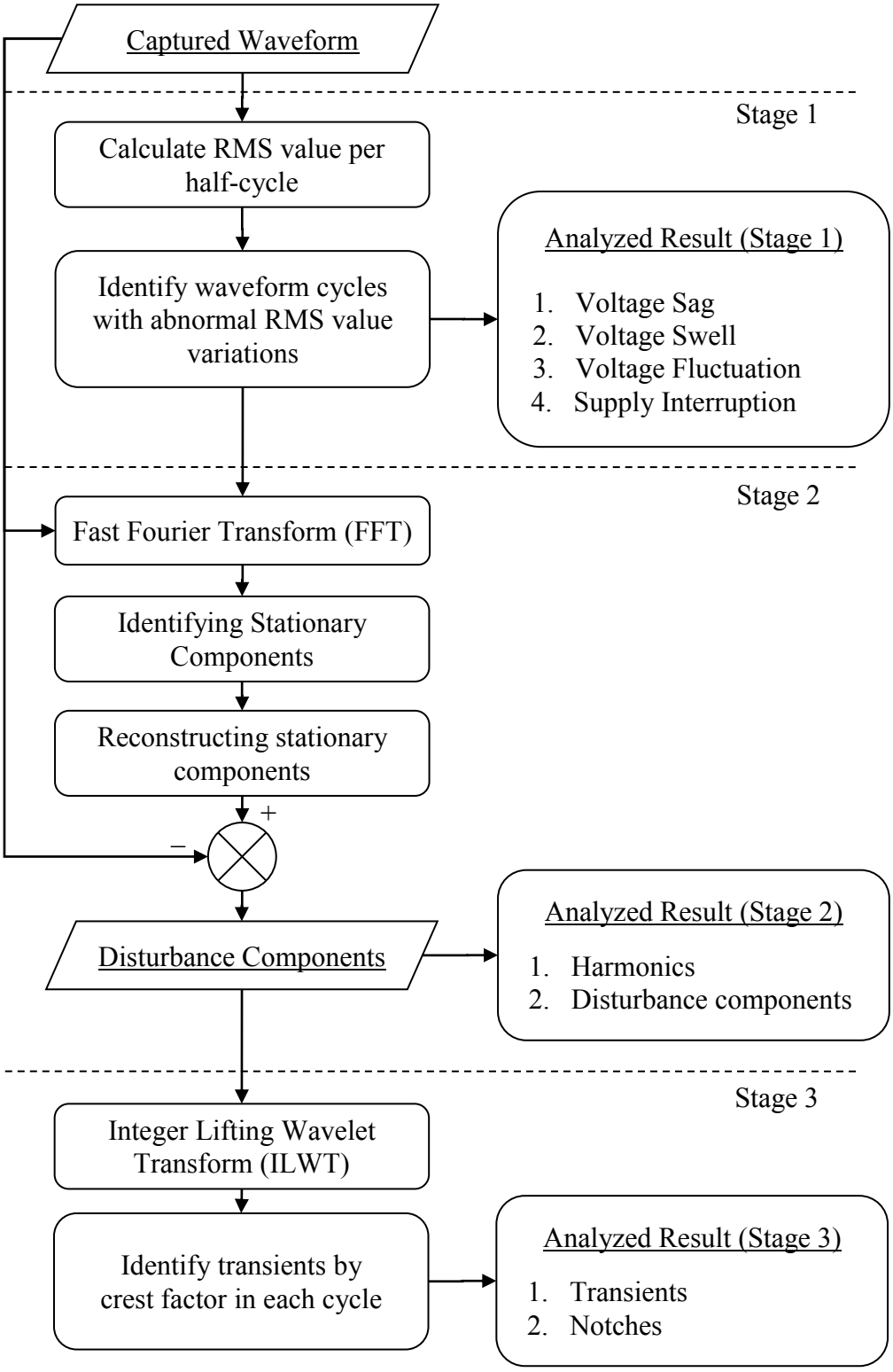

Fig. 3.4 Flowchart of the proposed algorithm

3.4 The Proposed Analysis Method for Time-Varying Harmonic and Disturbance

Concerning the non-uniform leakage problem of DWPT discussed in Chapter 2.3.3.2, an analysis method for time-varying harmonic and disturbance is proposed. The proposed method makes use of Discrete Wavelet Transform (DWT) and frequency shifting property of Hilbert transform (HT) to decompose electric waveform into uniform frequency bands. Spectra of the electric waveform are iteratively shifted to lower side of frequency spectrum, and DWT is applied on the shifted spectra of the electric waveform successively. Only the lowest frequency band, which suffers least leakage problem (Fig. 2.6), is taken out from the shifted spectra one at a time; hence, the non-uniform leakage problem is avoided, unlike DWPT. Basic approach of the proposed algorithm is illustrated in Fig. 3.5.

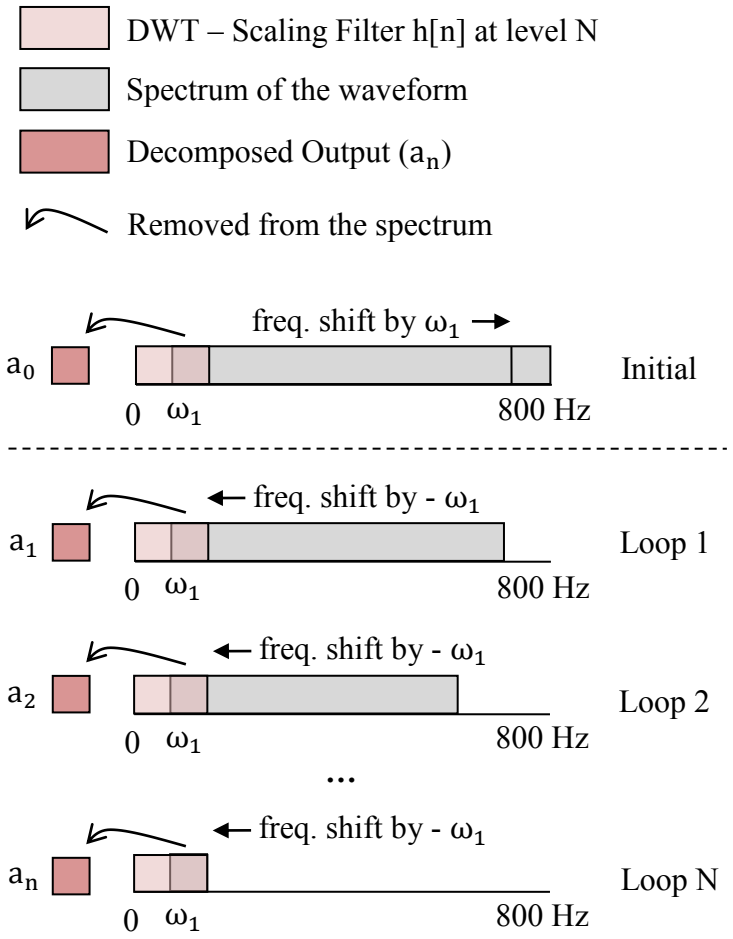

Fig. 3.5 Basic frequency shifting concept of the proposed algorithm

Firstly DWT is applied to obtain the approximation coefficients (aj) of the waveform. The number of levels of decomposition is dependent on the desired bandwidth of the approximation coefficients. With a sampling frequency of 1600 Hz, a bandwidth of 200 Hz would require two levels of decomposition. In any case, the desired bandwidth must be larger than the spectra offset ω_1 or otherwise the spectrum cannot be fully covered and some frequency components will be lost. Secondly, the approximation coefficients are converted into time domain data by inverse DWT (iDWT), and are subtracted from the input waveform. This is to make sure that the positive frequency component in the spectrum is not shifted to the negative frequency region which creates unwanted frequency components in the next step. Thirdly the spectra of the waveform are shifted by a fixed offset ω_1 (e.g. 25 Hz) to the lower frequency spectrum using HT. The extent of spectra shifting is dependent on the frequency contents of the waveform. While FFT can be used to provide a rough idea of the frequency spectrum of the waveform, it is found that a 25/30 Hz fixed offset is sufficient for common power quality analysis. The above steps are repeated until the entire spectrum is shifted to 0 Hz. All approximation coefficients thus obtained can be used for estimating harmonics (e.g. RMS, THD). The instantaneous amplitude, frequency and phase are estimated by HT. Fig. 3.6 shows the flowchart of the proposed algorithm. Detailed steps are described below.

Initial:

Step 1: $$s_{-1}[n] = \mathrm{Re}\left(\left(x[n] + j \cdot H[x[n]]\right) \cdot e^{j\omega_1 n}\right)$$

Step 2: $$a_0[n] = \mathrm{DWT}(s_{-1}[n])$$

Step 3: $$r_0[n] = \mathrm{iDWT}(a_0[n])$$

Step 4: $$s_0[n] = x[n] - \mathrm{Re}\left(\left(r_0[n] + j \cdot H[r_0[n]]\right) \cdot e^{-j\omega_1 n}\right)$$

Loop: Step 5 to 7, where, m = 1, 2, 3 … $(fs/(2 \cdot \omega_1) - 1)$ (until the spectra are shifted to 0Hz)

Step 5: $$a_m[n] = \mathrm{DWT}(s_{m-1}[n])$$

Step 6: $x_m[n] = s_{m-1}[n] - \mathrm{iDWT}(a_m[n])$

Step 7: $s_m[n] = \mathrm{Re}\left(\left(x_m[n] + j \cdot H[x_m[n]]\right) \cdot e^{-j\omega_1 n}\right)$

where

$x[n]$ is the input waveform data sequence

a_n is the approximation coefficient

s_n is the shifted waveform

ω_1 is the spectra shifting offset (25/30 Hz)

fs is the sampling frequency of $x[n]$

r_0 is the transition variable for Steps 3 & 4

It should be noted that the waveform is first shifted by ω_1 in Step 1 instead of $-\omega_1$ as in Step 7. This would ensure that the first output of the algorithm will have the same bandwidth as subsequent outputs. In order to avoid aliasing problem in the upper part of the frequency spectrum due to the increase in frequency (ω_1), in Step 4, r_0 is shifted back to its original frequency spectrum and is subtracted from $x[n]$, as the original $x[n]$ is not affected by the aliasing problem. The iterative processes in Step 5 to 7 are the same as described: in Step 5 the shifted waveform is decomposed by DWT; in Step 6 the approximation coefficients are inversely transformed and subtracted from $x_m[n]$; in Step 7 $x_m[n]$ is shifted again for the next iteration.

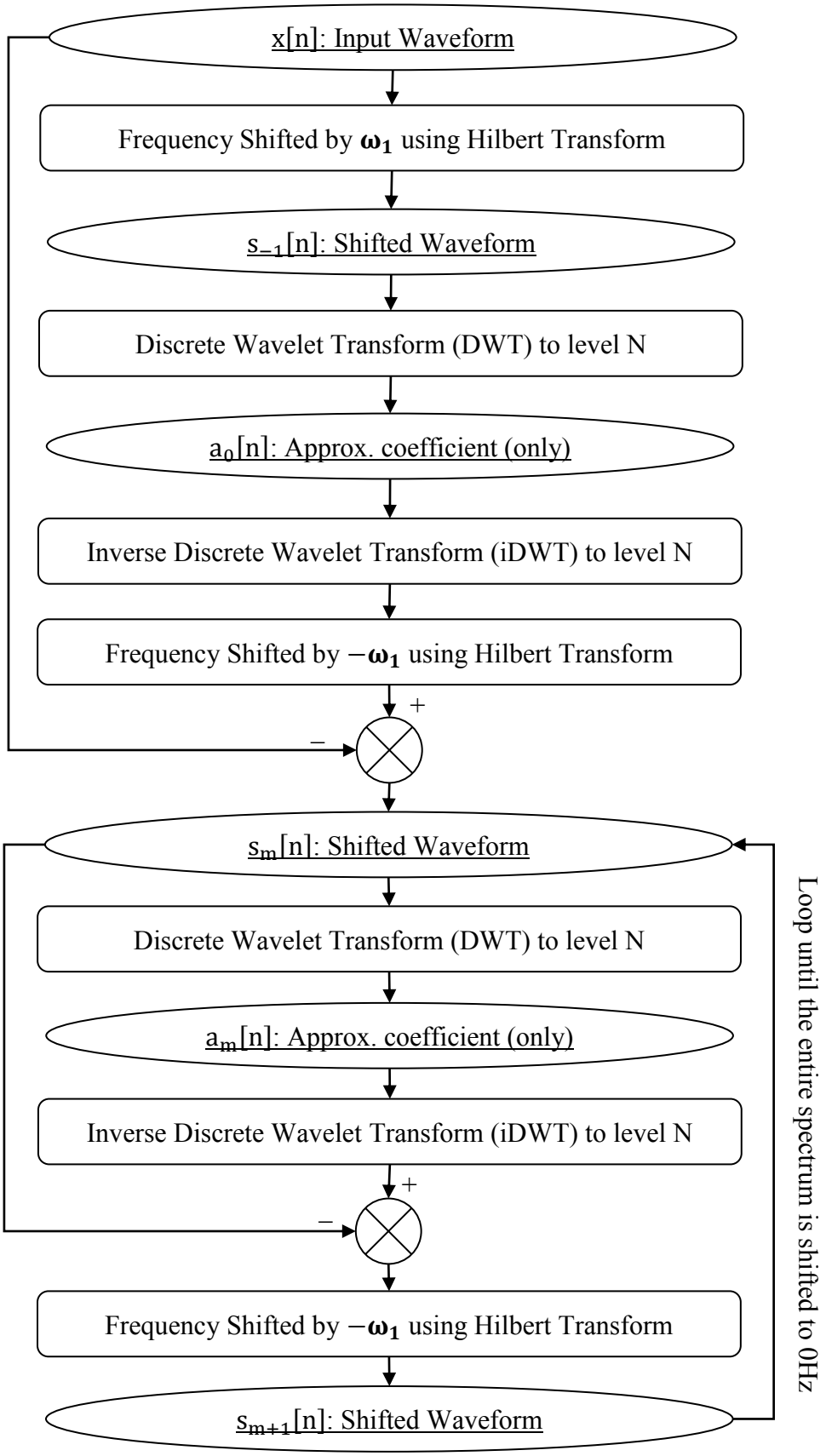

Fig. 3.6 Flowchart of the proposed algorithm

Fig. 3.7 shows the frequency property of the proposed algorithm. For illustration purpose, the sampling frequency of the waveform (x[n]) and the desired bandwidth are set as 1600 Hz and 50 Hz respectively. The decomposition level in DWT and the shifting offset (ω_1) is 4 Hz and 25 Hz respectively. Thereafter, monotone signals from 0 to 800 Hz in step of 0.1 Hz are fed into the algorithm individually to show the frequency property of the algorithm. In order to show the frequency property clearly, the output approximation coefficients are inversely transformed into time domain and shifted back to their original spectrum. The amplitude is calculated by averaging the instantaneous amplitude of the output of HT. 32 frequency bands with a uniform bandwidth of 25 Hz are decomposed. Except for the frequency bands at the two ends of the frequency spectrum, any two '25 Hz' frequency bands can be combined into a '50 Hz' frequency band, as shown in Fig. 3.8, which is then adapted for analyzing integer harmonics. The '25 Hz' frequency bands can also be combined in any adaptive manner for the analysis of non-integer harmonics.

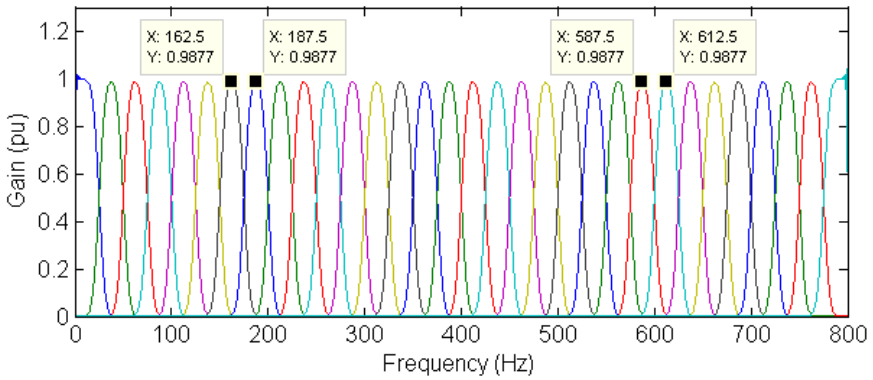

Fig. 3.7 Frequency bands of the proposed algorithm

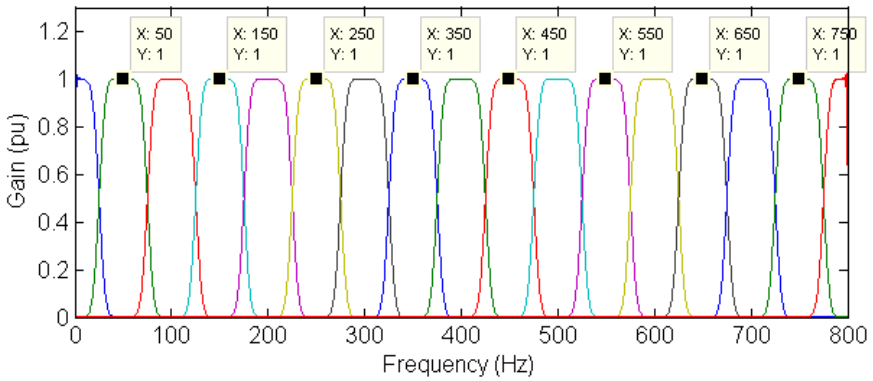

Fig. 3.8 Combined frequency bands of the proposed algorithm adapted for integer harmonics

3.5 Summary

In this chapter, the three proposed methods of this research study are presented. Firstly, the compression algorithm for voltage and current waveforms are introduced. It is dedicated for applications of electric power monitoring. It compresses stationary and non-stationary components of electric waveforms by different processes. Discrete Fourier transform is performed to compress the stationary components into sinusoidal functions, while Integer Lifting Wavelet transform, adaptive threshold, and Huffman coding are applied to compress the non-stationary components. The compression algorithm helps the electric waveform to be preserved and transmitted with lower requirements on memory storage and networking bandwidth; hence, it enables continuous waveform recording and monitoring to be realized with fewer resources.

Secondly, the identification algorithm for electric power disturbances is presented. The proposed identification algorithm is capable of identifying disturbances for both voltage waveform and current waveform. There are three stages in the identification algorithm. It identifies various kinds of disturbances in different stages. Moreover, its second stage is almost identical to the compression algorithm; hence, their processes and data can be shared to enhance computational efficiency, when they are integrated together.

Thirdly, the analysis method for time-varying harmonics and disturbances is presented. It utilizes Discrete Wavelet transform (DWT) and Hilbert transform (HT) to analyze harmonics and disturbances in electric waveforms. Similar to Discrete Wavelet Packet transform (DWPT), it decomposes electric waveforms into multiple frequency bands for analysis. Using HT and DWT, electric waveforms are shifted in frequency spectrum and decomposed into frequency bands iteratively. Unlike DWPT, the non-uniform leakage problem of the decomposed frequency bands is successfully avoided.

The three proposed methods – the compression algorithm, the identification algorithm, and the analysis method are aimed at enhancing capabilities of transient monitoring and analysis for existing electric power monitoring systems. In order to evaluate their feasibility and performance, a prototype electric power monitoring system integrated with the three proposed methods is developed and presented in next chapter.

Chapter 4

Development of Prototype Power Quality Monitoring System

4.1 Introduction

In order to implement the three proposed algorithms presented in the previous chapter, a prototype electric power monitoring system is developed. The prototype is developed to monitor and analyze disturbances of electric power systems in real-time. Moreover, it is aimed at realizing real-time electric waveform monitoring on low-speed communication networks.

The prototype has two main components – the prototype meter and the central monitoring system. Their data communications are carried out by low-speed wireless network – ZigBee. The architecture of the system is shown in Fig. 4.1.

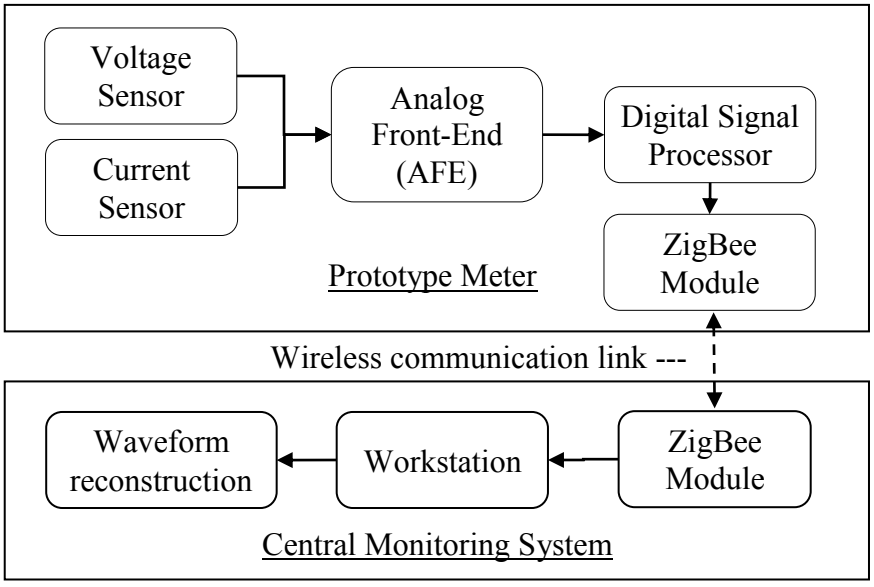

Fig. 4.1 Architecture of the proposed power quality monitoring system

The prototype meter is a custom built embedded system for data (e.g. waveform) sampling, processing and analyzing. It consists of five main components – voltage sensor, current sensor, Analog Front-End (AFE), Digital Signal Processor (DSP) and the Zigbee Module. On the other hand, a workstation (e.g. a traditional desktop computer) interfacing with a Zigbee Module is acting as the central monitoring system. Custom-made software is installed on the workstation to reconstruct, analyze and display captured waveforms.

4.2 Prototype meter

As in any embedded computer systems, they are always made up by hardware and software. In this case, the hardware is those five main components showed in Fig. 4.1. They are utilized to sample, process and transmit data. The software determines how the data is being sampled, processed and transmitted. The major software components in this prototype meter are the waveform compression and the disturbance identification algorithm.

4.2.1 Hardware Implementation

In order that both AC and DC can be measured, a Hall Effect current sensor is utilized in the prototype for both AC and DC current measurement. It is rated at 20 A with 20 kHz bandwidth and 1% accuracy. Moreover, a Hall Effect voltage sensor is also utilized for voltage isolation. Its bandwidth and accuracy is 10 kHz and 1% respectively.

Outputs of the sensors are then passed through an Analog Front-End (AFE), which is implemented with analog anti-aliasing filters, operational amplifiers and a 12-bit Analog-to-Digital Converter (ADC). Low-power DSP (e.g. TMS320C6747) from Texas Instrument is utilized to retrieve the data from ADC and to execute the proposed algorithms. Furthermore, ZigBee module is operating at 2.4GHz with a transmission rate of 250kbps. Fig. 4.2 shows a photograph of the prototype meter. Table 4.1 summarizes specifications of the prototype meters. Models of major components are shown in Table 4.2. The Analog Front-End is self-developed. Its circuit diagram is shown in Appendix III.

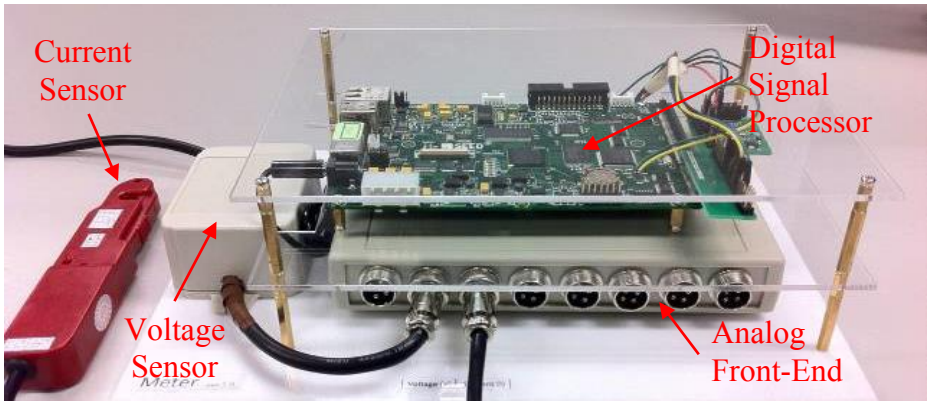

Fig. 4.2 Photograph of the prototype meter

Table 4.1
Specifications of the Prototype Meter

Parameter	Value	Unit
Basic Parameters		
Supply Voltage	+12	V
Supply Current	500	mA
Monitoring Capabilities		
Rated AC Voltage	220	V (RMS)
Rated AC Current	20	A (RMS)
Rated DC Voltage	400	V
Rated DC Current	30	A
Sampling Frequency	12.8	kHz
Frequency Bandwidth	4	kHz

Table 4.2
Major Components of the Prototype Meter

Item	Model
Digital Signal Processor	SEED DEC-L137
Voltage Sensor	ChenYang CYHVS300T
Current Sensor	Chengdu Jingfeng JT10T31
Analog Front-End	Refer to Appendix III for circuit diagram

4.2.2 Software Implementation

The software of the prototype meter is implemented on the Real-Time Operation System provided by Texas Instrument for their DSP. The software is divided into three

processing threads to handle various tasks more dynamically in an on-demand style. Architecture of the prototype meter software is shown in Fig. 4.3.

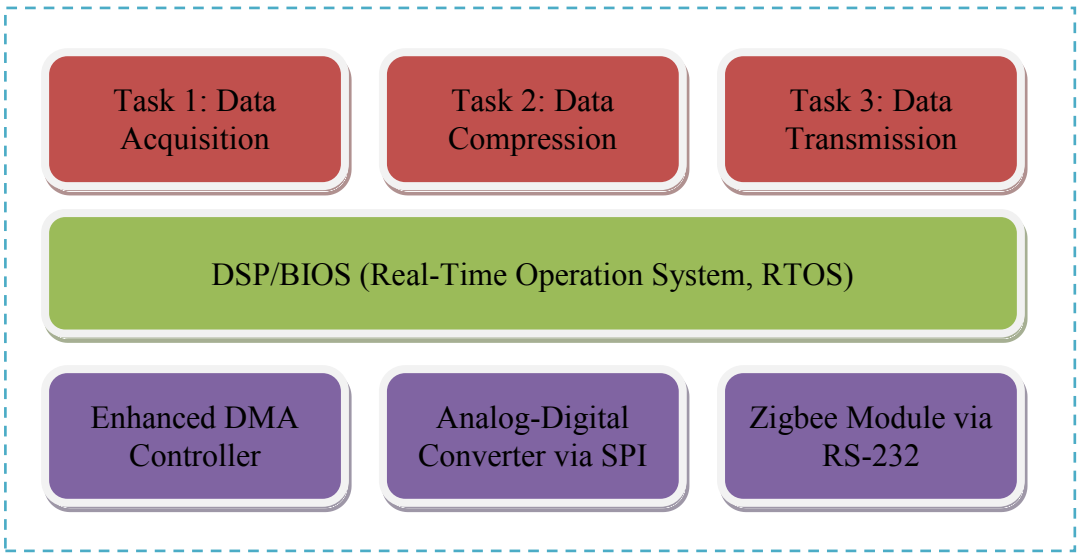

Fig. 4.3 Architecture of prototype meter software

Task 1 on data acquisition handles the ADC data communication which utilizes the DMA controller for fast data transfer. After the data is ready, task 2 executes waveform compression and disturbance identification algorithm. Once task 2 is finished, task 3 transmits the compressed data to the Zigbee Module. It can be noted that the three tasks are not executed in a sequential style. Task 1 always has the first priority to interrupt the others for immediate data extraction from the ADC. On the other hand, task 3 has to wait for the acknowledgement from Zigbee Module. As a result, the tasks are working concurrently all the time.

4.3 Central Monitoring System

The central monitoring system is mainly the custom made software for waveform reconstruction and analysis, which is executed on a workstation with a Zigbee communication interface. Microsoft Visual Studio is employed as the development platform for the custom made software. The software is able to store the compressed data, to reconstruct the waveform, to calculate power quantities and to perform the Fast Fourier transform. Screenshots of the software is shown in Fig 4.4 to Fig. 4.7.

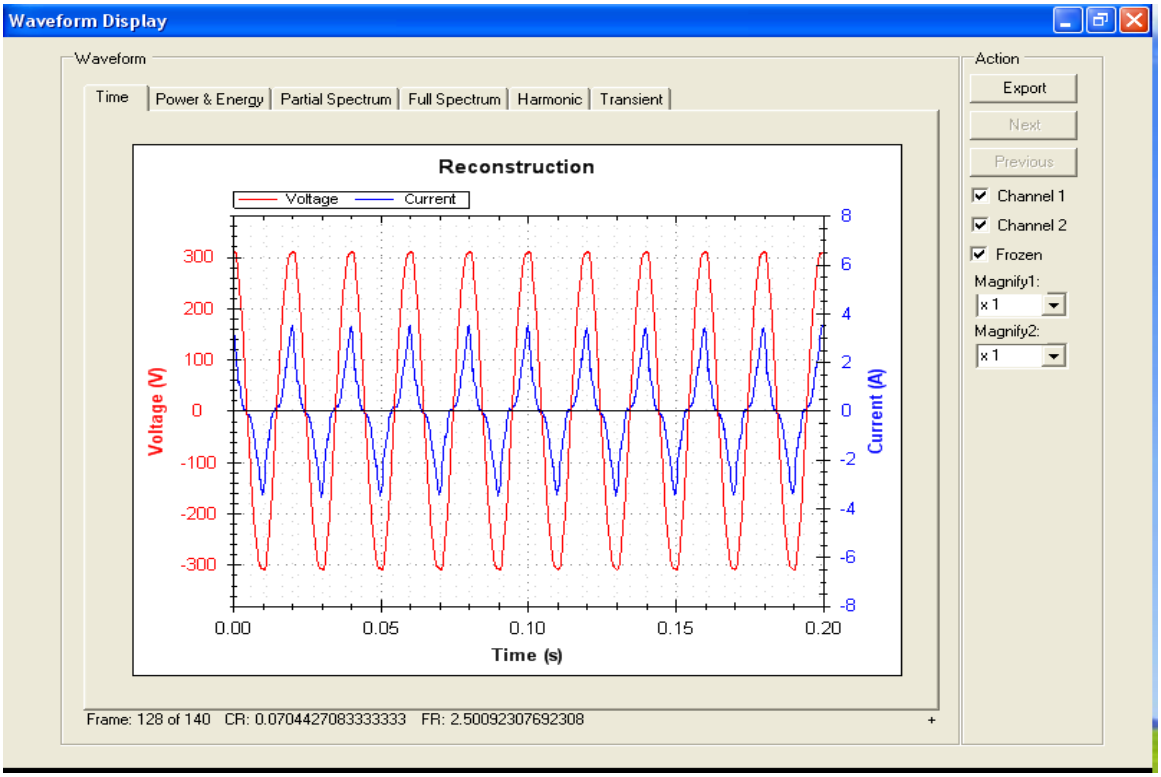

Fig. 4.4 Screenshot of the analysis software – waveform display

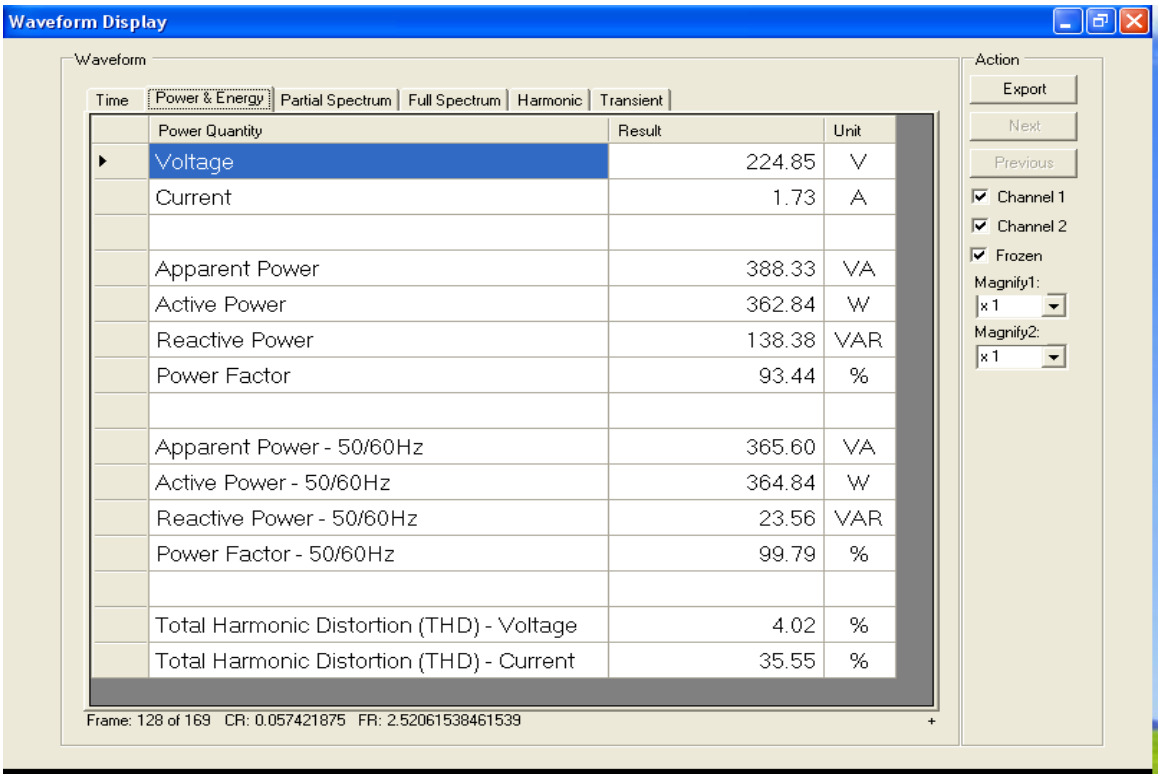

Fig. 4.5 Screenshot of the analysis software – power quantities

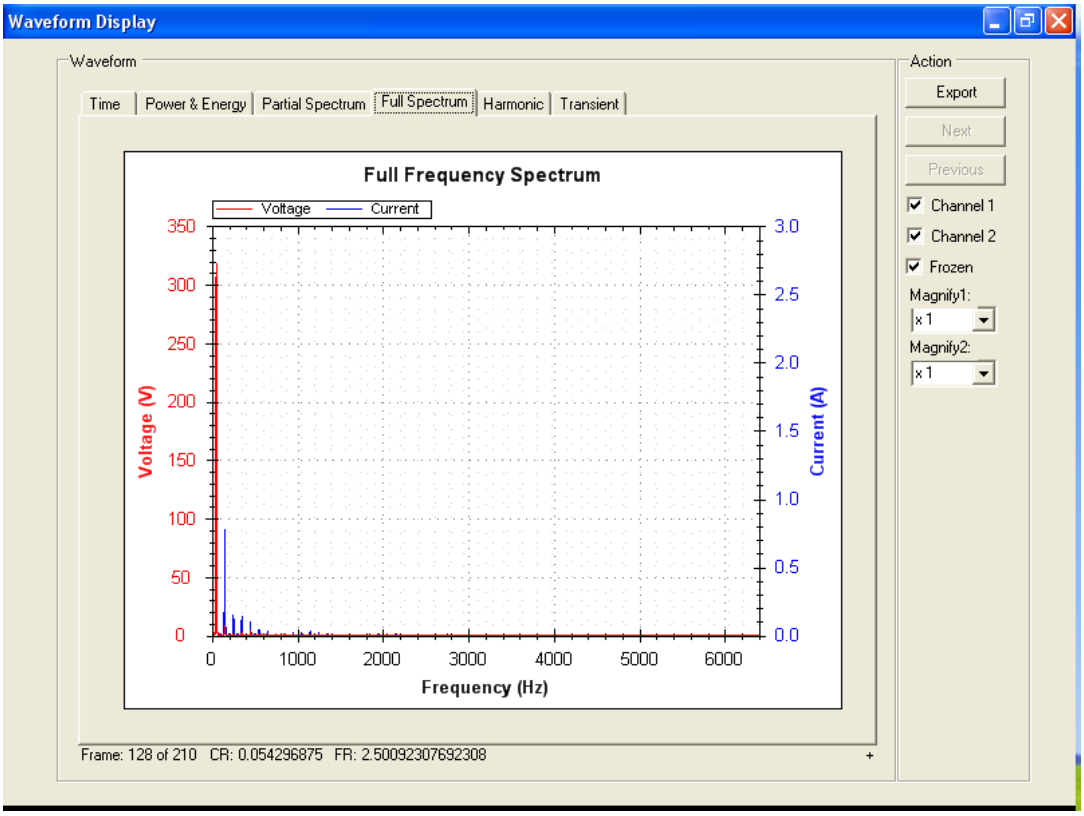

Fig. 4.6 Screenshot of the analysis software – frequency spectrum

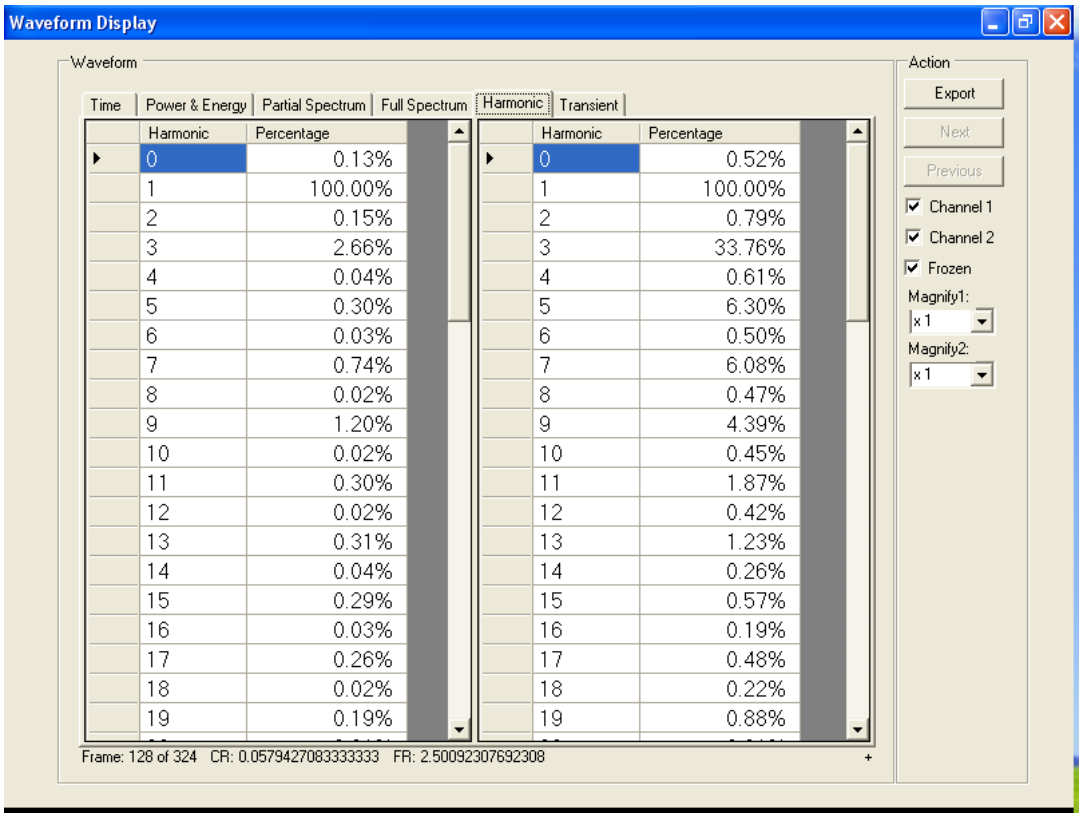

Fig. 4.7 Screenshot of the analysis software – harmonics

4.4 Summary

A prototype electric power monitoring system integrated with the three proposed methods of this thesis is successfully developed. Real-time electric waveform and disturbance monitoring are realized. The entire prototype is made up by two parts – the prototype meter and also the central monitoring system. The prototype meter is responsible for capturing data and monitoring the status on the power system. It executes both the waveform compression and disturbance identification algorithm. The central monitoring system is a management software program, which is executed on a workstation. It stores, reconstructs and displays the data obtain from the prototype for analysis. The wireless data communicate link between the prototype meter and the central monitoring system is established by Zigbee.

Chapter 5

Testing the Proposed Methods

5.1 Introduction

In order to evaluate feasibilities and performances of the three proposed methods – the compression algorithm, the disturbance algorithm and the analysis method, tests were performed. In the tests, the prototype electric power monitoring system was utilized to capture and analysis electric waveforms and disturbances. Some tests were performed in laboratory with specialized equipment to simulate real situations and scenarios of electric power systems. Other tests were carried out on site for a real-life electric distribution system. Different tests were designed and performed for each of the proposed methods to evaluate their feasibilities and performances. Tests and results for the three proposed methods are presented successively in this chapter.

5.2 Tests and Results of the Compression Algorithm

In order to evaluate the compression algorithm, experiments and field tests were conducted. Results of the tests are summarized into compression ratio (CR) and signal-to-noise ratio (SNR). In the experiments, typical electric power disturbances, such as sag, swell, and transient, were simulated. Environment of the experiments was controlled via a multi-functional power supply. On the other hand, the field test was carried out in an uncontrolled environment, where an electric supply of a local utility company was monitored for months by the prototype monitoring system.

5.2.1 Methodology

The prototype meter, which is discussed in Chapter 4, is utilized to capture and compress electric waveforms in the tests. Waveforms of voltage and current are sampled at 12.8 kHz, and their samples are quantized into 12-bits by an analog-to-digital converter (ADC). The duration of each captured electric waveform is 0.2s (10 cycles at 50 Hz).

In the compression process, non-stationary components of the electric waveforms are decomposed into 4 resolutions by integer LWT with Daubechies-4 wavelet. The performance of the compression algorithm is then evaluated under various threshold settings for wavelet coefficients. Moreover, the wavelet packet method [19, 24] without stationary component separation is adopted for comparison purpose. Performance evaluations are conducted for the following scenarios:

(1) the compression algorithm with adaptive threshold:

(a) initial foreground and background thresholds of 1 and 2;

(b) initial foreground and background thresholds of 1 and 8;

(2) the compression algorithm with fixed threshold; and

(3) the wavelet packet method without the stationary component separation in fixed threshold.

While the adaptive threshold of (1) is already discussed in Chapter 3.2, the fixed threshold of (2) and (3) is defined as,

$$\text{wavelet coefficient } (wc) = \begin{cases} 0 & , \ |\text{wc}| < th \\ \left\lfloor \frac{wc}{sfactor} + \frac{1}{2} \right\rfloor & , \ |\text{wc}| \geq th \end{cases}, \tag{5.1}$$

where $\text{th} = 1, 2, 4, \ldots \text{n}$; $\text{sfactor} = 2^{\lfloor \log_2(\text{th}) \rfloor} = 1,2,4,8,16, \ldots$

The fixed threshold truncates wavelet coefficients (*wc*) below the threshold (*th*), and downscales the magnitude of wavelet coefficients above the threshold (*th*). The scale-down factor (*sfactor*) in (5.1) is in power of 2 to match with the binary operation in electronic devices.

During the performance tests, threshold settings in scenarios (1), (2) and (3) were started from 1 for prefect reconstruction. Then they were incremented in factor of 2 to imitate various compression ratios. The compression ratio (CR) and the signal-to-noise ratio (SNR) defined in equations (5.2) and (5.3) are used to evaluate the waveform

compression performance. A high SNR represents good preservation of waveform information and a high CR represents effective compression. The performance of the proposed algorithm is hence evaluated for achieving an optimal compromise between SNR and CR.

$$\text{Compression Ratio (CR)} = \frac{\text{original file size}}{\text{compressed file size}}, \tag{5.2}$$

$$\text{SNR(dB)} = 10\log_{10}\left(\frac{\sum_{n=0}^{N-1}\|x[n]\|^2}{\sum_{n=0}^{N-1}\|x[n]-\tilde{x}[n]\|^2}\right), \tag{5.3}$$

where $x[n]$ and $\tilde{x}[n], n = 0,1,\ldots,N-1$ are the original and the reconstructed signal data respectively.

5.2.2 Experiments

The setup of the experiments is shown in Fig. 5.1. A multi-functional AC power supply is utilized to simulate electricity supplies of electric power systems, while a lamp box containing electronic-controlled fluorescent lamps and incandescent lamps is utilized to simulate a group of nonlinear loads. Voltage and current are monitored by the prototype meter.

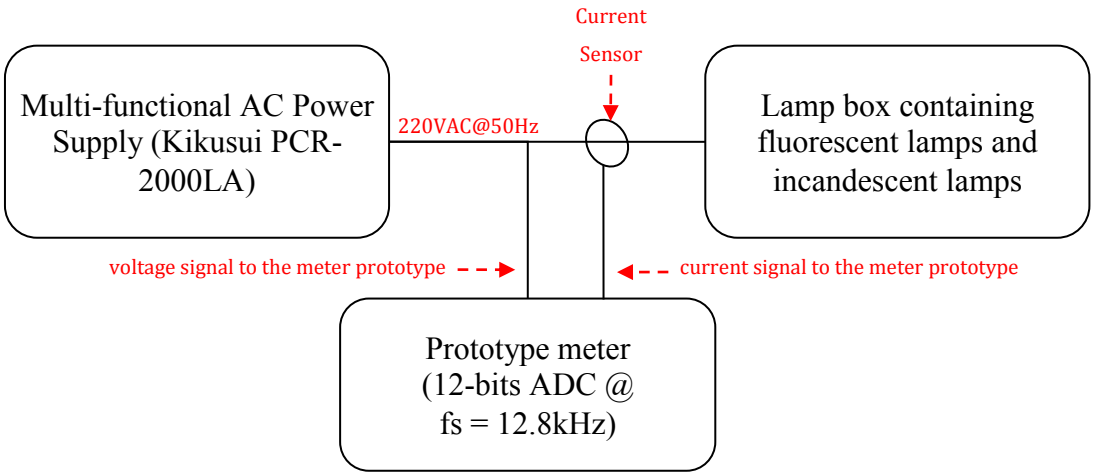

Fig. 5.1 Equipment setup for the experimental tests

Ten common electric power quality problems (e.g. harmonics, flicker, and transient) were tested. They were deemed sufficient to evaluate the performances of the compression

algorithm. The waveforms of each power quality problem and their corresponding performance charts (SNR versus CR) are presented in the following sub-sections. It should be noted that an SNR of 70dB in the performance charts is close to perfect reconstruction, and an SNR of 30dB was set as a lower bound in the tests. A summary of compression performance is given in Section 5.2.4

Test 1: Steady supply voltage free from harmonics

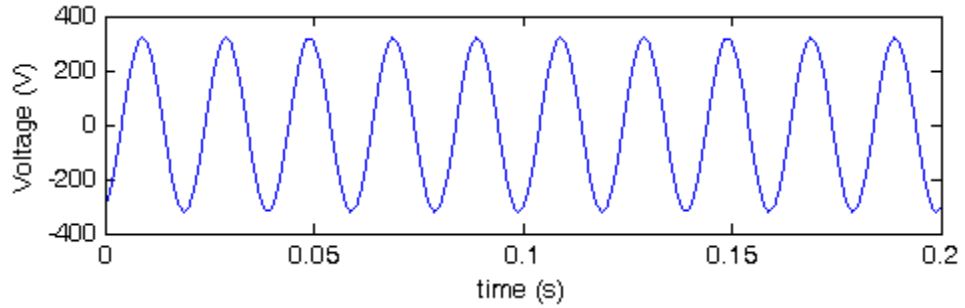

Fig. 5.2 Steady supply voltage waveform free from harmonics

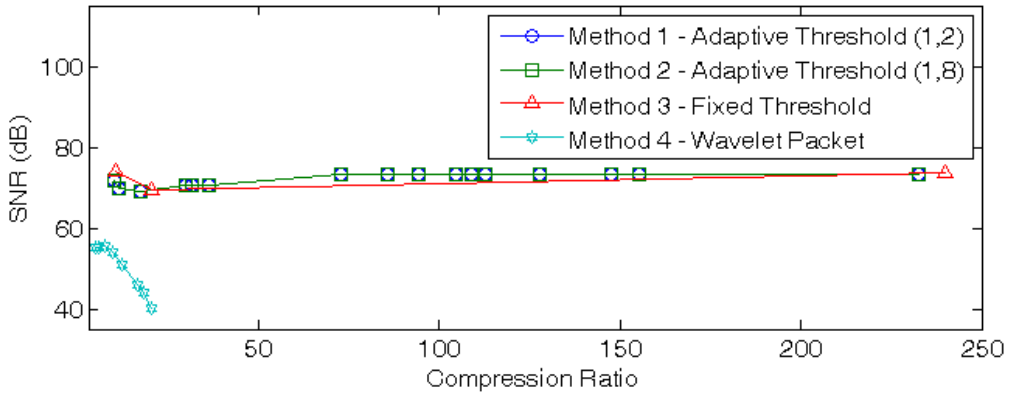

Fig. 5.3 Compression ratio of the waveform in Fig. 5.2

Test 2: Steady supply voltage with harmonic components (3rd-1.1%, 5th–2.1%, 7th–1.3%, 9th–0.5%)

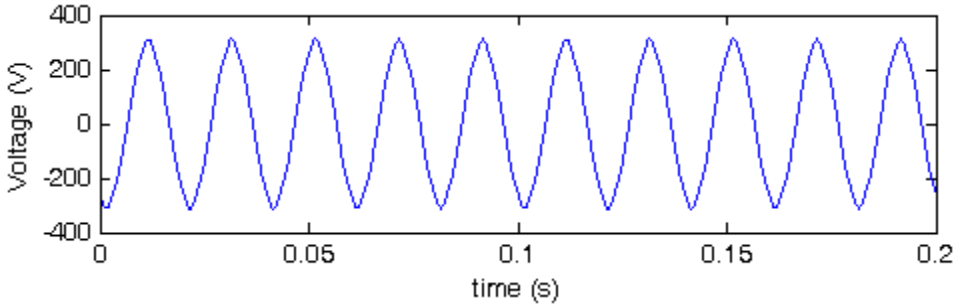

Fig. 5.4 Steady supply voltage waveform with four harmonic components

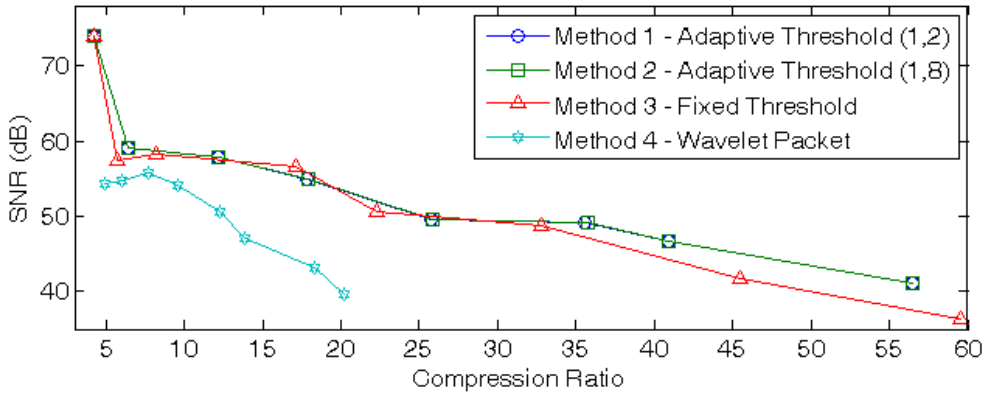

Fig. 5.5 Compression ratio of the waveform in Fig. 5.4

Test 3: Harmonic current drawn by the lamp box

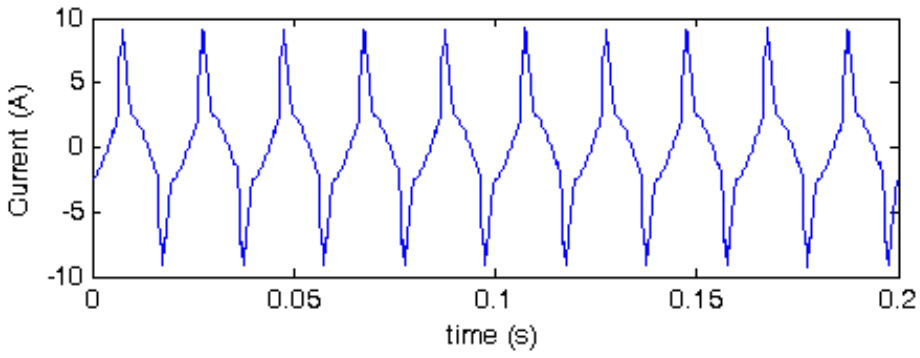

Fig. 5.6 Harmonic current waveform drawn by the lamp box

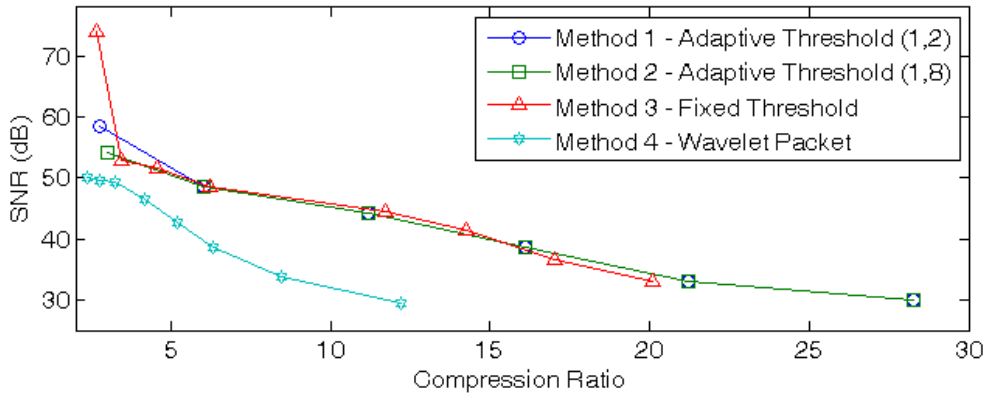

Fig. 5.7 Compression ratio of the waveform in Fig. 5.6

Test 4: Voltage Swell to 130%

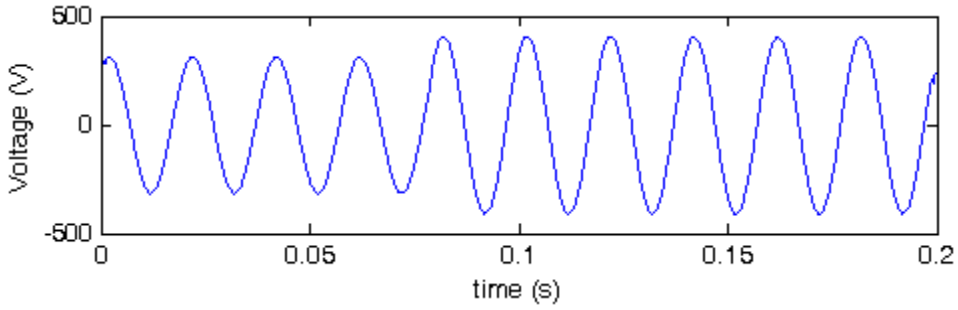

Fig. 5.8 Voltage swell waveform

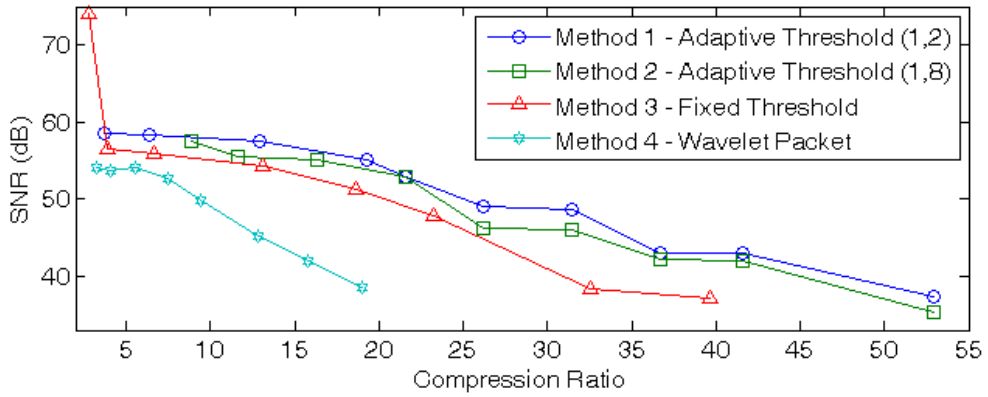

Fig. 5.9 Compression ratio of the waveform in Fig. 5.8

Test 5: Voltage Sag to 70%

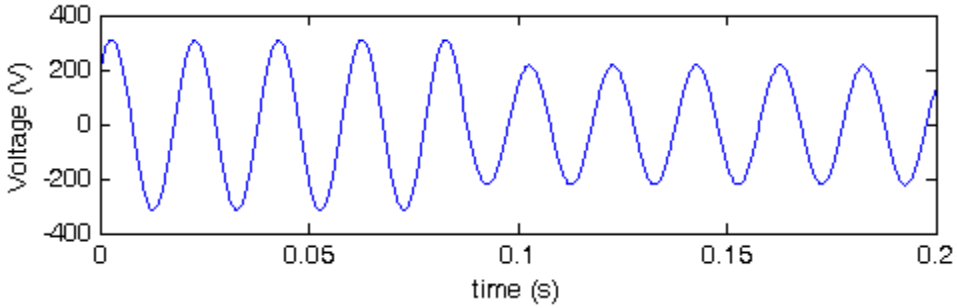

Fig. 5.10 Voltage sag waveform

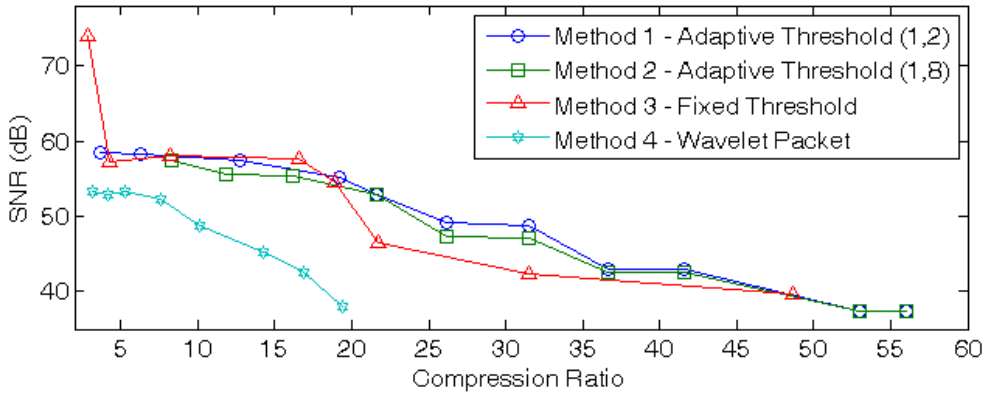

Fig. 5.11 Compression ratio of the waveform in Fig. 5.10

Test 6: Voltage Interruption

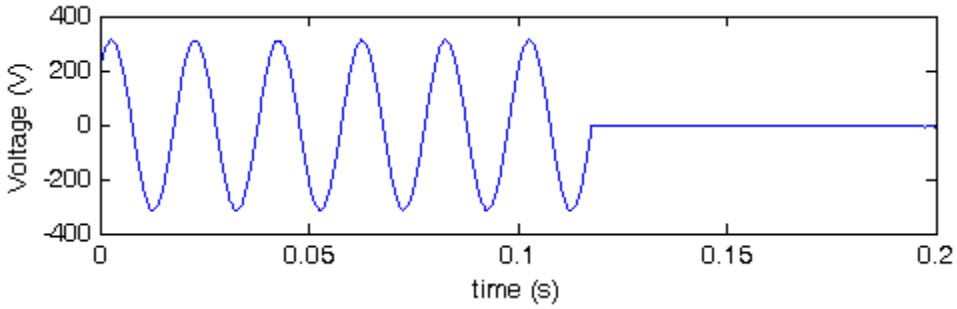

Fig. 5.12 Voltage interruption waveform

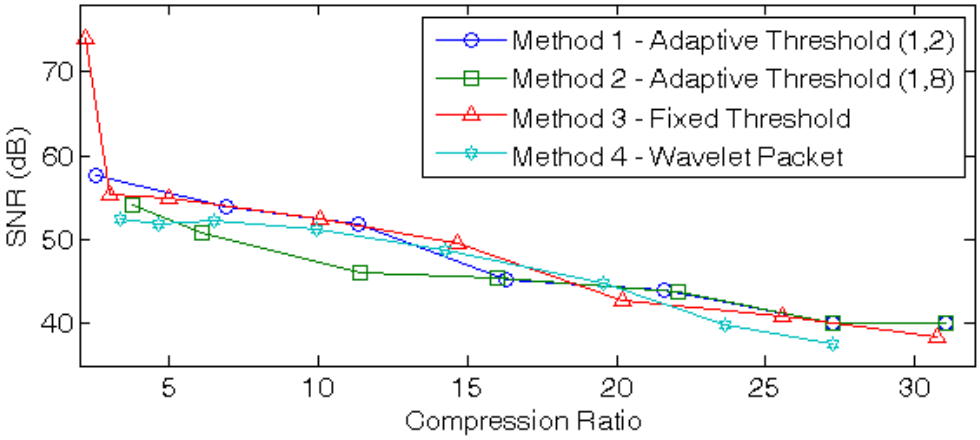

Fig. 5.13 Compression ratio of the waveform in Fig. 5.12

Test 7: Steady supply voltage with oscillatory Transient

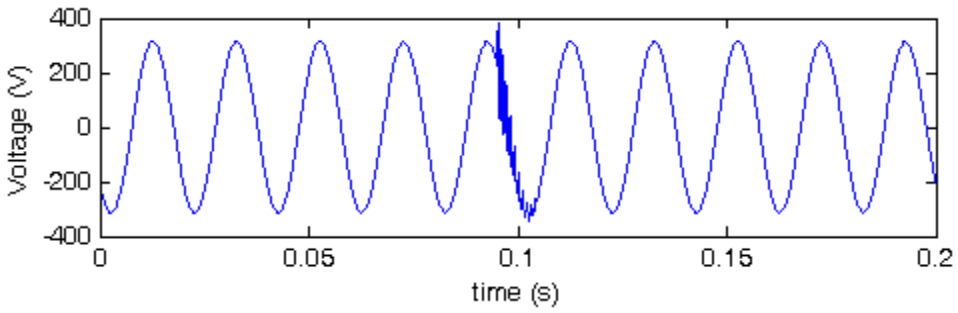

Fig. 5.14 Steady supply voltage with oscillatory transient waveform

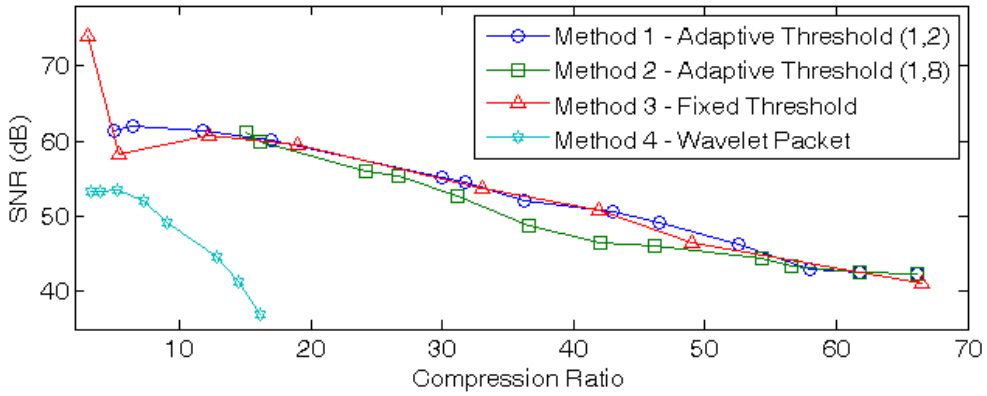

Fig. 5.15 Compression ratio of the waveform in Fig. 5.14

Test 8: Steady supply voltage with impulsive transient

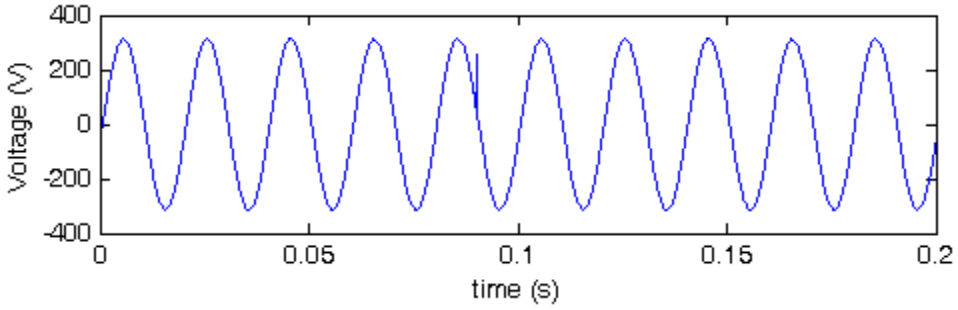

Fig. 5.16 Steady supply voltage with impulsive transient waveform

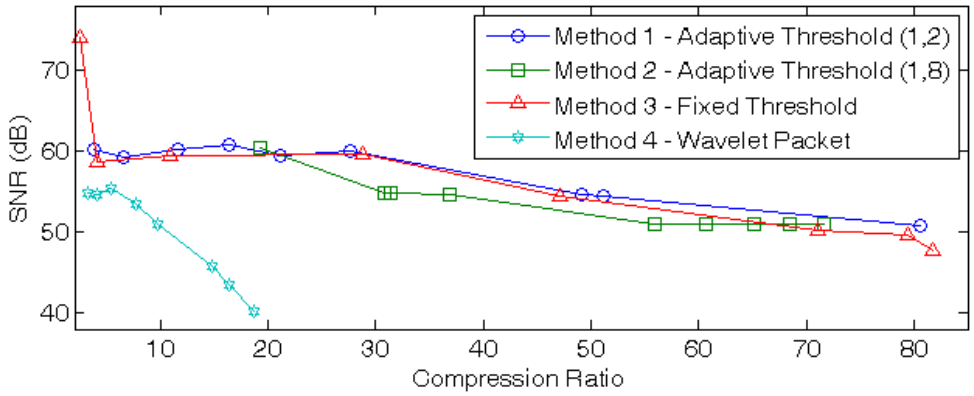

Fig. 5.17 Compression ratio of the waveform in Fig. 5.16

Test 9: Steady supply voltage with notches

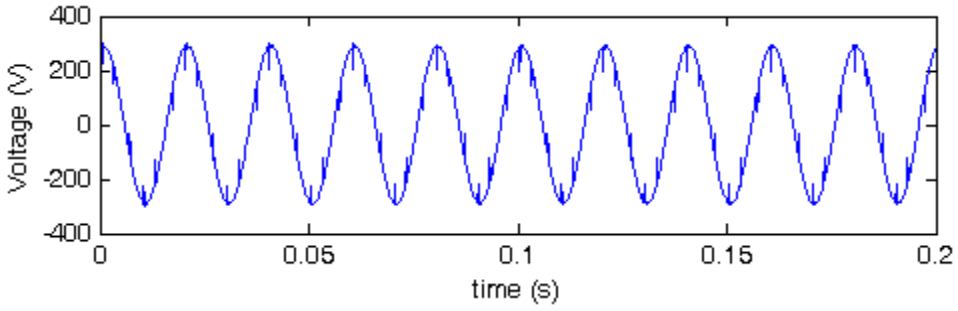

Fig. 5.18 Steady supply voltage with notches waveform

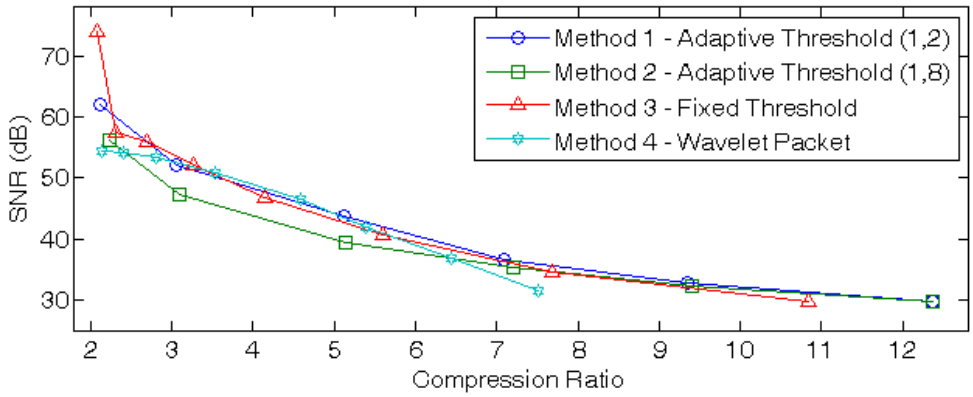

Fig. 5.19 Compression ratio of the waveform in Fig. 5.18

Test 10: Flickering supply voltage

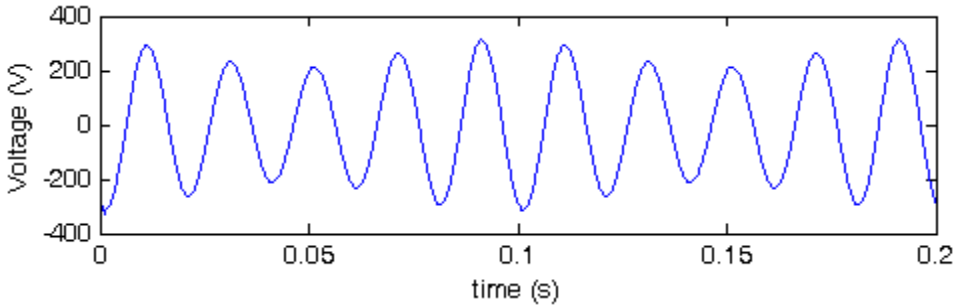

Fig. 5.20 Flickering supply voltage waveform

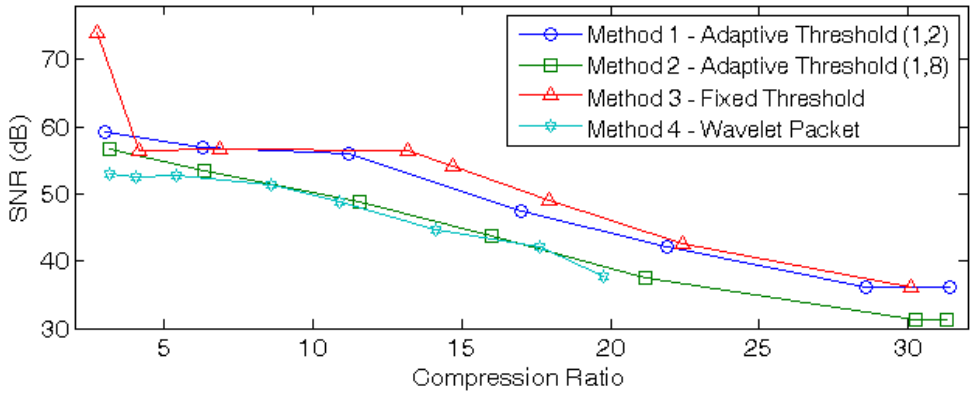

Fig. 5.21 Compression ratio of the waveform in Fig. 5.20

5.2.3 Field Test

The field tests were conducted in an uncontrolled environment. A real electric supply of a local utility company is monitored for a month through an electric outlet in the university building. Moreover, the electric outlet was connected with a group of electric appliances, which are used by students in the building. An example of the captured voltage and current waveform are shown in Fig. 5.22 and 5.24 respectively. Results of the field tests are averaged and are shown in Fig. 5.23 and 5.25.

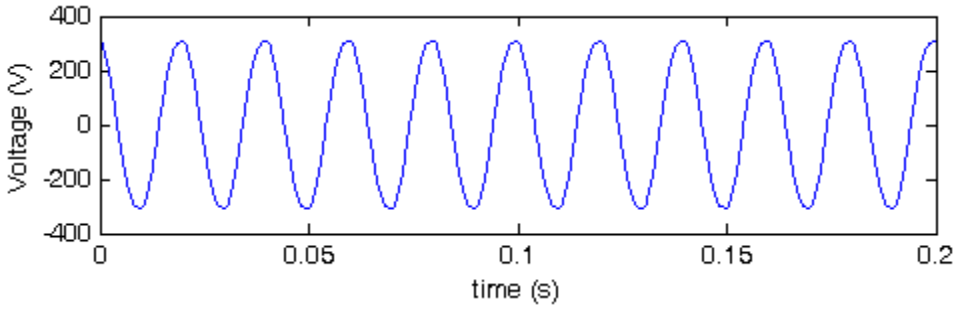

Fig. 5.22 An example of captured voltage waveform in the field test

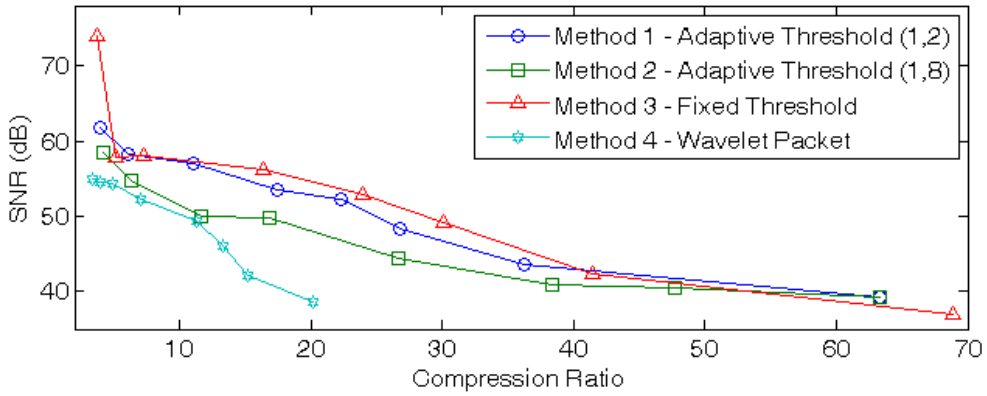

Fig. 5.23 Averaged compression ratio of captured voltage waveforms

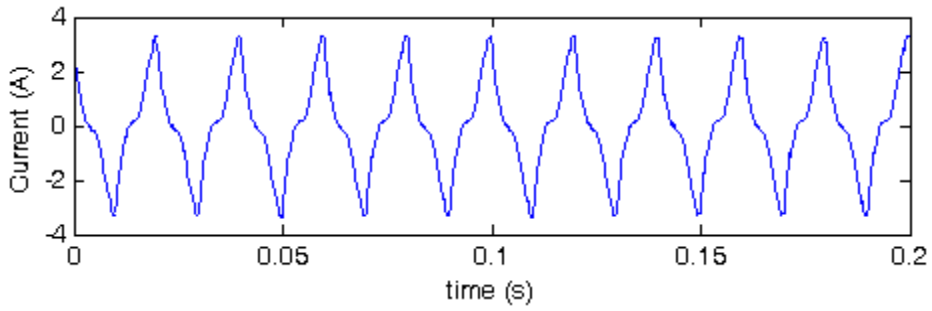

Fig. 5.24 An example of captured current waveform in the field test

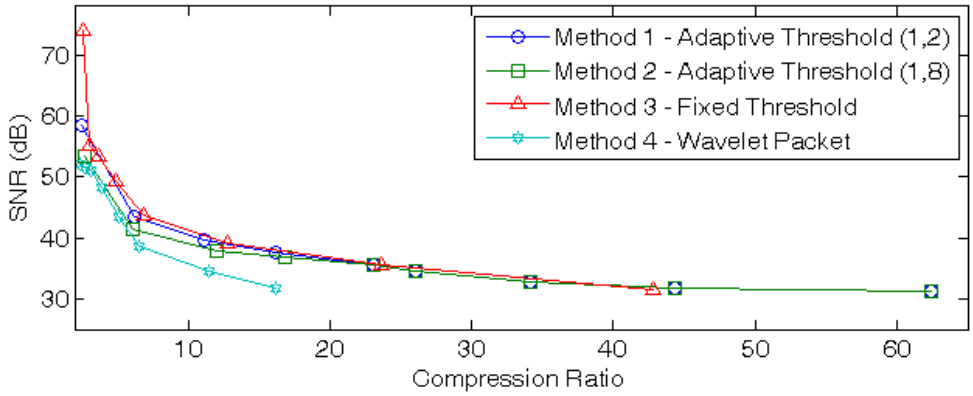

Fig. 5.25 Averaged compression ratio of captured current waveform

5.2.4 Summary of Compression Performance

As revealed by the experiments and the field test, SNR and CR are dependent on the type of power quality (PQ) events. It is observed from the experiments that:

1. For interruptions and notches, the performances of the proposed algorithm and the WPT based method are comparable. For other PQ events, the proposed algorithm outperforms the WPT based method.

2. For PQ events with significant stationary components (Tests 1 - 3), threshold settings would not affect the compression results significantly, because the adaptive threshold was only applied to non-stationary components. In Test 1 where its voltage is purely sinusoidal, its SNRs remain constant for all CRs. In Tests 2 and 3, there are variations in SNRs for different threshold settings, because harmonic components generated by the multi-functional AC power supply are not strictly stationary, which is close to real life situation.

3. In Tests 4 - 8, the SNR vs. CR performance of the adaptive threshold is slightly better than the fixed threshold. Besides, the adaptive threshold has introduced smaller errors in the transients of Tests 7 and 8.

4. In Test 9, although all four scenarios have similar SNR vs. CR performance, the adaptive threshold does support the perfect reconstruction of notches.

5. In Test 10, the proposed algorithm with the fixed threshold has a slightly better SNR vs. CR performance. It can be concluded that for waveforms with small variations such as voltage sag, swell and flickering, the adaptive threshold is comparable or slightly better than the fixed threshold. Moreover the background threshold setting is important in achieving an optimal SNR vs. CR performance.

The results obtained from the field test have also confirmed that the proposed compression algorithm outperforms the WPT based method. In terms of SNR vs. CR performance, the fixed threshold is better than the adaptive threshold. However, it should be noted that the adaptive threshold had an initial background threshold of 2 and 8, and the main advantage of the adaptive threshold is in preserving significant features of electric waveforms.

5.3 Tests and Results of the Identification Algorithm

Case studies were performed to evaluate the disturbance identification algorithm. Typical electric power disturbances were generated by a multi-functional AC power supply for the case studies. The prototype electric power monitoring system integrated with the identification algorithm was utilized to identify the generated disturbances. Experiment setup is shown in Fig. 5.1, which is the same as the experiments for the compression algorithm.

In order to visualize the procedures of the identification algorithm in detail, results of each stage of the identification algorithm are provided; hence, the RMS value in Stage 1, the frequency spectrum and extracted disturbance in Stage 2, and the crest factor and peak value in Stage 3 are included in the results for each case study.

5.3.1 Voltage swell

A voltage swell identified by the identification algorithm is shown in Fig. 5.26 (a). Its RMS value calculated in Stage 1 is presented in Table 5.1. From the RMS table, an increase in RMS value is observed in the 5th cycle, and a 10% voltage swell is identified from the 5th to the 10th cycle.

The frequency spectrum and the extracted disturbance obtained in Stage 2 are shown in Fig. 5.26 (b) and (c) respectively. Table 5.2 shows the crest factor and the peak value calculated for each cycle of the high frequency disturbance. As the peak values are small, no disturbance is identified.

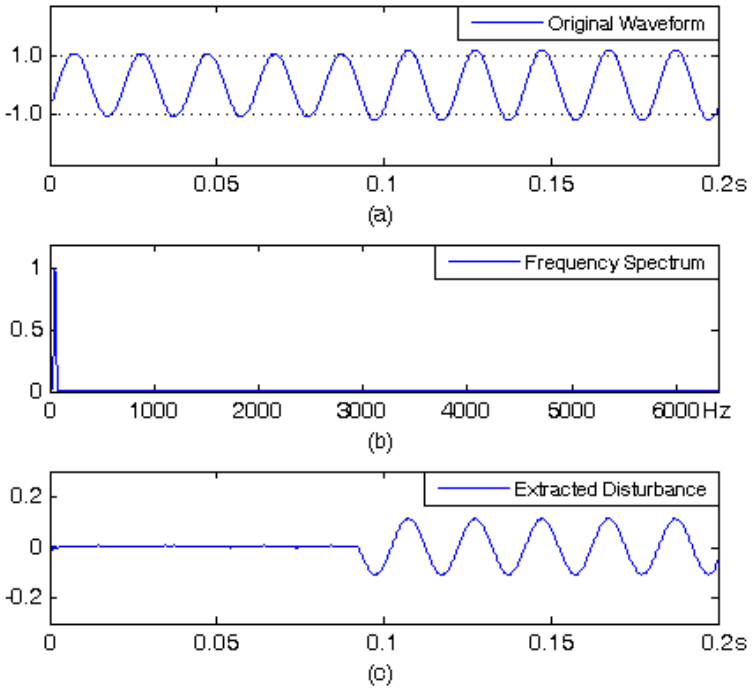

Fig. 5.26 (a) Voltage swell, (b) Frequency spectrum, (c) Extracted disturbance

Table 5.1
Half-cycle RMS value calculated in Stage 1

Cycle	1st half	2nd half
1	0.71	0.70
2	0.71	0.70
3	0.71	0.70
4	0.71	0.70
5	0.71	0.77
6	0.79	0.78
7	0.79	0.78
8	0.78	0.78
9	0.79	0.78
10	0.78	0.78

Table 5.2
Peak value & Crest Factor calculated in Stage 3

Cycle	Peak value	RMS value	Crest Factor
1	0.01	0.00	8.57
2	0.00	0.00	2.24
3	0.00	0.00	2.21
4	0.00	0.00	2.18
5	0.00	0.00	2.17
6	0.00	0.00	2.12
7	0.00	0.00	2.28
8	0.00	0.00	2.21
9	0.00	0.00	2.50
10	0.00	0.00	2.68

5.3.2 Voltage – impulsive transient

A voltage transient identified by the identification algorithm is shown in Fig. 5.27 (a). Its RMS value calculated in Stage 1 is shown in Table 5.3. From the RMS table, a decrease in RMS value is observed in the 1st half of the 6th cycle. The RMS values of other cycles are normal.

The frequency spectrum and the extracted disturbance obtained in Stage 2 are shown in Fig. 5.27 (b) and (c) respectively. Table 5.4 shows the crest factor and the peak value calculated for each cycle of the high frequency disturbance. Both crest factor and peak value in the 6th cycle is significantly large, hence a transient is identified.

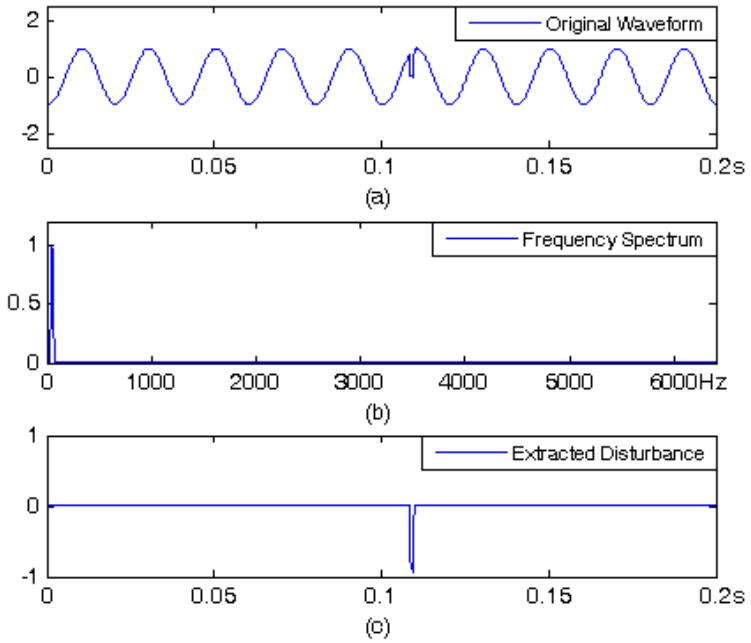

Fig. 5.27 (a) Impulsive transient, (b) Frequency spectrum, (c) Extracted disturbance

Table 5.3
Half-cycle RMS value calculated in Stage 1

Cycle	1st half	2nd half
1	0.70	0.70
2	0.70	0.70
3	0.70	0.70
4	0.70	0.70
5	0.70	0.70
6	0.63	0.70
7	0.70	0.70
8	0.70	0.70
9	0.70	0.70
10	0.70	0.70

Table 5.4
Peak value & Crest Factor calculated in Stage 3

Cycle	Peak value	RMS value	Crest Factor
1	0.01	0.01	1.68
2	0.01	0.01	1.42
3	0.01	0.01	1.53
4	0.01	0.01	1.49
5	0.01	0.01	1.49
6	0.94	0.20	4.70
7	0.01	0.01	1.54
8	0.01	0.01	1.54
9	0.02	0.01	1.54
10	0.02	0.01	1.57

As shown in Table 5.4, a transient is identified in Stage 3. The peak value and the crest factor at the 6th cycle are significantly larger than others.

5.3.3 Current – impulsive transient

A current transient identified by the identification algorithm is shown in Fig. 5.28 (a). This is the lighting load current captured simultaneously with the voltage transient in Fig. 5.27 (a). Its RMS value calculated in Stage 1 is presented in Table 5.5. From the RMS table, a significant RMS value is observed in the 1st half of the 6th cycle. The RMS values of other cycles are normal.

The frequency spectrum and the extracted disturbance obtained in Stage 2 are shown in Fig. 5.28 (b) and (c) respectively. Table 5.6 shows the crest factor and the peak value calculated for each cycle of the high frequency disturbance. Both crest factor and peak value of the 6th cycle is significantly larger, hence a transient is identified.

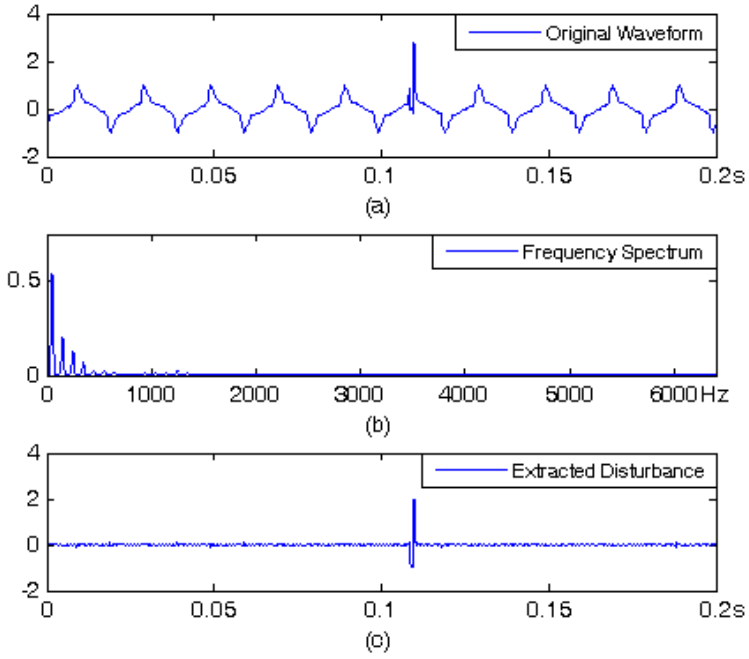

Fig. 5.28 (a) Impulsive transient, (b) Frequency spectrum, (c) Extracted disturbance

Table 5.5
Half-cycle RMS value calculated in Stage 1

Cycle	1st half	2nd half
1	0.42	0.42
2	0.42	0.42
3	0.42	0.42
4	0.42	0.42
5	0.42	0.42
6	0.52	0.44
7	0.42	0.42
8	0.42	0.42
9	0.42	0.42
10	0.42	0.42

Table 5.6
Peak value & Crest Factor calculated in Stage 3

Cycle	Peak value	RMS value	Crest Factor
1	0.09	0.02	3.93
2	0.09	0.02	4.09
3	0.09	0.02	3.96
4	0.08	0.02	3.62
5	0.08	0.02	3.52
6	1.97	0.29	6.68
7	0.08	0.02	3.34
8	0.08	0.03	2.97
9	0.07	0.03	2.75
10	0.08	0.03	2.83

5.3.4 Oscillating Transient

An oscillating transient identified by the identification algorithm is shown in Fig. 5.29 (a). Its RMS value calculated in Stage 1 is presented in Table 5.7. From the RMS table, a significant RMS value is observed in the 1st half of the 6th cycle. The RMS values of other cycles are normal.

The corresponding frequency spectrum and the extracted disturbance obtained in Stage 2 are shown in Fig. 5.29 (b) and (c) respectively. Table 5.8 shows the crest factor and the peak value calculated for each cycle of the high frequency disturbance. Both crest factor and peak value in the 6th cycle is significantly larger, hence a transient is identified.

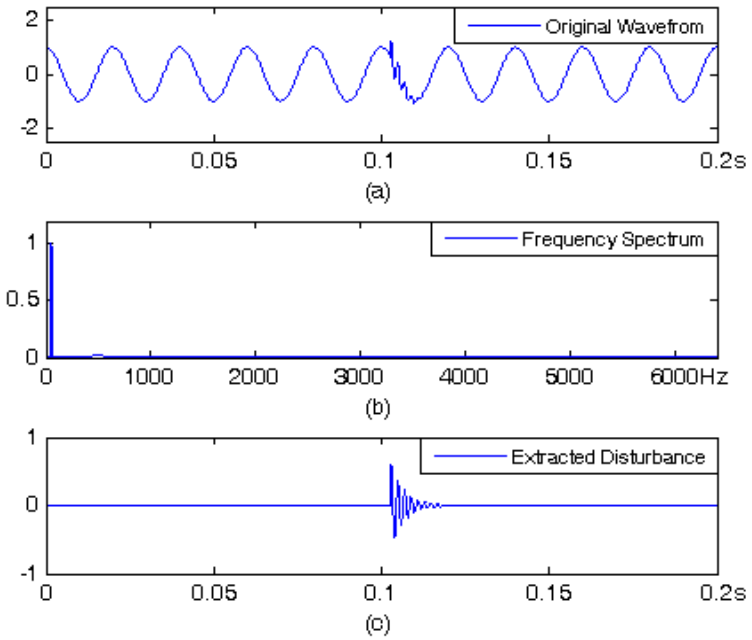

Fig. 5.29 (a) Oscillating transient, (b) Frequency spectrum, (c) Extracted disturbance

Table 5.7
Half-cycle RMS value calculated in Stage 1

Cycle	1st half	2nd half
1	0.71	0.71
2	0.71	0.71
3	0.71	0.71
4	0.71	0.71
5	0.71	0.71
6	0.74	0.71
7	0.71	0.71
8	0.71	0.71
9	0.71	0.71
10	0.71	0.71

Table 5.8
Peak value & Crest Factor calculated in Stage 3

Cycle	Peak value	RMS value	Crest Factor
1	0.00	0.00	1.59
2	0.00	0.00	1.59
3	0.00	0.00	1.59
4	0.00	0.00	1.59
5	0.00	0.00	1.59
6	0.61	0.14	4.37
7	0.01	0.00	4.82
8	0.00	0.00	1.59
9	0.00	0.00	1.59
10	0.00	0.00	1.59

5.3.5 Notches

A notches disturbance identified by the identification algorithm is shown in Fig. 5.30 (a). Its RMS value calculated in Stage 1 is presented in Table 5.9. From the RMS table, no disturbance is identified.

The frequency spectrum and the extracted disturbance obtained in Stage 2 are shown in Fig. 5.30 (b) and (c) respectively. Table 5.10 shows the crest factor and the peak value calculated for each cycle of the high frequency disturbance. As the crest factor and peak value in all cycles are significantly larger, hence more than one transient is identified and it is classified as a notches.

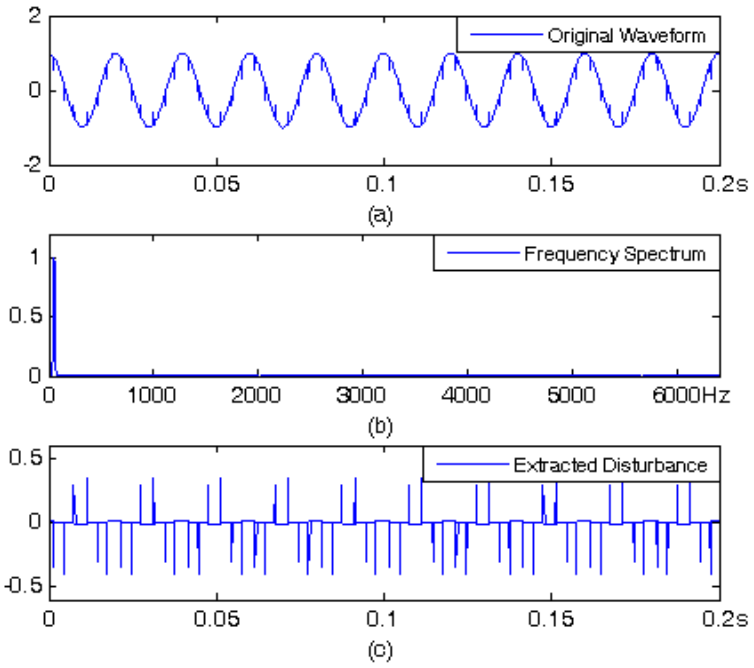

Fig. 5.30 (a) Notches, (b) Frequency spectrum, (c) Extracted disturbance

Table 5.9
Half-cycle RMS value calculated in Stage 1

Cycle	1st half	2nd half
1	0.70	0.70
2	0.70	0.70
3	0.70	0.70
4	0.70	0.70
5	0.70	0.70
6	0.70	0.70
7	0.70	0.70
8	0.70	0.70
9	0.70	0.70
10	0.70	0.70

It is evident from Table 5.10 that the peak value and the crest factor estimated for each cycle are far from the nominal value. Therefore there are transients in each cycle of the voltage waveform, leading to a conclusion that the disturbance is a notches.

Table 5.10
Peak value & Crest Factor calculated in Stage 3

Cycle	Peak value	RMS value	Crest Factor
1	0.40	0.05	7.46
2	0.40	0.05	7.46
3	0.40	0.05	7.46
4	0.40	0.05	7.46
5	0.40	0.05	7.46
6	0.40	0.05	7.46
7	0.40	0.05	7.46
8	0.40	0.05	7.46
9	0.40	0.05	7.46
10	0.40	0.05	7.46

5.4 Tests and Results of the Analysis Method

Five computer simulation tests and an experiment were conducted to evaluate the performance of the proposed analysis method for PQ analysis. Settings of the tests were as follows:

Sampling frequency : 6400 Hz

DWT decomposition level : 6 levels

Shifting offset (ω_1) : 25 Hz

Wavelet – Daubechies : “db20” (length 40)

Sampling window : 0.2 s (10/12-cycle, IEC61000-4-7).

The Daubechies “db20” wavelet is adopted in all the tests. This wavelet has been widely used for PQ analysis [4, 55].

5.4.1 Simulation Test - Harmonics and Inter-harmonics

The synthesized waveform defined by (5.4) is shown in Fig. 5.31. There are nine harmonic components including seven integer harmonics and two inter-harmonics (475 Hz and 775 Hz) as detailed in Table 5.11.

$$x[n] = \sum_m a_m \cos(2\pi n f_m + \theta_m) \tag{5.4}$$

In order to estimate the instantaneous frequencies, amplitudes and phases, all outputs (approximation coefficients) of the algorithm are inversely transformed into time domain and then analyzed by Hilbert transform (HT). The time-frequency plot of the output is shown in Fig. 5.32.

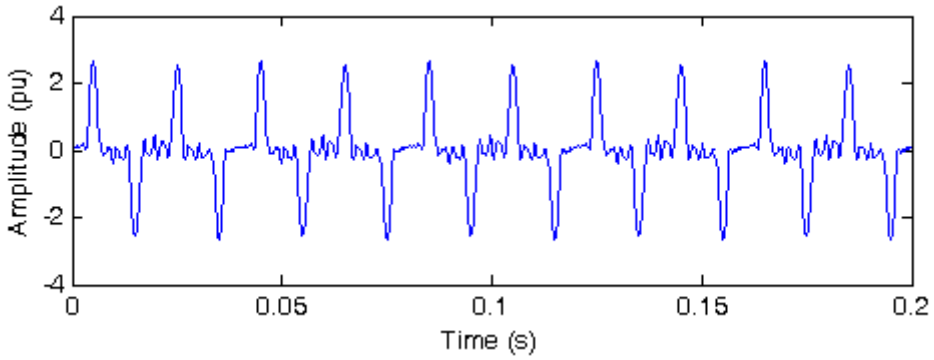

Fig. 5.31 Synthesized waveform with integer and non-integer harmonics

The output frequency bands are combined according to the frequency contents in each band. In this case frequency bands 25 - 50 Hz and 50 - 75 Hz are combined into 25 - 75 Hz for integer harmonics identification, and frequency bands 450 - 475 Hz and 475 - 500 Hz are combined into 450 - 500 Hz for non-integer harmonics identification. The frequencies, amplitudes and phases of the harmonic components are calculated by taking the means of the instantaneous values produced by HT. The results are presented in Table 5.11. It can be seen that the analysis method performs well compared with DWPT.

Fig. 5.33 shows the time-frequency analysis results of DWPT [54] by using the same wavelet (db20). For comparison, the DWPT results were inversed into time domain and analyzed by HT. Due to the leakage problem of the DWPT (as discussed in Section 3), the time-frequency spectrum plot shows fluctuating lines. In this case, HT is unable to provide monotone signals.

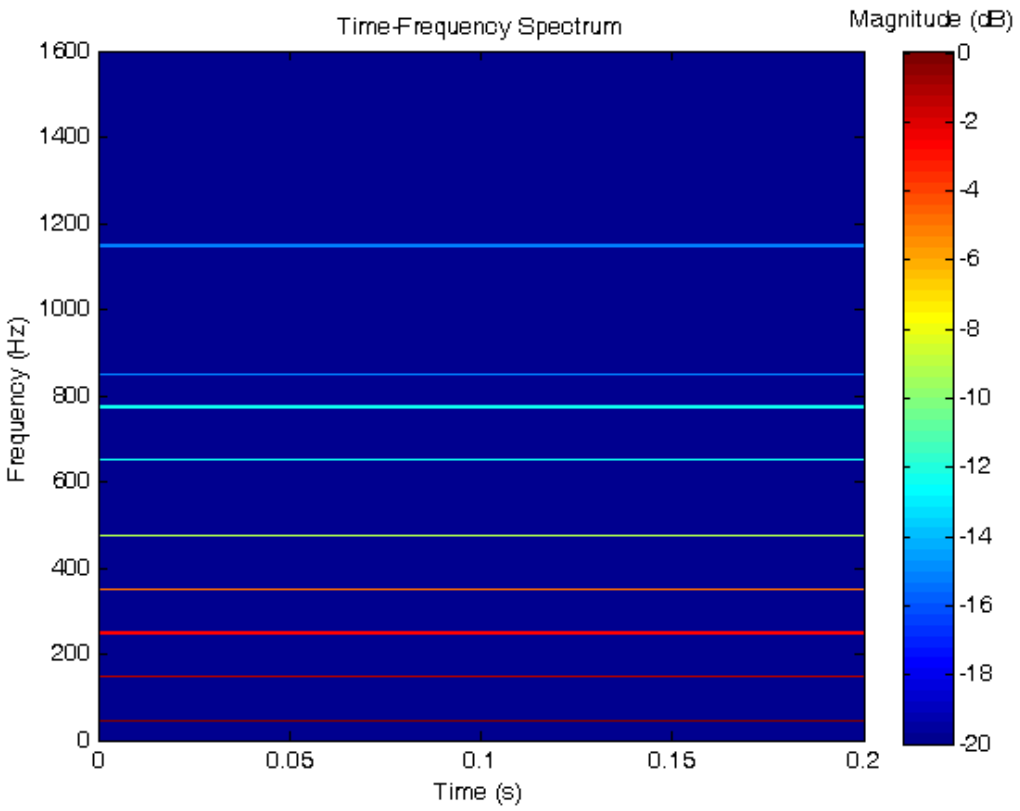

Fig. 5.32 Time-frequency analysis result of the synthesized waveform using the analysis method

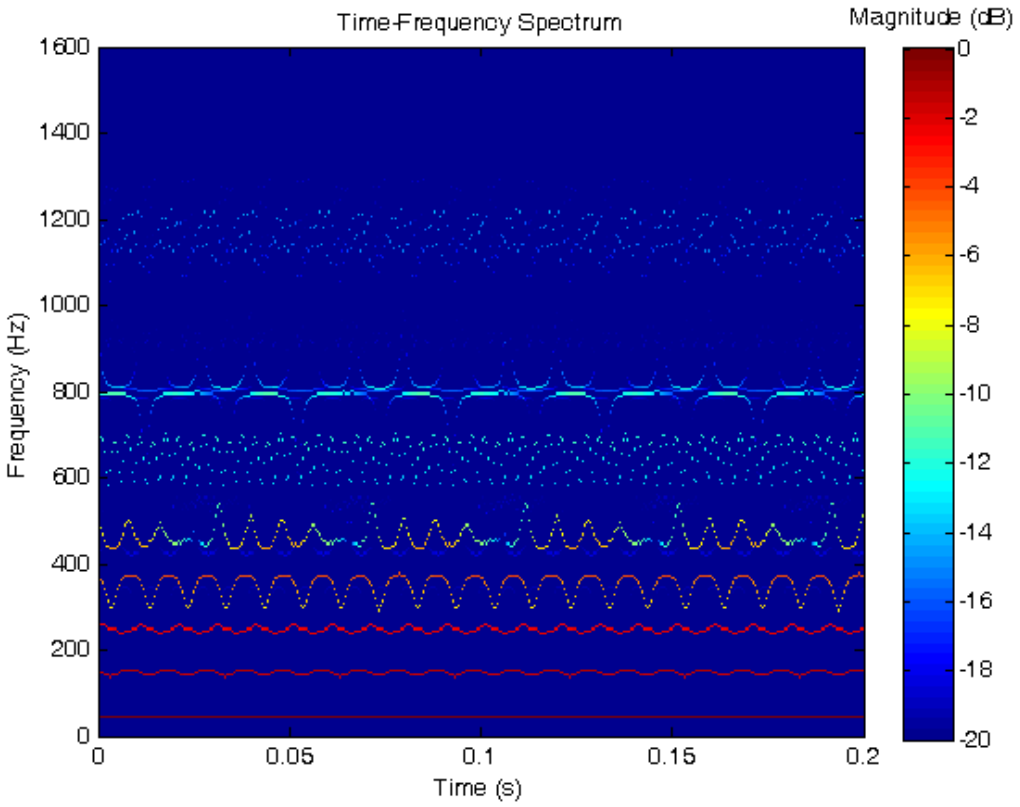

Fig. 5.33 Time-frequency analysis result of the synthesized waveform using DWPT

Table 5.11
Harmonics current estimated by the analysis method and DWPT

Synthesized Waveform			Results by the Proposed Algorithm			Results by DWPT		
Freq. (Hz)	Amp. (pu)	Phase (Degree)	Freq. (Hz)	Amp. (pu)	Phase (Degree)	Freq. (Hz)	Amp. (pu)	Phase (Degree)
50	1.00	-85.23	50	1.00	-85.23	50	1.00	-85.22
150	0.77	89.41	150	0.77	89.40	150	0.74	86.79
250	0.56	-91.02	250	0.56	-91.03	250	0.59	-85.93
350	0.32	88.52	350	0.32	88.51	350	0.29	89.73
475	0.12	-92.03	475	0.12	-92.03	475	0.14	-91.94
650	0.06	87.25	650	0.06	87.25	650	0.06	86.68
775	0.06	-93.48	775	0.06	-93.48	775	0.04	-89.53
850	0.03	85.63	850	0.03	85.63	850	0.03	92.77
1150	0.03	92.59	1150	0.03	92.59	1150	0.03	93.36

5.4.2 Simulation Test - Voltage Sag

The synthesized voltage waveform is shown in Fig. 5.34. It is a pure sinusoidal waveform at 50 Hz and a sag to 80 % happened at 0.1 s. A voltage sag to 80 % can commonly be caused by motor starting. The RMS value calculated from the sampled data is 0.6403. Fig. 5.35 shows the time-frequency plot of the output of the analysis method. The frequency of the voltage waveform is identified as 50 Hz, and the voltage sag appears as small spectra leakage found at around 0.1 s, with a frequency of approximately 100 Hz. Fig. 5.36 shows the instantaneous amplitudes of HT in the frequency band 25 - 75 Hz, in which the amplitude change is evident. The transitional amplitude variation near 0.1 s is due to the finite wavelet length, which is an inherent characteristic of HT. The RMS value estimated from the proposed algorithm is 0.6402. The RMS value calculated from DWPT [61] and the IEC61000-4-70 spectra grouping method are 0.6402 and 0.6401 respectively.

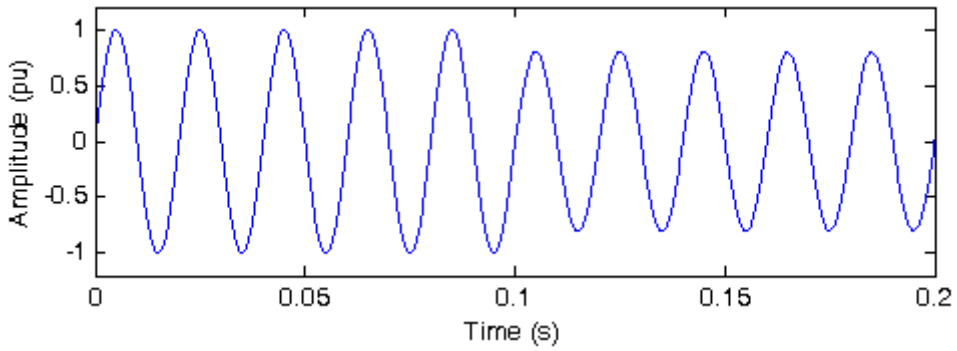

Fig. 5.34 Synthesized waveform with 20 % voltage sag at 0.1 s

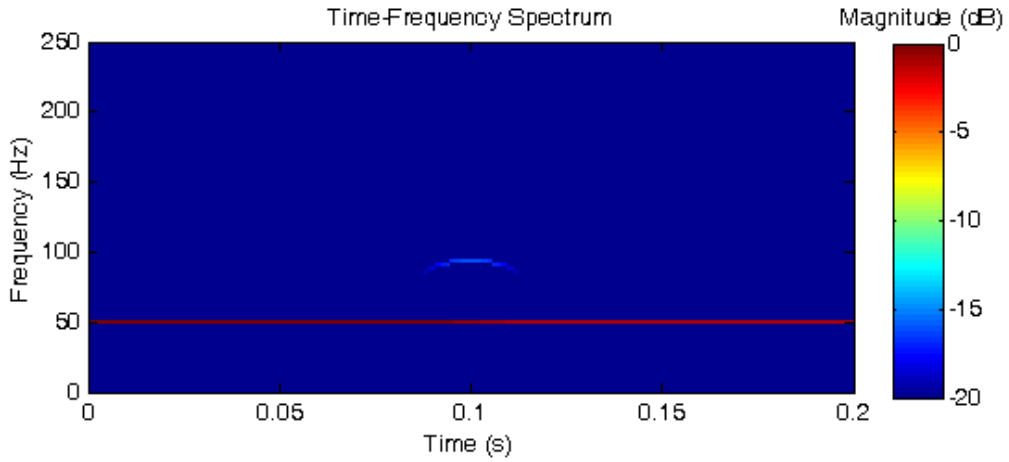

Fig. 5.35 Time-frequency analysis result of the voltage sag by the analysis method

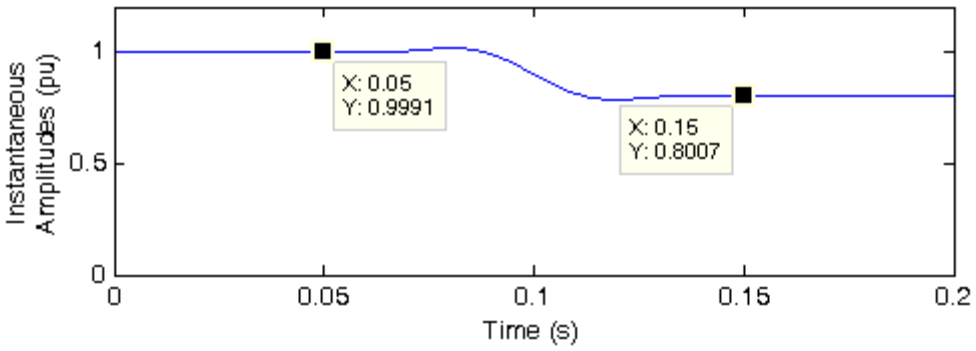

Fig. 5.36 Instantaneous amplitudes in frequency band 25 - 75 Hz

5.4.3 Simulation Test - Oscillating Transient

A 600 Hz oscillating transient is superimposed onto a pure sinusoidal voltage waveform at 50 Hz as shown in Fig. 5.37. The time-frequency plot by the analysis method is shown in Fig. 5.38. As shown, the fundamental component has a frequency of 50 Hz and exhibits constant amplitude. The oscillating transient has a frequency of 600 Hz and is found near 0.09 s, as indicated by the abrupt amplitude change.

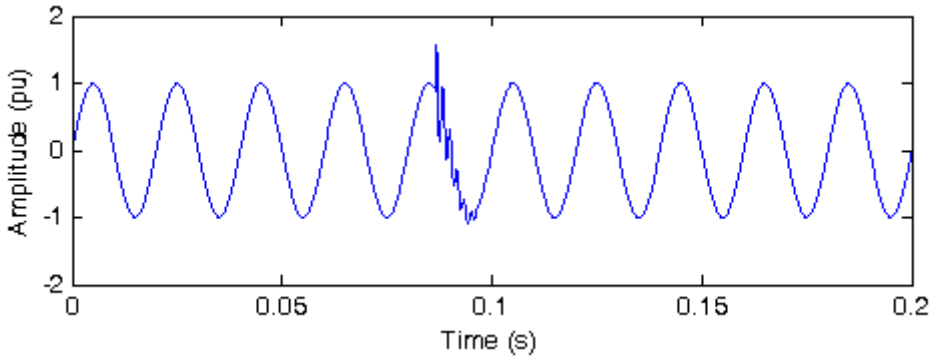

Fig. 5.37 Synthesized waveform with an oscillating transient

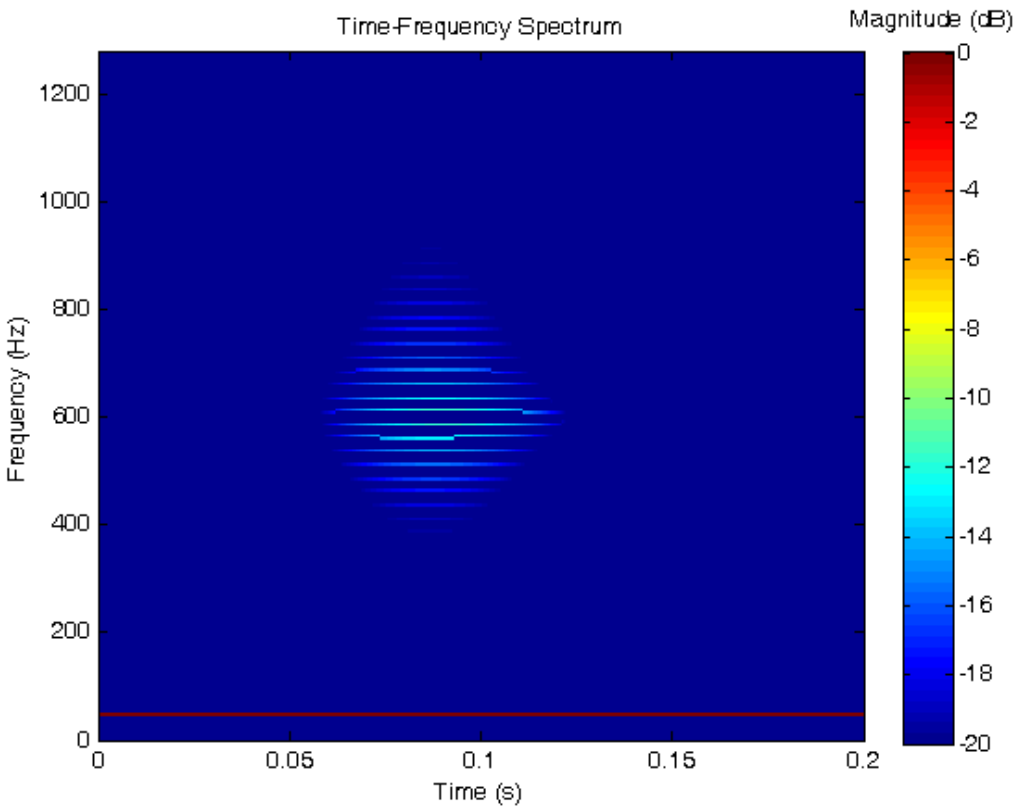

Fig. 5.38 Time-frequency analysis result of the waveform with an oscillating transient by the analysis method

5.4.4 Simulation Test - Voltage Fluctuations (Flicker)

The synthesized waveform defined by (5.5) is shown in Fig. 5.39. The amplitude of the waveform fluctuates between 0.8 and 1.2 times of the rated value. Fig. 5.40 shows the time-frequency plot generated by the analysis method. The voltage fluctuation is identified by the amplitude variation at 50 Hz.

$$x[n] = \cos(2\pi n f_0) \cdot (1 - v_f \cdot \cos(2\pi n f_f)), \tag{5.5}$$

where f_0 is 50 Hz, v_f is 0.2 and f_f is 10 Hz.

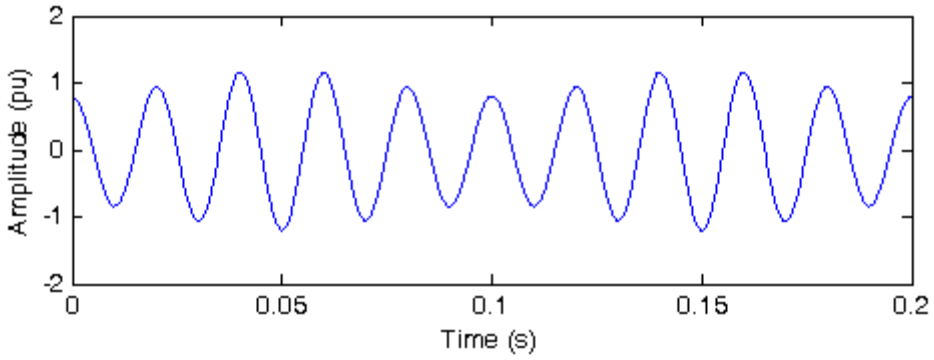

Fig. 5.39 Synthesized waveform with voltage fluctuation

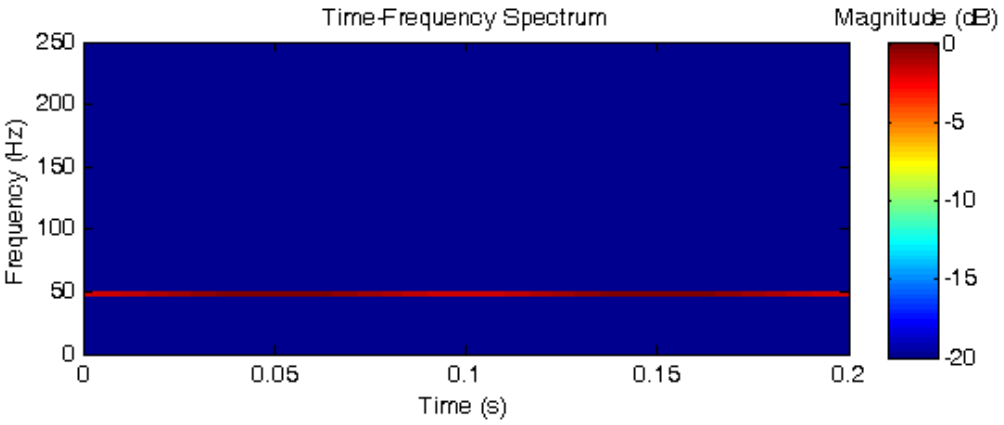

Fig. 5.40 Time-frequency analysis result of the waveform with voltage fluctuation by the analysis method

Fig. 5.41 shows the instantaneous amplitudes estimated by HT in the frequency band 25 - 75 Hz. The amplitude variation can be seen clearly. As a result, the analysis method is able to estimate the fundamental frequency of 50 Hz and the amplitude fluctuation of the synthesized waveform accurately.

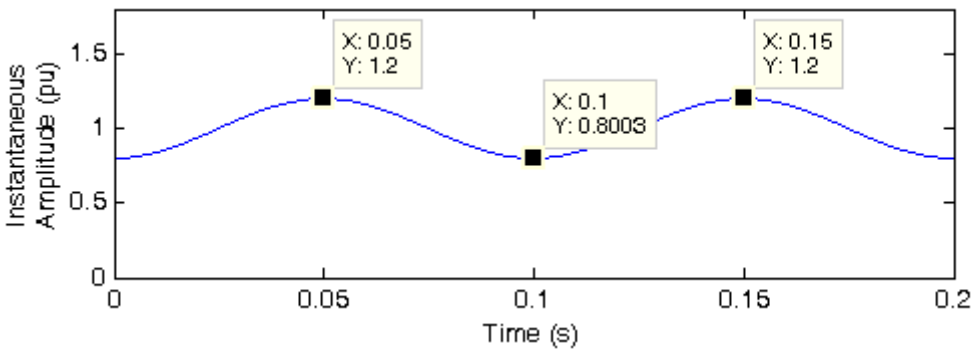

Fig. 5.41 Instantaneous amplitudes in frequency band 25 - 75 Hz

5.4.5 Simulation Test - Frequency variation

In the synthesized waveform, the fundamental frequency of the waveform changes from 50 Hz to 52 Hz at 0.1 s, as shown in Fig. 5.42. Fig. 5.43 shows the time-frequency plot generated by the analysis method, and the frequency variation is identified at 0.1 s. Fig. 5.44 shows the instantaneous frequency estimated by HT in the frequency band 25 - 75 Hz, the frequency variation can be seen clearly. The transitional frequency variation as seen in Fig. 5.44 is due to the finite wavelet length. Overall speaking the analysis method is able to estimate the frequency variation accurately.

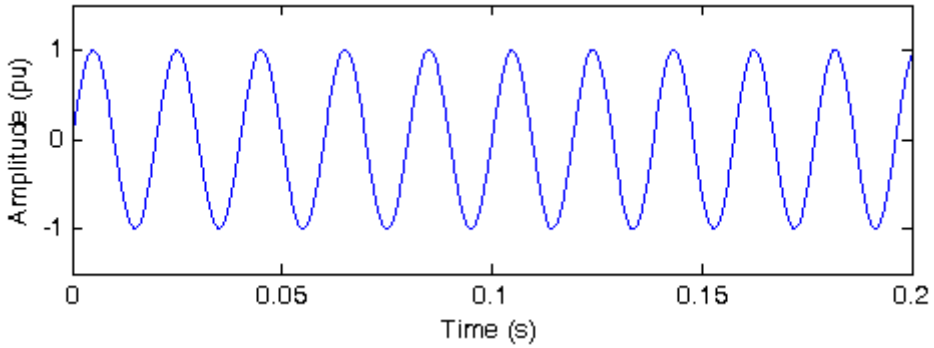

Fig. 5.42 Synthesized waveform with frequency change from 50 Hz to 52 Hz at 0.1 s

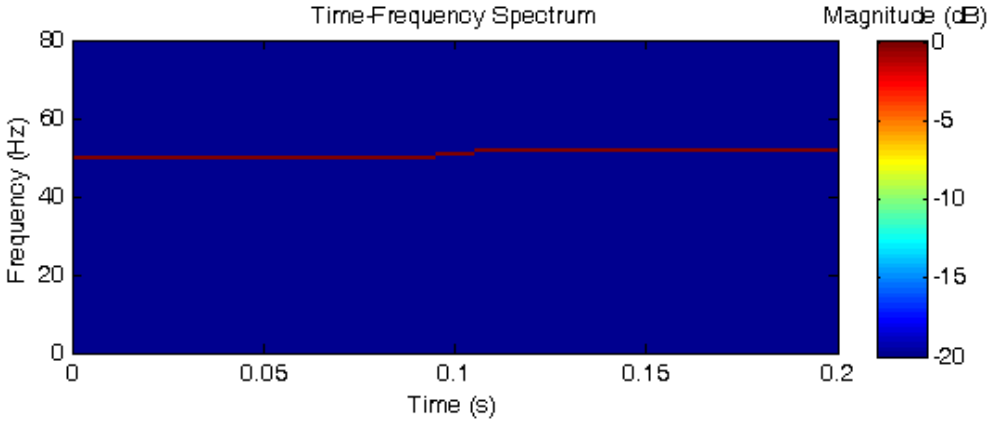

Fig. 5.43 Time-frequency analysis result of the waveform with frequency variation by the analysis method

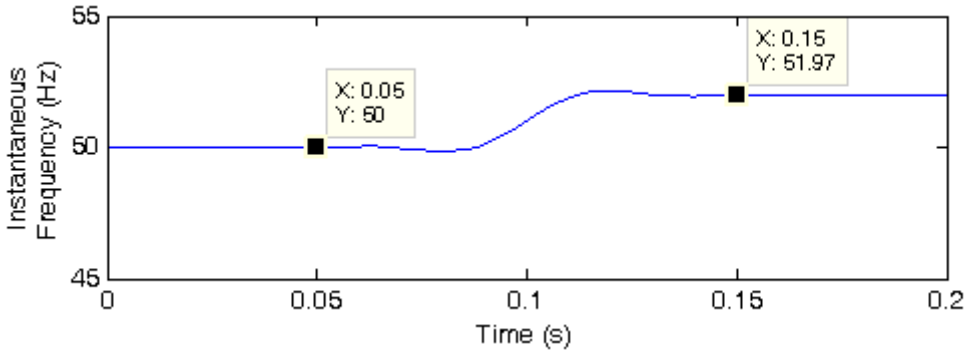

Fig. 5.44 Instantaneous frequencies in frequency band 25 - 75 Hz

5.4.6 Experiment

An experiment is conducted to demonstrate the practical usage of the proposed analysis method. Experiment setup is shown in Fig. 5.1, which is the same as the experiments of the compression algorithm. A multi-functional AC power supply was utilized to simulate electricity supplies of a real-life electric power system, while a lamp box containing electronic-controlled fluorescent lamps and incandescent lamps was utilized to simulate nonlinear loads. The prototype meter was utilized to capture waveforms of both voltage and current.

The multi-functional AC power supply was programmed to generate an approximately 10 % voltage sag, at a fundamental frequency of 50 Hz. Fig. 5.45 shows the voltage waveform. The measured voltage sag is 11 % and it appears from 0 s to 0.08 s. Fig. 5.46 shows the current waveform drawn by the lamp box. The abrupt change in supply voltage causes a current transient at approximately 0.077 s.

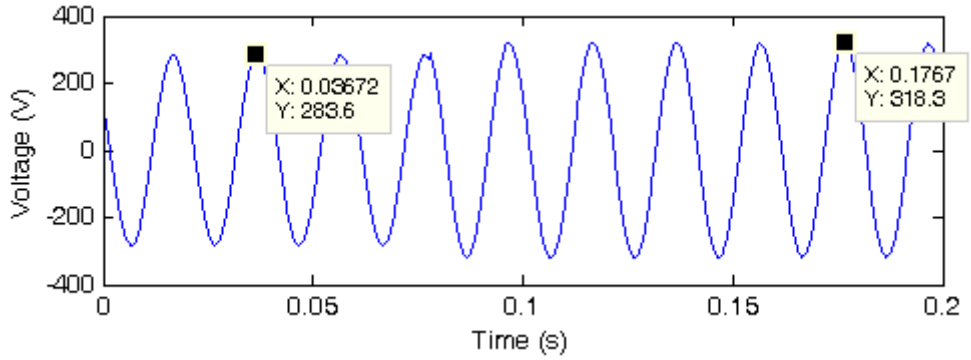

Fig. 5.45 Voltage sag generated by the power supply unit

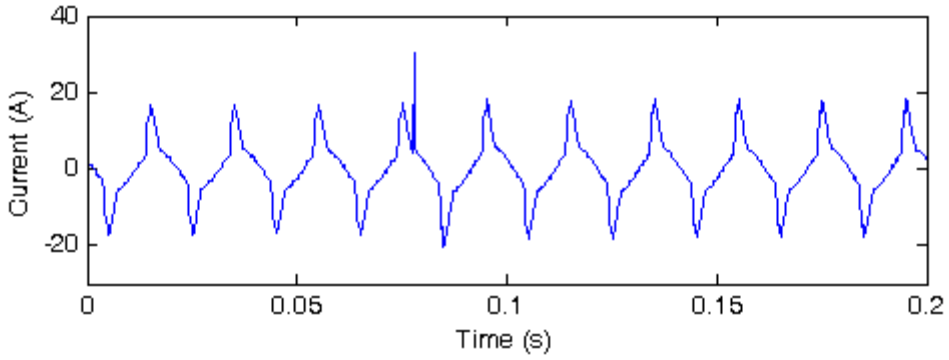

Fig. 5.46 Current drawn by the lamp box

The time-frequency plot of the voltage sag is shown in Fig. 5.47. The voltage frequency is identified as 50 Hz, and the high frequency component at around 0.07 s to 0.08 s denotes the amplitude change. Fig 5.48 shows the instantaneous amplitudes of the voltage waveform generated by the analysis method. It can be seen that the amplitude variations of the supply voltage are clearly identified and the voltage sag is 11 %.

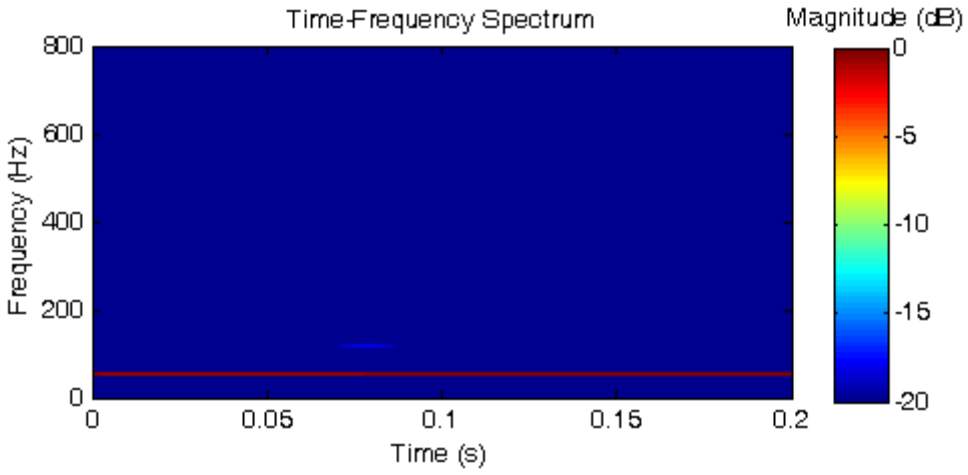

Fig. 5.47 Time-frequency analysis result of the captured voltage sag by the analysis method

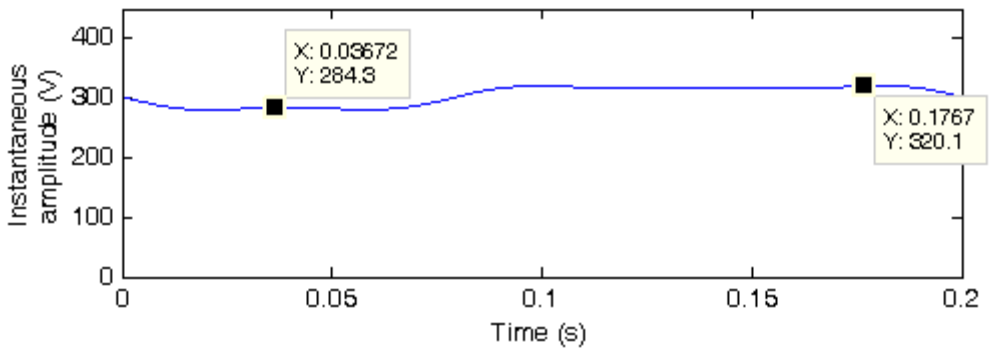

Fig. 5.48 Instantaneous amplitudes in frequency band 25 - 75 Hz of the voltage sag estimated by the analysis method

Fig 5.49 shows the time-frequency plot of the current waveform estimated by the analysis method. The transient in the current waveform is seen as a wide-spread abrupt amplitude change around 0.06 – 0.08 s. The current transient is caused by the amplitude change in voltage happened around 0.07 – 0.08 s.

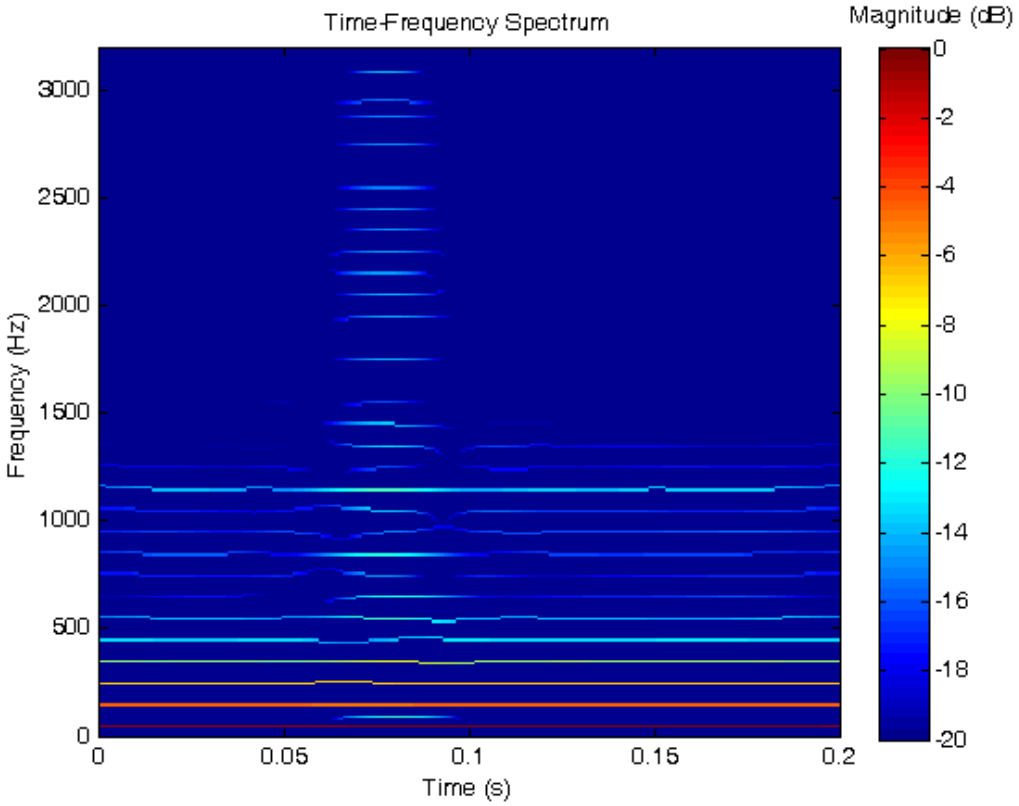

Fig. 5.49 Time-frequency analysis result of the current by the analysis method

Table 5.12 presents the current harmonics estimated by the analysis method, obtained by taking the means of their respective instantaneous values estimated by HT.

Table 5.12
Harmonics current estimated by the analysis method

Frequency (Hz)	Amplitude (A)	Phase (Degree)
50	9.87	72.05
150	3.65	-107.03
250	2.33	68.53
350	1.21	-108.14
450	0.48	102.02
550	0.45	-21.41
650	0.23	96.18
750	0.20	34.22
850	0.28	-75.33
950	0.25	116.06
1050	0.24	-18.72
1150	0.46	8.58
1250	0.17	-6.21
1350	0.17	-62.34
1450	0.13	33.86

5.5 Summary

Tests were performed to evaluate feasibilities and performances of the three proposed methods – the compression algorithm, the identification algorithm, and the analysis method. Since usages and purposes of the three proposed methods are not the same, different tests were designed and conducted for each of the proposed methods.

Firstly, experiments and a field test were performed for the compression algorithm. The tests evaluated the compression algorithm in terms of compression ratio (CR) and signal-to-noise ratio (SNR). In the experiments, different power quality events of an electric power system were simulated via a multi-functional AC power supply. On the other hand, the field test was performed in a real-life electric power distribution system. In the experiments and the field tests, the developed prototype electric power monitoring system

in Chapter 4 is utilized to capture and compress electric waveforms for performance evaluations.

Overall speaking, the compression algorithm is able to achieve a better SNR vs. CR performance than the WPT-based method. Besides, the adaptive threshold supports perfect reconstruction on significant features (e.g. transients) of electric waveforms, which is not feasible with the WPT-based method. The SNR and CR are dependent on the status of the electric power system and types of PQ events. In most cases, a compression ratio from 30 to 80 can be achieved at a SNR of 40dB. Hence, requirements on memory storage and networking bandwidth can be lowered significantly for remote monitoring of electric waveforms.

Secondly, experiments were performed for the identification algorithm. In the experiments, different electric power disturbances were generated by the multi-functional AC power supply. The prototype monitoring system was utilized to identify the generated disturbances. Analysis results of each stage of the identification algorithm are provided in detail so that the processes of the identification algorithm can be visualized readily.

As illustrated by the test results, both the feasibility and the effectiveness of the identification algorithm were verified. It is able to identify disturbances not only in voltage, but also in current. During the processes, stationary components are separated from electric power disturbances; hence, the identification algorithm is unaffected by time-varying harmonics of the current. As a result, it can identify voltage and current disturbances in the same way with simple power quantities, such as RMS value, peak value and crest factor, effectively.

Thirdly, simulation tests and an experiment were performed for the analysis method. In the simulation tests, synthesized electric waveforms were used to verify the accuracy and the effectiveness of the analysis method. Analyzed results were compared with the synthesized waveform features. Meanwhile, an experiment was performed to give a demonstration on practical usages of the analysis method.

Unlike Discrete Wavelet Packet transform (DWPT), the proposed analysis method does not have the non-uniform leakage problem as discussed in Section 2.3.3.2 of Chapter 2.

Hence, it outperformed DWPT for harmonic analysis in the tests. Furthermore, the approximated coefficients obtained from the analysis result can be used to calculate electric power quantities (e.g. RMS value). As shown in the tests, RMS value estimated by the analysis method is more accurate than the grouping method recommended in IEC61000-4-7. Also, the analysis method can be used to detect electric power quality problems (e.g. flickers) as shown in the tests.

In conclusion, the feasibilities and performances of the three proposed methods – the compression algorithm, the identification algorithm, and the analysis method were verified and demonstrated by the tests using the prototype electric power monitoring system.

Chapter 6

Conclusion

6.1 Conclusion of the Research Study

In this thesis, a novel electric power quality monitoring system is proposed for monitoring and analyzing transients in electric power systems. Compared with existing electric power quality monitoring systems, the proposed monitoring system is able to provide more detailed information and analysis on the status and disturbance events of electric power systems. Novelties of the proposed monitoring system are in three major aspects.

6.1.1 The Electric Waveform Compression Algorithm

Firstly, the proposed monitoring system is capable of providing not only traditional electric power quantities (e.g. Power factor, RMS value, and Harmonic Distortion) as in existing monitoring system, but also electric waveforms of voltage and current. Compared to the electric power quantities, the electric waveforms are more useful for troubleshooting in electric power systems as suggested in IEC 61000-4-30. The electric waveforms are neither averaged nor accumulated measurement results. They are raw measurement results which represent voltage and current status of electric power systems. They offer good time resolutions and flexibilities to analyze fast changing disturbance events happened in the electric power systems. They help electrical engineers to understand problems of electric power systems more easily. Such information cannot be obtained from mere electric power quantities.

Electric waveforms are desirable when dedicated troubleshooting in electric power systems is necessary. However, recording and transferring electric waveforms require a huge amount of computing memory and networking bandwidth. Hence, an electric

waveform compression algorithm is designed for the proposed monitoring system to lower the requirements on both memory and bandwidth.

This proposed compression algorithm is specially designed for applications in electric power monitoring systems. It can compress electric waveforms of voltage and current effectively. Stationary and non-stationary components of electric waveforms are separated and compressed by different means. Fast Fourier Transform is utilized to extract and model stationary components of electric waveforms in terms of cosine functions. The Integer Discrete Wavelet Transform, the adaptive threshold scheme and the Huffman coding are applied to compress non-stationary components. The adaptive threshold enables significant features (e.g. transient) in electric waveforms to be compressed and preserved with less error and prefect reconstruction is realized.

Performances of the proposed compression algorithm are successfully verified by the experiments and the field test. In most cases, a compression ratio from 30 to 80 can be achieved at a signal-to-noise ratio of 40dB.

6.1.2 The Disturbance Identification Algorithm

Secondly, the proposed monitoring system is capable of detecting and identifying electric power disturbances on electric power systems automatically. It can help in improving the reliability of electric power systems. Instead of being ignored or classified as unknown problems, disturbance events can be identified without manual inspections and spot tests. It can alert electrical engineers to carry out improvements and to avoid the same disturbance events from happening again. As a result, chances of equipment damages and malfunctions can be reduced, and the reliability of the electric power systems can be improved.

Unlike other existing disturbance identification algorithms, the proposed disturbance identification algorithm is capable of identifying electric power disturbance not only in voltage, but also in current. By separating stationary and non-stationary components in electric waveforms, a generalized approach to identify voltage and current disturbance with simple electric power quantities (e.g. RMS value) is proposed. Hence, it helps the proposed identification algorithm to identify more problems and disturbance events in electric power systems.

Moreover, the proposed identification algorithm is designed to work together with the proposed compression algorithm. Part of their processes and data, such as the separation of stationary and non-stationary components, are identical. Hence, they can share data and processes to enhance computational efficiency. A prototype meter integrated with the compression and identification algorithms is successfully developed for feasibility evaluations. The meter is embedded with a mid-range digital signal processor, and it can implement both algorithms for real-time applications. It is verified that the proposed algorithm and the prototype meter is able to perform remote electric waveform and disturbance monitoring on a low speed network (Zigbee) in real-time.

6.1.3 The Analysis Method for Time-Varying Harmonic and Disturbance

Thirdly, in addition to the waveform monitoring and the disturbance identification, the proposed monitoring system is integrated with a novel analysis method. The method can analyze recorded electric waveforms of the proposed monitoring system in time-frequency domain. It is especially useful for analyzing time-varying harmonics and disturbances in electric power systems. It can provide additional analytical information for electrical engineer to evaluate the problems and the status of electric power systems.

The proposed analysis method is similar to Discrete Wavelet Packet Transform (DWPT). It decomposes electric waveforms into multiple frequency bands for detailed analysis. By using Hilbert Transform (HT) and Discrete Wavelet Transform (DWT) together to decompose electric waveforms in a frequency-shifting manner, the non-uniform leaking problem inherent with DWPT has been overcome.

Performances of the proposed analysis method are verified by the tests. It outperforms DWPT in time-varying harmonics analysis, and it is suitable for analyzing various kinds of electric power disturbances, such as transients and voltage fluctuations.

6.1.4 The Proposed Electric Power Quality Monitoring System

Overall speaking, three novel methods are introduced for the proposed electric power quality monitoring system. Besides measuring traditional electric power quantities, the proposed monitoring system is also capable of monitoring electric waveforms,

identifying electric power disturbance, and analyzing time-frequency characteristics for time-varying harmonics and disturbances.

Electric power systems are facing more and more challenges, such as the penetration of renewable energy resources at various levels of the electric power systems, the installation of enormous electric vehicle charging networks, and numerous building integrated intelligent demand response management facilities. As a result, a robust power quality monitoring system that can perform real-time monitoring of the power quality and status of the electric power systems are indispensable. It is believed that such a system should form an integral part of the so called smart grid technology. It is hoped that the proposed electric power quality monitoring system may be able to relieve existing and potential problems of the future electric power systems under the smart grid technology.

6.2 Areas for Further Research

In this study, the proposed monitoring system is implemented as a prototype only; hence, the system architecture is relatively simple, containing only a prototype meter and a central monitoring system. The current system architecture is suitable for small scale monitoring only. Significant improvement works should be carried out (e.g. adding a sub-monitoring system) so that the future system can handle hundreds or even thousands of meters simultaneously.

Automatic control has been a trend in many industries. Self-healing is one of the major targets in future electric power systems i.e., smart gird technology. The proposed monitoring system in this study has provided a solid foundation in analyzing and identifying problems for electric power systems. Based on this study, a self-diagnosis system which can automatically analyze and locate problems on electric power systems, is to be explored and developed for the smart gird applications.

Experiences tell us that many serious problems (e.g. blackout) of electric power systems can be avoided, if preventive measures were carried out in the first place. In some scenarios, early signs of these problems can be found in the power quality information database recorded by the electric power quality monitoring system. However, operators of electric power systems are rarely aware of the significance of these records until problems occurred suddenly. Hence, an expert system, which can provide alerts for

operators to carry out preventive measures, is desired to be developed and integrated in the proposed electric power quality monitoring systems of this research study.

List of Publications

Journal papers

1. J. Y. C. Chan, N. C. F. Tse, and L. L. Lai, "A Coreless Electric Current Sensor with Circular Conductor Positioning Calibration," IEEE Transactions on Instrumentation and Measurement, vol. 62, pp. 2922-2928, 2013.

2. N. C. F. Tse, J. Y. C. Chan, W. H. Lau, and L. L. Lai, "Hybrid Wavelet and Hilbert Transform with Frequency-Shifting Decomposition for Power Quality Analysis," IEEE Transactions on Instrumentation and Measurement, vol. 61, pp. 3225-3233, 2012.

3. N. C. F. Tse, J. Y. C. Chan, W. H. Lau, J. T. Y. Poon, and L. L. Lai, "Real-Time Power-Quality Monitoring with Hybrid Sinusoidal and Lifting Wavelet Compression Algorithm," IEEE Transactions on Power Delivery, vol. 27, pp. 1718-1726, 2012.

Conference papers

4. J. Y. C. Chan, J. M. K. So, M. C. Leung, N. C. F. Tse, W. H. Lau, “Power Quality and Energy Usage of a Multi-Purpose Building in Hong Kong," in Advances in Power System Control, Operation and Management (APSCOM 2012), 9th International Conference on, 2012, pp. 1-6.

5. N. C. F. Tse, W. H. Lau, and J. Y. C. Chan, "ZigBee based smart metering network for monitoring building integrated electric vehicle charging circuits," in Power and Energy Society General Meeting, 2010 IEEE, 2010, pp. 1-5.

6. N. C. F. Tse, J. Y. C. Chan, and L. L. Lai, "Development of a smart metering scheme for building smart grid system," in Advances in Power System Control, Operation and Management (APSCOM 2009), 8th International Conference on, 2009, pp. 1-5.

7. N. C. F. Tse, W. W. Y. Ng, T. T. Chow, J. Chan, L. L. Lai, D. S. Yeung, and L. Jincheng, "Data Mining of Building Electrical Information Based on Radial Basis Function Neural Network," in Intelligent System Applications to Power Systems, 2009. ISAP '09. 15th International Conference on, 2009, pp. 1-4.

References

[1] Electromagnetic compatibility (EMC) - Part 4-7: Testing and measurement techniques - General guide on harmonics and interharmonics measurements and instrumentation, for power supply systems and equipment connected thereto, IEC 61000-4-7 ed2.1, Oct. 2009.

[2] Electromagnetic compatibility (EMC) - Part 4-30: Testing and measurement techniques - Power quality measurement methods, IEC 61000-4-30 ed2.0, Oct. 2008.

[3] IEEE Recommended Practice for Monitoring Electric Power Quality, IEEE Std 1159-2009 (Revision of IEEE Std 1159-1995), Jun. 2009.

[4] J. Barros and R. I. Diego, "Analysis of Harmonics in Power Systems Using the Wavelet-Packet Transform," *IEEE Trans. Instrumentation and Measurement*, vol. 57, no. 1, pp. 63-69, Jan. 2008.

[5] "Sustainable Development indicators - Theme 4: Ensuring a secure and reliable gas and electricity supply," [Online]. Available: https://www.ofgem.gov.uk/ofgem-publications/59150/ensuring-secure-and-reliable-gas-and-electricity-supply.pdf [Accessed: Nov. 18 2013].

[6] "Coal & Electricity," [Online]. Available: http://www.worldcoal.org/coal/uses-of-coal/coal-electricity/ [Accessed: Nov. 18 2013].

[7] D. Chapman, "Power Quality Application Guide – Cost: The Cost of Poor Power Quality," [Online]. Available: http://www.copperinfo.co.uk/power-quality/downloads/pqug/21-the-cost-of-poor-power-quality.pdf [Accessed: Nov. 18 2013].

[8] A.V. Oppenheim, A.S. Wilsky and I.T. Young, Signals and Systems, Prentice Hall, 1983.

[9] Oppenheim AV, Schafer RW. Discrete-Time Signal Processing. Prentice-Hall, 1989.

[10] N. E. Huang and S. S. P. Shen, *Hilbert-Huang Transform and Its Applications*. Singapore: World Scientific, 2005.

[11] S. Haykin, Communication Systems, John Wiley & Sons, 2000

[12] S. Mallat, A Wavelet Tour of Signal Processing, The Sparse Way, Academic Press, Dec. 2008.

[13] W. Sweldens, "The lifting scheme: A construction of second generation wavelets," SIAM J. Math. Anal., vol. 29, no. 2, pp. 511-546, 1997.

[14] I. Daubechies and W. Sweldens, "Factoring wavelet transforms into lifting steps," J. Fourier Anal. Appl., vol. 4, no. 3, pp. 247-269, 1998.

[15] R. Calderbank, I. Daubechies, W. Sweldens, and B.-L. Yeo, "Wavelet transforms that map integers to integers," Appl. Comput. Harmon. Anal., vol. 5, no. 3, pp. 332-369, 1998.

[16] E. Muljadi, C. P. Butterfield, J. Chacon, H. Romanowitz, "Power quality aspects in a wind power plant," IEEE Power Engineering Society General Meeting, Montreal, Que., 18-22 Jun. 2006.

[17] H. D. Mathur, L. B. F. Leite, H. Siguerdidjane, Y. K. Bhateshvar, "Study of impact of wind power penetration on frequency stabilization in multi-area power system," 8th International Symposium on Advanced Topics in Electrical Engineering (ATEE), Bucharest, 23-25 May 2013.

[18] S. Santoso, E. J. Powers and W. M. Grady, "Power quality disturbance data compression using wavelet transform methods," IEEE Trans. Power Delivery, vol. 12, no. 3, pp. 1250-1257, Jul. 1997.

[19] T. B. Littler and D. J. Morrow, "Wavelets for the analysis and compression of power system disturbances," IEEE Trans. Power Delivery, vol. 14, no. 2, pp. 358-364, Apr. 1999.

[20] P. K. Dash, B. K. Panigrahi, D. K. Sahoo and G. Panda, "Power quality disturbance data compression, detection, and classification using integrated spline wavelet and S-transform," IEEE Trans. Power Delivery, vol. 18, no. 2, pp. 595-600, Apr. 2003.

[21] M. V. Ribeiro, J. M. T. Romano and C. A. Duque, "An improved method for signal processing and compression in power quality evaluation," IEEE Trans. Power Delivery, vol. 19, no. 2, pp. 464-471, Apr. 2004.

[22] M. V. Ribeiro, S. H. Park, J. M. T. Romano and S. K. Mitra, "A Novel MDL-based Compression Method for Power Quality Applications," IEEE Trans. Power Delivery, vol. 22, no. 1, pp. 27-36, Jan. 2007.

[23] N. Otsu, "A Threshold Selection Method from Gray-Level Histograms," IEEE Trans. Systems, Man and Cybernetics, vol. 9, no. 1, pp. 62-66, Jan. 1979.

[24] E. Y. Hamid and Z. I. Kawasaki, "Wavelet-based data compression of power system disturbances using the minimum description length criterion," IEEE Trans. Power Delivery, vol. 17, no. 2, pp. 460-466, Apr. 2002.

[25] M. H. J. Bollen, "What is power quality?," Electric Power Systems Research, vol. 66, no. 1, pp. 5-14, Jul. 2003.

[26] W. E. Brumsickle, D. M. Divan, G. A. Luckjiff, J. W. Freeborg, R. L. Hayes, "Power quality and reliability," IEEE Industry Applications Magazine, vol. 11, no. 1, pp. 48-53, Jan. 2005.

[27] IEEE Guide for Identifying and Improving Voltage Quality in Power Systems, IEEE Std. 1250-2011, Mar. 2011.

[28] L. Xie, P. M. S. Carvalho, L. A. F. M. Ferreira, J. H. Liu, B. H. Krogh, N. Popli, M. D. Ilic, "Wind Integration in Power Systems: Operational Challenges and Possible Solutions," Proceedings of the IEEE , vol. 99, no.1, pp. 214,232, Jan. 2011.

[29] R. G. Stockwell, L. Mansinha and R. P. Lowe, "Localization of the complex spectrum: the S transform," IEEE Trans. Signal Processing, vol. 44, no. 4, pp. 998-1001, Apr. 1996.

[30] A. M. Gaouda, M. A. Salama, M. R. Sultan, and A. Y. Chikhani, "Power Quality Detection and Classification Using Wavelet- Multi resolution Signal Decomposition," IEEE Trans. Power Delivery, Vol. 14, no. 4, pp. 1469-1476, Oct. 1999.

[31] S. Santoso, J. P. Edward, W. M. Grady and A. C. Parsons, "Power quality disturbance waveform recognition using wavelet-based neural classifier - Part 1: Theoretical foundation," IEEE Trans. Power Delivery, vol. 15, no. 1, pp. 222-228, Jan. 2000.

[32] S. Santoso, J. P. Edward, W. M. Grady and A. C. Parsons, "Power quality disturbance waveform recognition using wavelet-based neural classifiers - Part 2: Application," IEEE Trans. Power Delivery, vol. 15, no. 1, pp. 229-235, Jan. 2000.

[33] S. Kaewarsa, K. Attakitmongcol and T. Kulworawanichpong, "Recognition of power quality events by using multiwavelet-based neural networks," Int J Electrical Power and Energy Systems, vol. 30, no. 4, pp. 254-260, May 2008.

[34] M. Oleskovicz, D. V. Coury, O. D. Felho, W. F. Usida, A. A. F. M. Carneiro and L. R. S. Pires, "Power quality analysis applying a hybrid methodology with wavelet

transforms and neural networks," Int J Electrical Power and Energy Systems, vol. 31, no. 5, pp. 206-212, Jun. 2009.

[35] C. N. Bhende, S. Mishra, B. K. and Panigrahi, "Detection and classification of power quality disturbances using S-transform and modular neural network," Electric Power Systems Research, vol. 78, no. 1, pp. 122-128, Jan. 2008.

[36] S. Mishra, C.N. Bhende and B.K. Panigrahi, "Detection and Classification of Power Quality Disturbances Using S-Transform and Probabilistic Neural Network," IEEE Trans. Power Delivery, vol. 23, no. 1, pp. 280-287, Jan. 2008.

[37] S. Haykin, Neural Networks: A Comprehensive Foundation, Prentice Hall, 1999.

[38] "Smart Grid," [Online]. Available: http://energy.gov/oe/technology-development/smart-grid [Accessed: Nov. 18 2013].

[39] R. G. Stockwell, "S-transform analysis of gravity wave activity from a small scale network of airglow imagers," Ph.D. thesis, University of Western Ontario, London, Ontario, Canada, 1999.

[40] S. Qian and D. Chen, "Discrete Gabor transform," IEEE Trans. Signal Processing, vol. 41, no. 7, pp. 2429-2438, Jul. 1993.

[41] W. Mecklenbräuker and F. Hlawatsch, The Wigner Distribution: Theory and Applications in Signal Processing. Elsevier Science, 1997.

[42] S. C. Pei and J. J. Ding, "Relations Between Gabor Transforms and Fractional Fourier Transforms and Their Applications for Signal Processing," IEEE Trans. Signal Processing, vol. 55, no. 10, pp. 4839-4850, Oct. 2007.

[43] N. E. Huang, S. S. P. Shen, et al, Hilbert-Huang Transform and Its Applications. Singapore: World Scientific, 2005.

[44] R. Yan and R X. Gao, "A Tour of the Hilbert-Huang Transform: An Empirical Tool for Signal Analysis," IEEE Instrumentation & Measurement Magazine, vol. 10, no. 5, pp. 40-45, Oct. 2007.

[45] N. E. Huang, M. C. Wu, S. R. Long, S. P. Shen, W. Qu, P. Gloersen, K. L. Fan, "A confidence limit for the empirical mode decomposition and the Hilbert spectral analysis," Proc. Royal Soc. A, vol. 459, no. 2037, pp. 2317-2345, Sep. 2003.

[46] S. Santoso, E.J. Powers, W.M. Grady and P. Hofmann, "Power quality assessment via wavelet transform analysis," IEEE Trans. Power Delivery, vol. 11, no. 2, pp. 924-930, Apr. 1996.

[47] J. Liang, S. Elangovan and J. B. X. Devotta, "A wavelet multiresolution analysis approach to fault detection and classification in transmission lines," International

Journal of Electrical Power & Energy Systems, vol. 20, no. 5, pp. 327-332, Jun. 1998.

[48] D. G. Ece, and O. N. Gerek, "Power quality event detection using joint 2-D-wavelet subspaces," IEEE Tran. Instrumentation and Measurement, vol. 53, no. 4, pp. 1040-1046, Aug. 2004.

[49] M. Uyar, S. Yildirim and M. T. Gencoglu, "An effective wavelet-based feature extraction method for classification of power quality disturbance signals," Electric Power Systems Research, vol. 78, no. 10, pp. 1747-1755, Oct. 2008.

[50] M. Oleskovicz, D. V. Coury, O. D. Felho, W. F. Usida, A. A. F. M. Carneiro and L. R. S. Pires, "Power quality analysis applying a hybrid methodology with wavelet transforms and neural networks," International Journal of Electrical Power & Energy Systems, vol. 31, no. 5, pp. 206-212, Jun 2009.

[51] C. C. Liao, H. T. Yang and H. H. Chang, "Denoising Techniques With a Spatial Noise-Suppression Method for Wavelet-Based Power Quality Monitoring," IEEE Tran. Instrumentation and Measurement, vol. 60, no. 6, pp. 1986-1996, Jun. 2011.

[52] W. K. Yoon and M. J. Devaney, "Power measurement using the wavelet transform," IEEE Trans. Instrumentation and Measurement, vol. 47, no. 5, pp. 1205-1210, Oct. 1998.

[53] E. Y. Hamid and Z. I. Kawasaki, "Wavelet packet transform for RMS values and power measurements," IEEE Power Engineering Review, vol. 21, no. 9, pp. 49-51, Sep. 2001.

[54] V. L. Pham and K. P. Wong, "Antidistortion method for wavelet transform filter banks and nonstationary power system waveform harmonic analysis," IEE Proc. Generation, Transmission and Distribution, vol. 148, no. 2, pp. 117-122, Mar. 2001.

[55] C. Parameswariah and M. Cox, "Frequency characteristics of wavelets," IEEE Trans. Power Delivery, vol. 17, no. 3, pp. 800-804, Jul. 2002.

[56] J. L. J. Driesen and R. J. M. Belmans, "Wavelet-based power quantification approaches," IEEE Tran. Instrumentation and Measurement, vol. 52, no. 4, pp. 1232-1238, Aug. 2003.

[57] J. Barros and R. I. Diego, "Application of the wavelet-packet transform to the estimation of harmonic groups in current and voltage waveforms," IEEE Trans. Power Delivery, vol. 21, no. 1, pp. 533-535, Jan. 2006.

[58] L. Eren, M. Unal and M. J. Devaney, "Harmonic Analysis Via Wavelet Packet Decomposition Using Special Elliptic Half-Band Filters," IEEE Tran. Instrumentation and Measurement, vol. 56, no. 6, pp. 2289-2293, Dec. 2007.

[59] F. Vatansever and A. Ozdemir, "Power parameters calculations based on wavelet packet transform," International Journal of Electrical Power & Energy Systems, vol. 31, no. 10, pp. 596-603, Nov. 2009.

[60] W. G. Morsi and M. E. El-Hawary, "Novel power quality indices based on wavelet packet transform for non-stationary sinusoidal and non-sinusoidal disturbances," Electric Power Systems Research, vol. 80, no. 7, pp. 753-759, Jul. 2010.

[61] A. H. Ghaemi, H. Askarian Abyaneh and K. Mazlumi, "Harmonic indices assessment by Wavelet Transform," International Journal of Electrical Power & Energy Systems, vol. 33, no. 8, pp. 1399-1409, Oct. 2011.

[62] N. C. F. Tse and L. L. Lai, "Wavelet-Based Algorithm for Signal Analysis," EURASIP Journal on Advances in Signal Processing, vol. 2007, no. 1, pp. 169-178, Jan 2007

[63] P. K. Dash, B. K. Panigrahi and G. Panda, "Power quality analysis using S-transform," IEEE Trans. Power Delivery, vol. 18, no. 2, pp. 406-411, Apr. 2003.

[64] P. K. Dash and M. V. Chilukuri, "Hybrid S-transform and Kalman filtering approach for detection and measurement of short duration disturbances in power networks," IEEE Tran. Instrumentation and Measurement, vol. 53, no. 2, pp. 588-596, Apr. 2004.

[65] X. Xiao, F. Xu and H. Yang, "Short duration disturbance classifying based on S-transform maximum similarity," International Journal of Electrical Power & Energy Systems, vol. 31, no. 7, pp. 374-378, Sep. 2009.

[66] S. H Cho, G. Jang and S. H. Kwon, "Time-Frequency Analysis of Power-Quality Disturbances via the Gabor–Wigner Transform," IEEE Trans. Power Delivery, vol. 25, no. 1, pp. 494-499, Jan. 2010.

[67] N. Senroy, S. Suryanarayanan and P. F. Ribeiro, "An Improved Hilbert–Huang Method for Analysis of Time-Varying Waveforms in Power Quality," IEEE Trans. Power Systems, vol. 22, no. 4, pp. 1843-1850, Nov. 2007.

[68] S. Shukla, S. Mishra and B. Singh, "Empirical-Mode Decomposition With Hilbert Transform for Power-Quality Assessment," IEEE Trans. Power Delivery, vol. 24, no. 4, pp. 2159-2165, Oct. 2009.

Appendix I

A Coreless Electric Current Sensor with Circular Conductor Positioning Calibration

---

(Please see the next page)

A Coreless Electric Current Sensor With Circular Conductor Positioning Calibration

John Y. C. Chan, *Student Member, IEEE,* Norman C. F. Tse, *Member, IEEE,* and Loi Lei Lai, *Fellow, IEEE*

***Abstract*—This paper presents a novel coreless current sensor unit for measuring electrical current of circular conductors. The proposed sensor unit consists of three magnetic field sensors and a microcontroller unit (MCU). The new sensor unit does not need a bulky magnetic core necessary for magnetic field concentration, and can be used in the same way as conventional current transformers (CTs). An algorithm is developed to calibrate the outputs of the magnetic field sensors (e.g., Hall effect integrated circuits (ICs) with respect to the relative position of the current-carrying circular conductor. The algorithm can be implemented on a low-cost MCU for automatic real-time operation. Unlike other coreless magnetic field sensors that need to be fixed onto the conductor for accurate current measurement, the proposed sensor unit affords a more flexible installation option. A hardware prototype is constructed for the proposed coreless current sensor unit. The performance evaluation results show that the accuracy of the proposed sensor unit is comparable to the conventional magnetic core CTs.**

***Index Terms*—Automatic position calibration, coreless current sensing, magnetic field sensor.**

I. Introduction

UNLIKE voltage that can be measured directly, current is always measured through indirect means. While a few current sensing technologies make use of Ohm's law [1]–[3], many others rely on magnetic field phenomena, including Hall effect [4], [5], Faraday's law of induction [6], [7], and Faraday effect [8], [9].

Current transformer (CT) and Hall effect current transformer (HCT) are the most popular current measurement equipment. They are largely applied in electrical power distribution systems for alternating current (AC) measurement [10]. HCT can also measure direct current (DC). It is used extensively in power electronic circuits or battery-powered equipment, such as inverters, renewable energy sources, and motor vehicles. These applications require both high frequency AC and DC current measurement [5]. For measuring the AC of a circular conductor, CT and HCT are equipped with a magnetic toroidal core (e.g., silicon steel or ferrite material) for magnetic field concentration. The high permeability of the magnetic core helps to amplify the magnetic flux produced by the current, thus improving both the measurement sensitivity and interference immunity significantly. As the magnetic core can maintain a uniform magnetic flux regardless of the conductor's position [11], these current sensors are more flexible in installation.

Another popular AC sensor is the Rogowski coil (RC) [12]–[14]. RC is basically a coreless CT, which offers many advantages, including: 1) it does not suffer from magnetic core saturation and hysteresis problems; 2) a faster response than CT [12] can be achieved due to low coil inductance; and 3) RC with flexible construction (e.g., nonrigid plastic core) is much lighter than CT and HCT, and is more convenient and flexible in installation. The only drawback is RC's measurement accuracy is affected by the position of the conductor that is reported to be ranged 0.2%–3% [15].

The magnetic field sensor (e.g., Hall effect IC) used in the HCT is a feasible coreless current sensing option. Similar to HCT, it supports both AC and DC measurement. As magnetic core is not provided, this sensor is normally fixed onto print circuit board (PCB), and must be in close proximity with the current-carrying path [15], [16]. Meanwhile in [17], a novel solution is proposed for applying coreless Hall effect sensors to measure current in a large cable, with special attention to immunity to external magnetic field interference. Similar to many other approaches [18], these magnetic field sensors need to be fixed onto the cable directly. Sensor calibration is required to cater for the effects of conductor diameter, conductor shape, conductor insulation thickness, and installation method on the measured magnetic field strength.

In order to provide a more flexible solution for measuring the current of a circular conductor by a coreless sensor, an approach that utilizes three magnetic field sensors and a microcontroller unit (MCU) for automatic sensing calibration is proposed in this paper. The proposed coreless current sensing unit can be used in a similar fashion as the conventional CT, HCT, or clamp meter, yet possesses the features of coreless sensors. Both AC and DC can also be measured. The paper is organized as follows. Section II discusses the relationship between the distance and the magnetic field strength produced by a circular electrical conductor. In Section III, the proposed

Manuscript received October 18, 2012; revised January 10, 2013; accepted February 18, 2013. Date of publication July 3, 2013; date of current version October 7, 2013. The Associate Editor coordinating the review process was Dr. E. Fiorucci.

J. Y. C. Chan is with the Division of Building Science, Technology, City University of Hong Kong, Kowloon, Hong Kong SAR, and also with the School of Engineering and Mathematical Sciences, City University London, London EC1V 0HB, U.K. (e-mail: yaucchan@cityu.edu.hk).

N. C. F. Tse is with the Division of Building Science, Technology, City University of Hong Kong, Hong Kong (e-mail: bsnorman@cityu.edu.hk).

L. L. Lai is with the Energy Strategy, Planning, Policy Support, Research and Development Centre, State Grid Energy Research Institute, Beijing 100052, China (e-mail: l.l.lai@ieee.org).

Color versions of one or more of the figures in this paper are available online at http://ieeexplore.ieee.org.

Digital Object Identifier 10.1109/TIM.2013.2266051

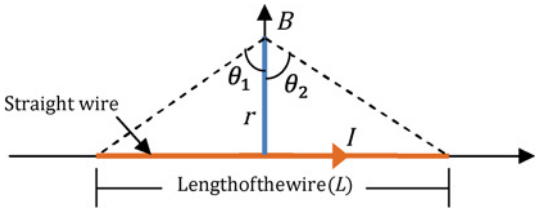

Fig. 1. Magnetic field produced by the current in a straight wire.

coreless current sensor unit integrated with an automatic positioning calibration algorithm is introduced. Section IV describes the construction of the prototype sensor unit. The performance evaluation is presented in Section V. Sections VI contains the conclusions.

II. Magnetic Field Strength of Circular Current-Carrying Conductor

According to Ampere's circuital law, the strength of the magnetic field generated by a current-carrying conductor is directly proportional to the current magnitude. From Biot–Savart law, the magnetic field produced by a straight wire in free space can be written as [19]

$$B = \frac{\mu_0 I}{4\pi r}(\sin\theta_2 - \sin\theta_1) \tag{1}$$

where B is the magnetic flux density, μ_0 is the permeability of free space, I is the current magnitude, r is the distance from the center of the conductor, and θ_1 and θ_2 are the angles shown in Fig. 1.

When the length of the wire L is infinite [19], the angles θ_1 and θ_2 in (1) tend to be - 90 and 90, respectively. The magnetic field produced by the current of the infinite straight wire can be represented as

$$B = \frac{\mu_0 I}{2\pi r}. \tag{2}$$

Equation (2) is commonly adopted to approximate the magnetic field emitted from a straight wire with finite length, provided that the distance r is much shorter than L [18]. This is the case when a magnetic field sensor is closely attached to a long straight wire. Moreover, (2) reveals that the magnetic field is inversely proportional to the distance from the center of the straight wire. As the measured flux density is dependent on the overall diameter of the wire, calibration is therefore required when a sensor is directly attached to the wire surface [17], [18].

III. Proposed Coreless Current Sensor Unit With Automatic Positioning Calibration

In order to automate the calibrating process discussed in Section II, the proposed coreless current sensor unit utilizes three magnetic sensors together with an MCU to estimate the relative distances of the cable from the sensors. The concept of the automatic calibration algorithm is illustrated in Fig. 2. Instead of attaching directly to the conductor surface, the magnetic field sensors (e.g., Hall effect IC) are soldered onto

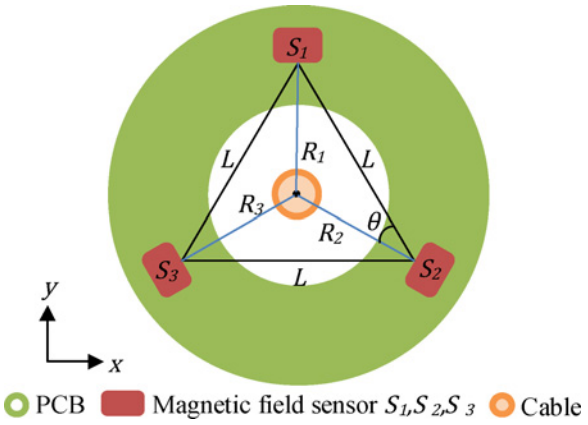

Fig. 2. Conceptual diagram of the coreless current sensor unit.

a PCB in the form of an equilateral triangle. The sensor unit resembles a conventional toroidal core CT, but with the magnetic core replaced by a plastic one. This sensor unit can be used even when the physical size of the conductor is much smaller than the magnetic field sensor. As there is no magnetic core for magnetic field concentration, the magnetic flux density measured by each sensor varies with the distance from the conductor. The first step is to position the conductor, after which the calibration can be performed. The positioning calibration algorithm is derived as follows.

As shown in Fig. 2, the magnetic field sensors are fixed onto the PCB with known interdistances. The position of the conductor is to be estimated from the magnetic flux density measured by the individual sensors. From (2), the magnetic flux density measured by the magnetic field sensors S_1, S_2, and S_3 can be approximated as

$$B_1 = \frac{\mu_0 I}{2\pi R_1} \tag{3}$$

$$B_2 = \frac{\mu_0 I}{2\pi R_2} \tag{4}$$

$$B_3 = \frac{\mu_0 I}{2\pi R_3} \tag{5}$$

where B_1, B_2, and B_3 are the magnetic flux densities measured by the magnetic field sensors S_1, S_2, and S_3, respectively; is the permeability of free space; I is the current flowing in the conductor; R_1, R_2, and R_3 are the distances between the center of the conductor and S_1, S_2, and S_3, respectively. Substituting (4) and (5) into (3), we get

$$R_2 = R_1 \times \frac{B_1}{B_2} \tag{6}$$

and

$$R_3 = R_1 \times \frac{B_1}{B_3}. \tag{7}$$

Let

$$m = \frac{B_1}{B_2} \tag{8}$$

and

$$n = \frac{B_1}{B_3} \tag{9}$$

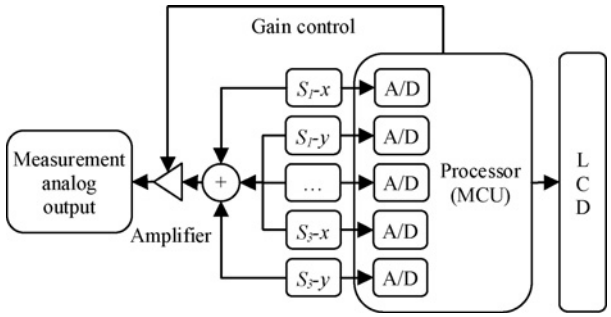

Fig. 3. Schematic block diagram of the prototype current sensor unit.

by the Law of Cosine, the relationship of R_1, R_2, and R_3 and θ can be written as

$$R_1^2 = L^2 + R_2^2 - 2LR_2\cos\theta \tag{10}$$

$$R_3^2 = L^2 + R_2^2 - 2LR_2\cos(60-\theta) \tag{11}$$

where R_1, R_2, R_3, θ, and L are as shown in Fig. 2.

By substituting (6), (7), (8), and (9) into (10) and (11), the following expressions in terms of R_1 and θ are obtained

$$R_1^2 = L^2 + (mR_1)2 - \cos\theta \text{ and} \tag{12}$$

$$(nR_1)^2 = L^2 + (mR_1)^2\cos(60-\theta). \tag{13}$$

Solving (12) and (13), we get

$$R_1 = \sqrt{\frac{2L^2}{\left(m^2+n^2+1+\sqrt{3(2m^2+2n^2+2m^2n^2-m^4-n^4-1)}\right)}}. \tag{14}$$

Similarly R_2 and R_3 can be obtained by using (6) and (7), and the conductor current (I) can be estimated by (3).

The positioning calibration algorithm is implemented on a low-cost MCU for real-time automatic application. It should be noted that the proposed algorithm is designed for circular conductors, and the magnetic field sensors used are capable to measure the magnetic flux density on x and y axes only. This means that the plane of the magnetic sensors should be perpendicular to the axis of the conductor, as illustrated in Figs. 2 and 4. Otherwise additional magnetic sensors should be included to measure the magnetic flux density along the z-axis.

IV. Construction of the Prototype Sensor Unit

The schematic block diagram of the prototype sensor unit is shown in Fig. 3. The prototype sensor unit consists of a low-cost MCU (e.g., Texas Instruments MSP430), magnetic field sensor ICs, an LCD display, and a variable gain amplifier. The prototype current sensor unit can provide both numerical and analog output, similar to a conventional clamp meter.

The operation of the sensor unit is as follows. The MCU acquires data from the magnetic field sensors S_1, S_2, and S_3 (Fig. 2) through analog-to-digital converters (ADCs), and estimates the distances R_1, R_2, and R_3 (Fig. 2). The conductor current is estimated using (12)–(13) and (3)–(5). The LCD display and the analog amplifier gain are also controlled by the MCU.

TABLE I
Specifications of the Prototype Sensor Unit

Parameter	Value	Unit
Supply Voltage	±5	V
Current Range	0.1 to 10	A
Sensitivity	10	mV/A
Bandwidth (-3dB)	DC to 15	kHz
Accuracy	±0.053	A

Each magnetic field sensor measures the magnetic flux density on x and y axes (e.g., GMW 2SA-10G or Melexis MLX91204), therefore totally six ADCs are needed. The magnitudes of B_1, B_2, and B_3 in (3)–(5) can be obtained by applying the Pythagorean Theorem (15) to the respective measured x and y values

$$B = \sqrt{B_x^2 + B_y^2} \tag{15}$$

where B_x and B_y are the measured magnetic flux densities on the x- and the y-axis, respectively, and B is the magnitude of the flux density (e.g., B_1, B_2, and B_3).

Fig. 4 shows the layout of the prototype coreless current sensor unit. In order to facilitate testing and design modification, the magnetic field sensors are installed on a sensor board. The MCU, the variable gain amplifier, and the LCD display are assembled on the MCU board. The block diagram of the variable gain amplifier circuit is shown in Fig. 5. Digital potentiometers (e.g., Maxim Integrate MAX5497) are adopted to control the amplitude gain of the amplifier through the MCU. The assembled sensor board and the MCU board are shown in Figs. 6 and 7, respectively. The prototype sensor unit is designed to operate from 0.1 to 10 A, with the output sensitivity tuned to 10 mV/A, adjustable by the variable gain amplifier. The overall bandwidth is 15 kHz which is mainly limited by the bandwidth of the magnetic field sensors. The maximum error as discussed in Section V is 0.053 A. Table I summarizes the specifications of the prototype sensor unit.

V. Performance Evaluation of the Prototype Sensor Unit

The test platform made use of a multifunctional AC power supply unit (Kikusui PCR-500) to supply a steady AC power to a resistive load through a step-down voltage transformer (220 V/6 V, 300 VA). The test platform is shown in Figs. 8 and 9. The current in the test circuit is measured simultaneously by the prototype current sensor unit and a class-A power quality (PQ) meter (Hioki PW3198). For comparison purpose, a digital oscilloscope (OSC) is used to read the analog output of the prototype sensor unit and the voltage output of the step-down transformer. Table II presents the specifications of the measuring devices in the test platform.

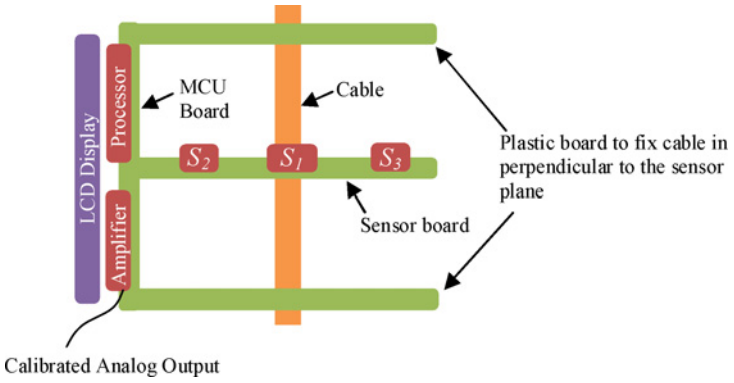

Fig. 4. Layout of the prototype coreless current sensor unit.

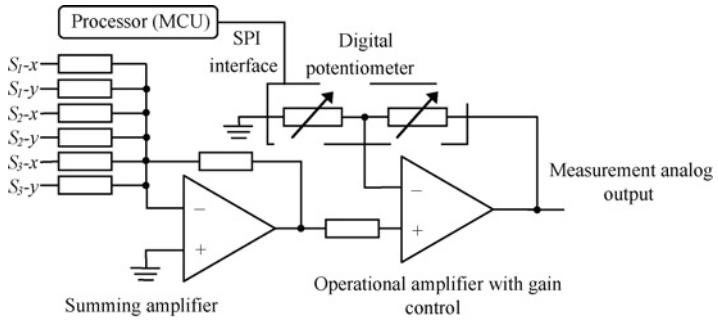

Fig. 5. Block diagram of the variable gain amplifier circuit.

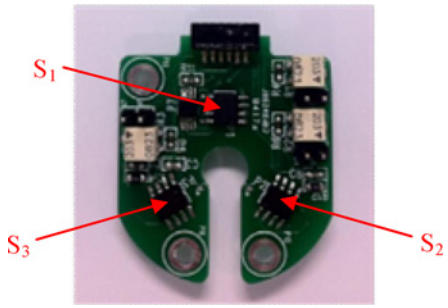

Fig. 6. Sensor board assembly.

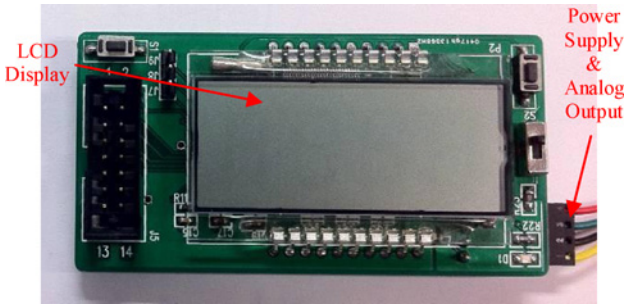

Fig. 7. MCU board assembly.

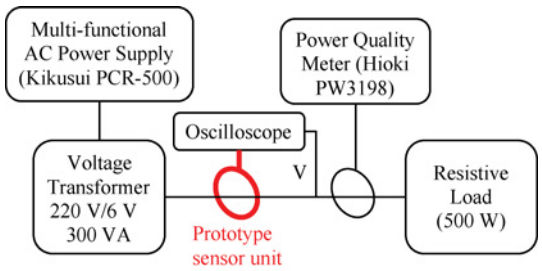

Fig. 8. Layout of the test platform.

Fig. 9. Photos of the test platform.

A binding board is used to fix the conductor in various positions inside the sensor unit (Fig. 10). Three positions are chosen for conducting the measurement as shown in Fig. 11.

During the test, the prototype current sensor unit is evaluated from 0.1 to 10 A at Positions 1, 2, and 3. The readings of the prototype current sensor unit are obtained from RMS measurement function of the digital OSC, as in Fig. 13. All measurements are taken after the test platform has been stabilized for 5 min. The measurement results with the conductor at Positions 1, 2, and 3 are shown in Tables III–V, respectively.

TABLE II
SPECIFICATIONS OF THE DEVICES IN THE TEST PLATFORM

Device	Parameter	Value	Unit
Multi-functional AC Power Supply (Kikusui PCR-500)	Output Voltage	1 to 280	V
	Output Power	500	VA
	Line Regulation Stability	±0.1	%
	Load Regulation Stability	±0.2	V
Voltage Transformer	Voltage Ratio	220 / 6	V
	Power Rating	300	VA
Power Quality Meter (Hioki PW3198)	Current Range (Configured)	0 to 50	A
	Overall Accuracy	±0.5% rdg. ±0.06 A	-
	RMS measurement method	10	cycle
Digital Oscilloscope (UTD2102CEL)	Bandwidth	100	MHz
	Vertical Sensitivity(Configured)	50	mV/div
Resistive Load	Resistance	0.625	Ohm
	Power Rating	500	W

TABLE III
MEASUREMENT RESULTS (POSITION 1)

Supply Current (A rms)	AC Supply Output Voltage (V rms)	Oscilloscope Measured Voltage (V rms)	Measured Current (A rms)		
			PQ meter	Prototype	Difference
0.10	1.9	0.065	0.103	0.126	0.022
0.30	6.1	0.195	0.311	0.294	0.017
0.50	10.1	0.323	0.516	0.486	0.029
1.00	20.1	0.678	1.082	1.043	0.039
2.00	39.0	1.270	2.011	1.973	0.038
3.00	59.1	1.920	3.042	2.989	0.053
5.00	98.2	3.200	5.058	5.042	0.016
8.00	155.9	5.080	8.049	8.023	0.026
10.00	194.8	6.310	10.049	10.030	0.019

TABLE IV
MEASUREMENT RESULTS (POSITION 2)

Supply Current (A rms)	AC Supply Output Voltage (V rms)	Oscilloscope Measured Voltage (V rms)	Measured Current (A rms)		
			PQ meter	Prototype	Difference
0.10	1.9	0.065	0.103	0.128	0.025
0.30	6.1	0.193	0.310	0.297	0.013
0.50	10.1	0.322	0.513	0.493	0.020
1.00	20.1	0.669	1.029	1.048	0.019
2.00	39.0	1.260	2.002	1.992	0.010
3.00	59.1	1.910	3.031	3.013	0.018
5.00	98.2	3.100	5.049	5.060	0.011
8.00	155.9	5.030	8.037	8.080	0.043
10.00	194.8	6.250	9.996	10.020	0.024

TABLE V
MEASUREMENT RESULTS (POSITION 3)

Supply Current (A rms)	AC Supply Output Voltage (V rms)	Oscilloscope Measured Voltage (V rms)	Measured Current (A rms)		
			PQ meter	Prototype	Difference
0.10	1.9	0.066	0.104	0.129	0.026
0.30	6.1	0.196	0.311	0.303	0.008
0.50	10.1	0.325	0.516	0.510	0.006
1.00	20.1	0.668	1.034	1.008	0.026
2.00	39.0	1.280	2.013	1.981	0.032
3.00	59.1	1.930	3.044	3.018	0.026
5.00	98.2	3.210	5.061	5.012	0.049
8.00	155.9	5.080	8.054	8.015	0.039
10.00	194.8	6.310	10.072	10.030	0.042

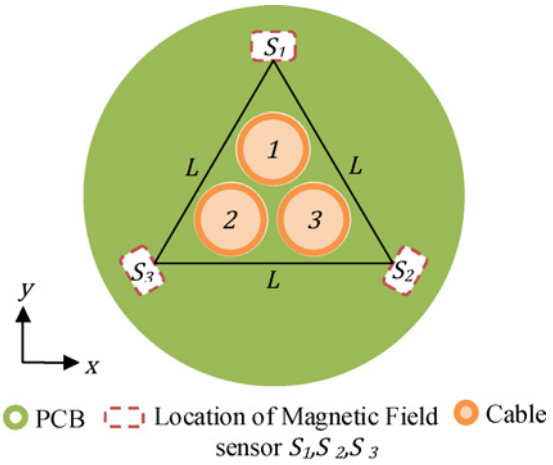

Fig. 10. Binding board to fix the conductor in three different positions.

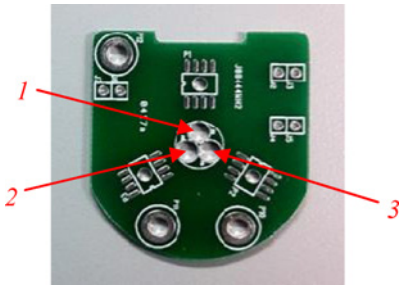

Fig. 11. Binding board assembly.

The observed maximum difference is 0.053 A (i.e., 0.53% of 10 A) at a supply current of 3 A (Table III). Taking into account the accuracy of PQ meter (Table II), the observed maximum difference has an uncertainty of +0.0752 A when the reading of PQ meter is 3.042 A. The average measurement difference between the PQ meter and the prototype current sensor unit is 0.026 A, corresponding to 0.26% at 10 A. Similarly the uncertainty of PQ meter at 10 A is +0.11 A.

The relative differences between the measured current of the PQ meter and the prototype sensor unit in the three conductor positions under various supply currents are summarized graphically in Fig. 12. The relative difference is estimated by

$$\text{Relative differnce}\,(\%) = \frac{I_m - I_p}{I_m} \times 100 \qquad (16)$$

where I_{m} and I_{p} are the measured current of the PQ meter and the prototype sensor unit, respectively.

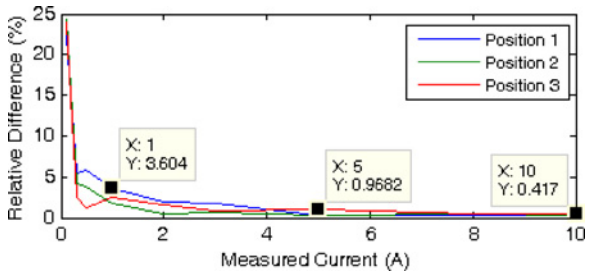

Fig. 12. Relative difference between the currents measured by the PQ meter and the prototype sensor unit.

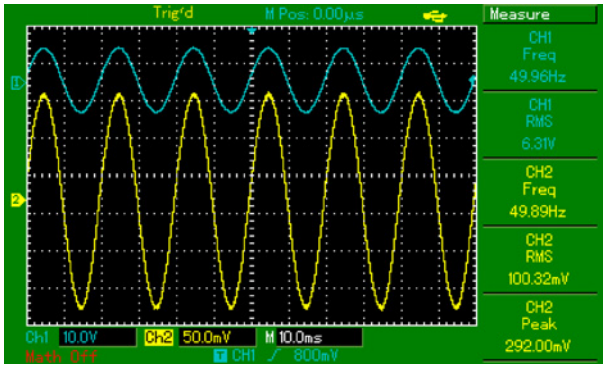

Fig. 13. Screenshot of the digital oscilloscope. Blue (upper) line: transformer output voltage. Yellow (lower) line: current measured by the prototype sensor unit.

Fig. 13 shows a screenshot captured by the digital OSC. On the screenshot, the output voltage of the AC power supply is 194.8 V rms, and the output voltage of the step-down transformer is 6.31 V (Channel 1 of the screenshot in blue). The current measured by the PQ meter is 10.072 A. The analog

output of the prototype sensor unit is 100.32 mV (Channel 2 of the screenshot in yellow), equivalent to a measured current of 10.032 A at a sensitivity of 10 mV/A (Table I).

VI. Conclusion

A prototype coreless current sensor unit was constructed for measuring AC and DC of a circular conductor. This sensor unit was composed of three magnetic field sensors and an MCU. A positioning calibration algorithm was developed for automatic sensor output calibration. It can be used to conduct current measurement of any circular conductors without the need of manual calibration. The sensor unit is able to locate the position of the conductor, and to calibrate the measured results of the magnetic field sensors accordingly. A prototype current sensor unit was constructed for verifying the measurement performance. It was verified that the accuracy of the proposed current sensor unit is comparable to the conventional CTs with current magnitudes ranged 0.1–10 A.

For future works, a functional mechanism will be designed to ease the fixing of the proposed magnetic field sensor unit perpendicularly to the circular conductor for onsite applications. A sensor unit with 3-D magnetic field measurement capability will also be experimented.

References

[1] C. M. Johnson and P. R. Palmer, "Current measurement using compensated coaxial shunts," in *IEEE Proc. Sci. Meas. Tech.*, vol. 141, no. 6, pp. 471–480, Nov. 1994.

[2] F. Castelli, "The flat strap sandwich shunt," *IEEE Trans. Instrum. Meas.*, vol. 48, no. 5, pp. 894–898, Oct. 1999.

[3] R. Ferrero, M. Marracci, and B. Tellini, "Analytical study of impulse current measuring shunts with cage configuration," *IEEE Trans. Instrum. Meas.*, vol. 61, no. 5, pp. 1260–1267, May 2012.

[4] L. Cristaldi, A. Ferrero, M. Lazzaroni, and R. T. Ottoboni, "A linearization method for commercial Hall-effect current transducers," *IEEE Trans. Instrum. Meas.*, vol. 50, no. 5, pp. 1149–1153, Oct. 2001.

[5] P. Poulichet, F. Costa, and E. Laboure, "A new high-current large-bandwidth DC active current probe for power electronics measurements," *IEEE Trans. Ind. Electron.*, vol. 52, no. 1, pp. 243–254, Feb. 2005.

[6] N. Locci and C. Muscas, "Hysteresis and eddy currents compensation in current transformers," *IEEE Trans. Power Del.*, vol. 16, no. 2, pp. 154–159, Apr. 2001.

[7] N. Kondrath and M. K. Kazimierczuk, "Bandwidth of current transformers," *IEEE Trans. Instrum. Meas.*, vol. 58, no. 6, pp. 2008–2016, Jun. 2009.

[8] T. W. Cease and P. Johnston, "A magneto-optic current transducer," *IEEE Trans. Power Del.*, vol. 5, no. 2, pp. 548–555, Apr. 1990.

[9] T. Sawa, K. Kurosawa, T. Kaminishi, and T. Yokota, "Development of optical instrument transformers," *IEEE Trans. Power Del.*, vol. 5, no. 2, pp. 884–891, Apr. 1990.

[10] A. Cataliotti, D. D. Cara, A. E. Emanuel, and S. Nuccio, "Current transformers effects on the measurement of harmonic active power in LV and MV networks," *IEEE Trans. Power Del.*, vol. 26, no. 1, pp. 360–368, Jan. 2011.

[11] E. Ramsden, *Hall effect Sensors: Theory and Application*, 2nd ed. Burlington, MA, USA: Newnes, 2006.

[12] D. A. Ward and J. L. T. Exon, "Using Rogowski coils for transient current measurements," *Eng. Sci. Educ. J.*, vol. 2, no. 3, pp. 105–113, Jun. 1993.

[13] E. Abdi-Jalebi and R. McMahon, "High-performance low-cost Rogowski transducers and accompanying circuitry," *IEEE Trans. Instrum. Meas.*, vol. 56, no. 3, pp. 753–759, Jun. 2007.

[14] M. Chiampi, G. Crotti, and A. Morando, "Evaluation of flexible Rogowski coil performances in power frequency applications," *IEEE Trans. Instrum. Meas.*, vol. 60, no. 3, pp. 854–862, Mar. 2011.

[15] S. Ziegler, R. C. Woodward, H. H. C. Iu, and L. J. Borle, "Current sensing techniques: A review," *IEEE Sensors J.*, vol. 9, no. 4, pp. 354–376, Apr. 2009.

[16] L. Law, "Measuring current with IMC Hall effect technology," *Sensors*, vol. 20, no. 11, pp. 29–32, Nov. 2003.

[17] C. Kun-Long and C. Nanming, "A new method for power current measurement using a coreless Hall effect current transformer," *IEEE Trans. Instrum. Meas.*, vol. 60, no. 1, pp. 158–169, Jan. 2011.

[18] T. Yuan-Pin, C. Kun-Long, and C. Nanming, "Design of a Hall effect current microsensor for power networks," *IEEE Trans. Smart Grid*, vol. 2, no. 3, pp. 421–427, Sep. 2011.

[19] D. K. Cheng, *Field and Wave Electromagnetics*. Canada: Addison-Wesley, 1989.

John Y. C. Chan (S'10) received the B.E. degree in computer engineering from the City University of Hong Kong, Hong Kong, in 2009.

Currently, he is pursuing the Ph.D. degree in electrical engineering at City University London, London, U.K. His current research interests include electrical power quality and embedded system design and signal processing.

Norman C. F. Tse (M'09) graduated from Hong Kong Polytechnic University (then Hong Kong Polytechnic), Hong Kong, in 1985, the M.Sc. degree from the University of Warwick, Coventry, U.K., in 1994, and the Ph.D. degree from City University London, London, U.K., in 2007.

He is an Associate in electrical engineering. Currently, he is with the Centre for Smart Energy Conversion and Utilization Research (CSCR), City University of Hong Kong, Hong Kong. His current research interests include power quality measurement and analysis, web-based power quality monitoring, harmonics mitigation, and building energy efficiency study.

Loi Lei Lai (SM'92–F'07) received the B.Sc. (first-class honors) and Ph.D. degrees from the University of Aston, Birmingham, U.K., and the D.Sc. degree from City University London (CUL), London, U.K.

Currently, he is the Director of the Energy Strategy, Planning, Policy Support, and Research and Development Center, State Grid Energy Research Institute, Beijing, China. He is also an Honorary Visiting Chair Professor with CUL, a Visiting Professor with Southeast University, Nanjing, China, a Guest Professor with Fudan University, Shanghai, China, and the Pao Yu Kong Chair Professor with Zhejiang University, Hangzhou, China.

Dr. Lai was a recipient of the IEEE Third Millennium Medal, the 2000 IEEE Power Engineering Society United Kingdom and Republic of Ireland Chapter Outstanding Engineer Award, the 2003 IEEE Power Engineering Society Outstanding Large Chapter Award, a Prize Paper by the IEEE Power and Energy Society Power Generation and Energy Development Committee in June 2006 and July 2009, and a high-quality paper prize from the International Association of Desalination, USA, in 1995. He is a fellow of The Institution of Engineering and Technology, U.K.

Appendix II

Source Code for the Algorithm

This appendix contains source code for the Frequency Shifting Discrete Wavelet Decomposition method described in Chapter 7. The listed source codes are in MATLAB syntax, and required to execute in MATLAB environment with its internal libraries and toolboxes (e.g. Wavelet Toolbox). The source codes are mainly separated in five MATLAB script files.

File 1: ihht_demo.m

This file contains a main routine to demonstrate the decomposition method. It executes various sub-routines to decompose the input waveform and to display the analyzed results.

```
function [im, ph, A, f, imf, ihht_wpt] = ihht_demo(wname, lv, sig, amp_ratio)

% ihht_demo
% ----------------------------------------
% Input:
%   wname: filter name
%   lv: decompose level
%   si: input signal
% Output:
%   ihh_wpt: output
% ----------------------------------------

% initial
slen = length(sig);
sig = sig(1:floor(slen/2)*2);

% create filter
[h0, h1] = wfilters(wname,'d');
[f0, f1] = wfilters(wname,'r');

% decompose
ht_wpt = ihht_wavelet_packet(6400, h0, h1, f0, f1, lv, sig);
```

```
% emd
imf = ihht_emd(ht_wpt, 0);

% find amp, freq, time
[ph,A,f,t] = hhspectrum(imf);
FFss = mean(f(:,640:end-639),2) * 6400;
AAss = mean(A(:,640:end-639),2);

% grouping
ihht_wpt = ihht_wpt_reorganization(FFss, AAss, ht_wpt, amp_ratio * 0.001, 32, 25);

% emd
imf = ihht_emd(ihht_wpt, amp_ratio * 0.002);

% find amp, freq, time
[ph,A,f,t] = hhspectrum(imf);
A = A(:,640:end-639);
f = f(:,640:end-639);
ph = ph(:,641:end-640);
imf = imf(:, 641:end-640);

% Truncate ihht_wpt.s
ihht_twpt = ihht_wpt_trim(ihht_wpt, 641, 640);

% plot grouping subbands
ihht_wpt_plot(ihht_twpt);

% mapping into a image
[im,tt,ff] = toimage(A,f);

% plot
disp_hhs(im, -22);
end

% Truncate ihht_wpt.s
function ihht_twpt = ihht_wpt_trim(ihht_wpt, startIndex, endIndex)

% Loop
for j = 1 : length(ihht_wpt.s)
   ihht_twpt.s{j} = ihht_wpt.s{j}(startIndex:end-endIndex);
end
end
```

File 2. ihht_wavelet_packet.m

This file contains a sub-routine to decompose the input waveforms.

```
function ht_wpt = ihht_wavelet_packet(fs, h0, h1, f0, f1, lv, sig)

% Decompose input signal to 2^lv subband by wavelet packet for ihht
% ----------------------------------------
% Input:
%   wname: filter name
%   lv: decompose level
%   si: input signal
% Output:
%   ihh_wpt: output
% ----------------------------------------

% initial
ss = sig;

time = 0 : 1/fs : (length(sig) / fs);

% shift stem
sstep = (fs/2)/(2^(lv+1));

% shift and decompose
for c = 1 : (2^(lv+1))

   % calculate shift frequency
   shift_freq = sstep * (c - 2) ; %shift -25, 0, 25, 50, 75....

   % shift signal
   ht_wave = real(hilbert(ss) .* exp(j*2*pi*time(1:end-1)*-shift_freq));

   % decompse
   wpt = wavelet_packet_decompose_1(h0, h1, f0, f1, lv, ht_wave);

   % shift signal
   rht_wave = real(hilbert(wpt.s00) .* exp(j*2*pi*time(1:end-1)*shift_freq));

   % save signal
   ht_wpt.s{c} = rht_wave;

   % cancal form the signal
   ss = ss - rht_wave;
end
end
```

File 3: ihht_emd.m

This file contains a sub-routine to organize the obtained results in file 2 for the Hilbert transform function in further analysis.

```
function imf = ihht_emd(ihht_wpt, th)

% emd for ihht_wpt
% ----------------------------------------
% Input:
%   ihh_wpt: signals
% Output:
%   imf: output
% ----------------------------------------

% Initial
imf = [];

% Loop
for j = 1 : length(ihht_wpt.s)
   if(max(abs(ihht_wpt.s{j}(641:end-640))) >= th)
      imf = [imf; ihht_wpt.s{j}];
   end
end
end
```

File 4: ihht_wpt_reorganization.m

This file contains a sub-routine to group decomposed frequency bands for harmonic and sub-harmonic analysis.

```
function ihht_wpt = ihht_wpt_reorganization(freq, amp, ht_wpt, th, ts, offset)
% re-organization structure of wpt
% ----------------------------------------
% Input:
%   freq: frequency of subbands
%   amp: amp of subbands
%   ht_wpt:
% ----------------------------------------

% initial
cnt = 1;
alen = length(ht_wpt.s);
slen = length(ht_wpt.s{1});

% loop
for c = 1 : length(freq)
   if(amp(c) >= th)

      % calculate boundary
      Lo_index = max(0, floor((freq(c)-(ts/2))/offset));
      Hi_index = min(alen-1, floor((freq(c)+(ts/2))/offset));
```

```
      % find it is similar
      if(amp(c) >= amp((Lo_index+1):(Hi_index+1)))
      if((freq(c) - offset) <= (freq((Lo_index+1):(Hi_index+1))))
      if((freq(c) + offset) >= (freq((Lo_index+1):(Hi_index+1))))

         % init
         ihht_wpt.s{cnt} = zeros(1, slen);

         % sum up
         for cc = (Lo_index+1) : (Hi_index+1)
           ihht_wpt.s{cnt} = ihht_wpt.s{cnt} + ht_wpt.s{cc};
         end

         % increment
         cnt = cnt + 1;
      end
      end
      end

   end

end
end
```

File 5: ihht_wpt_plot.m

This file contains a sub-routine to display the analysis result.

```
function ihht_wpt_plot(ihht_wpt)

% plot re-organizated wpt
% ----------------------------------------
% Input:
%   ihht_wpt: re-organizated wpt
%   lv: decomposed level
% ----------------------------------------

% Initial
pindex = [1:2:16, 2:2:16];

% Loop
for j = 0 : (length(ihht_wpt.s)-1)

   % create figure
   if(mod(j,16) == 0)
      figure;
```

```
    end

    % plot
    subplot(8, 2, pindex(mod(j,16)+ 1)), plot(ihht_wpt.s{j+1});
end
end
```

Appendix III

Circuit Diagrams of the Analog Front-End

This appendix shows circuits of the developed Analog Front-End (AFE) in Chapter 4. The circuits of the AFE can be divided into four major categories in terms of their functions. Their circuit diagrams are shown below:

Category 1: Power Supply

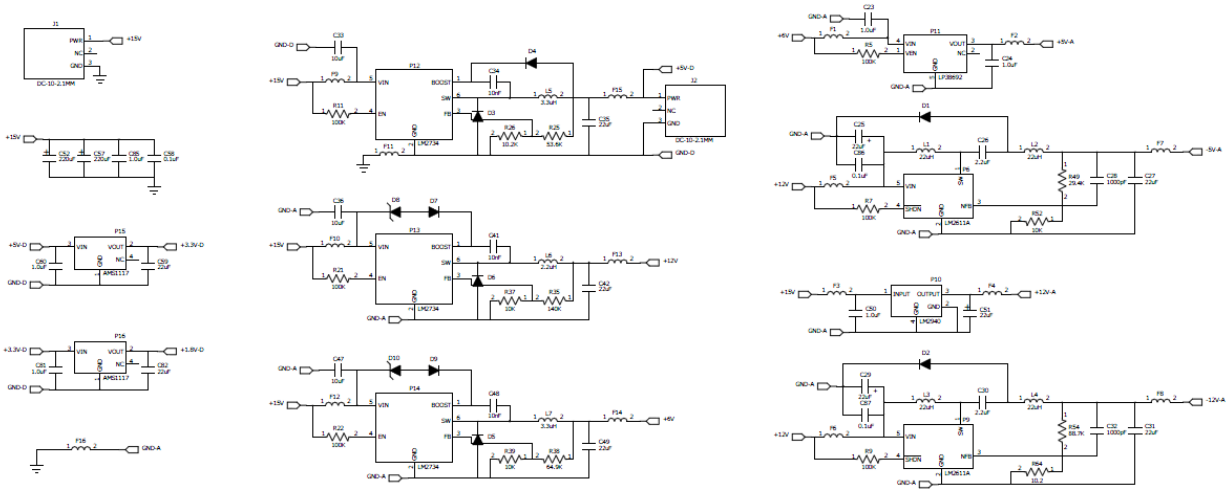

Category 2: Analog Filter and Voltage Sensing

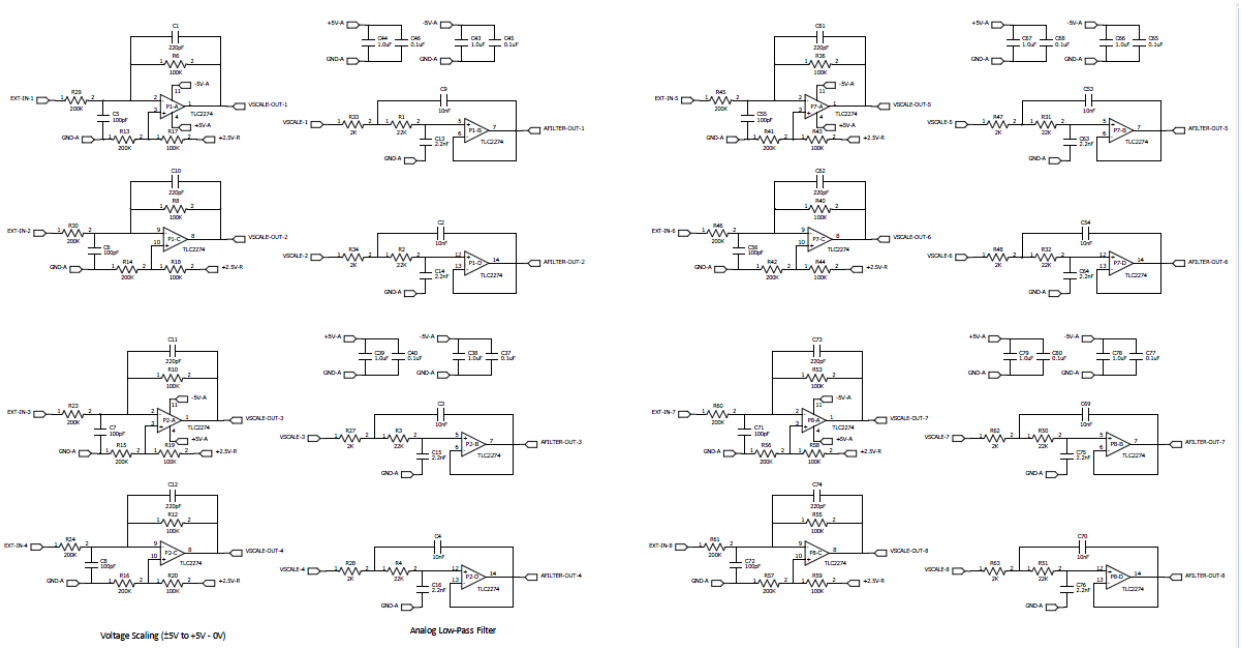

Category 3: Switches, A/D Converter and Voltage Reference

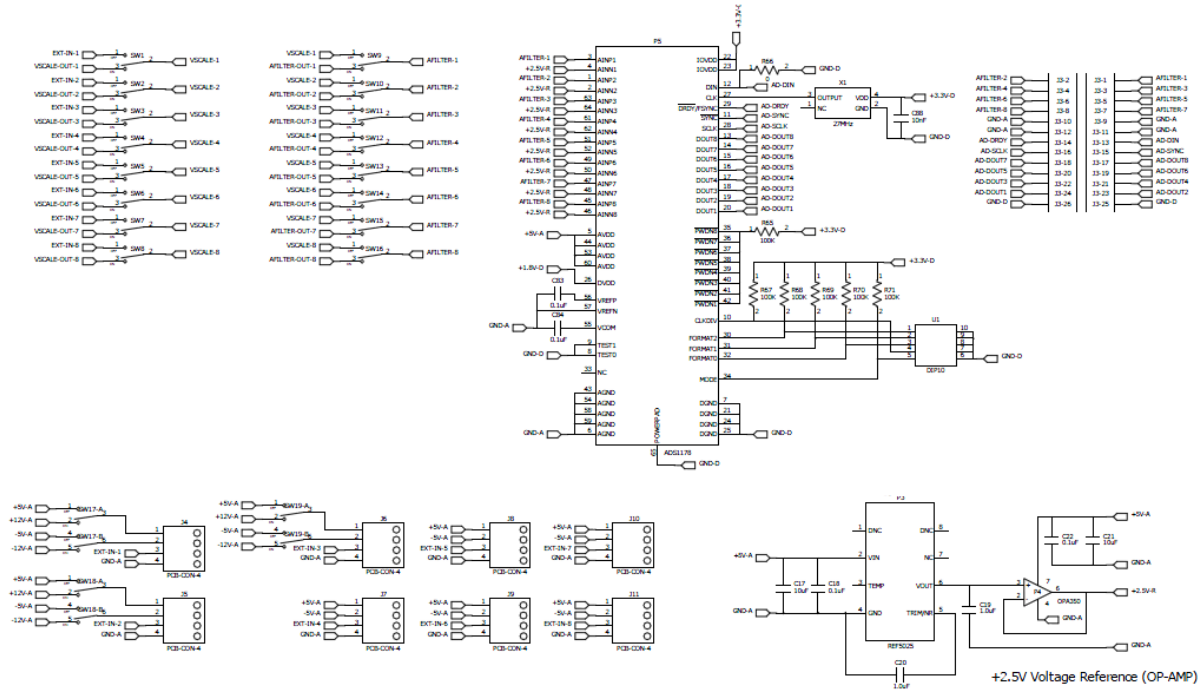

Category 4: A/D Converter - Sampling Clock